

**SPACE RESEARCH IN SLOVAKIA**

**2014 - 2015**



**SLOVAK ACADEMY OF SCIENCES**

**COSPAR**

**SLOVAK NATIONAL COMMITTEE**

APRIL 2016

ISBN 978-80-89656-09-7  
EAN 9788089656097

## Contents.

1.	EXPERIMENTS FOR MEASUREMENTS IN SPACE.....	4
	<i>J. Baláž, P. Bobík, K. Kudela</i>	
2.	SPACE PHYSICS, GEOPHYSICS AND ASTRONOMY.....	12
	<i>I. Dorotovič, R. Gális, K. Kudela, J. Masarik, A. Ondrášková, M. Revallo, J. Rybák, J. Tóth</i>	
3.	MATERIAL RESEARCH IN SPACE .....	51
	<i>J. Lapin</i>	
4.	REMOTE SENSING.....	56
	<i>I. Barka, T. Bucha, J. Feranec, Z. Klikušovská, M. Kopecká, Z. Kováčiková, J. Nováček, R. Pazúr, M. Rusnák, I. Sačkov, J. Sládek, M. Sviček</i>	
5.	SPACE METEOROLOGY.....	72
	<i>J. Kaňák, L. Okon, L. Méri, M. Jurašek, K. Hrušková, M. Zvolenský</i>	
6.	INSTITUTIONS PARTICIPATING IN SPACE RESEARCH IN SLOVAKIA. NATIONAL COMMITTEE OF COSPAR.....	88

# 1. EXPERIMENTS FOR MEASUREMENTS IN SPACE

*J. Baláž, P. Bobík, K. Kudela*

## 1.1. Experiment MEP-2 on board of RADIOASTRON space observatory

The programmable energetic particle spectrometer MEP-2, developed at the Department of Space Physics IEP-SAS in cooperation with Democritus University of Thrace, Xanthi, Greece and Institute for Space Research (IKI-RAN), Moscow, operates nominally on board of RADIOASTRON (Spektr-R) space observatory as a part of solar wind suite PLASMA-F (<http://www.plasma-f.cosmos.ru/en/instruments>). Since its launch on high-apogee orbit on 18 July 2011, MEP-2 delivered remarkable amount of valuable science data that are continuously archived and analysed.

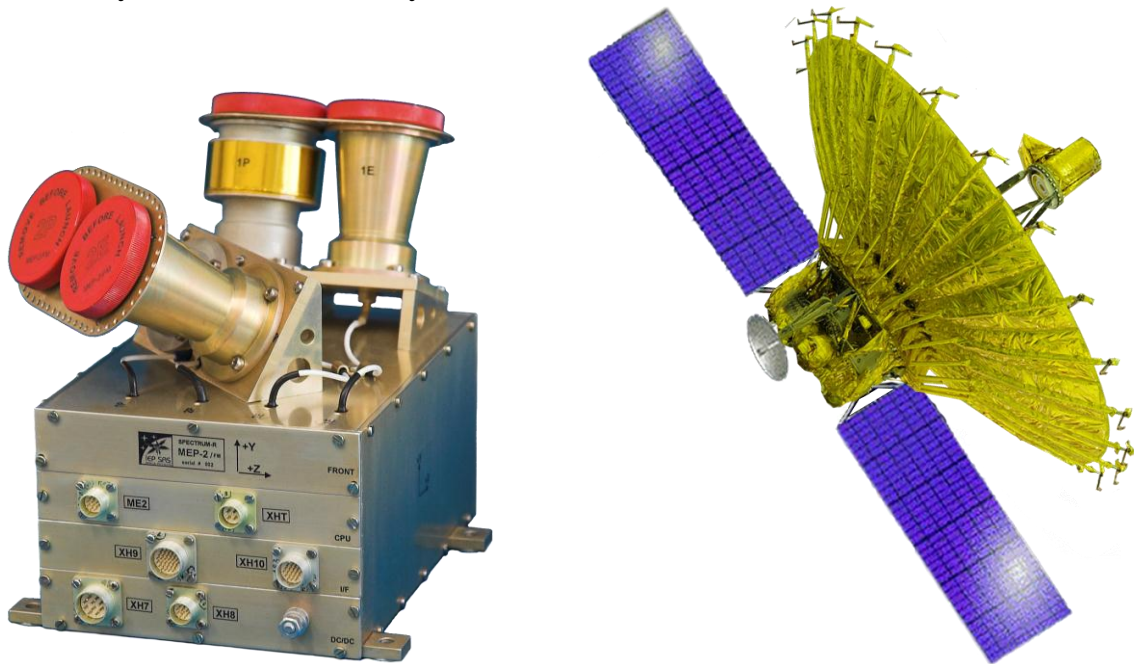


*Figure 1.1. Energetic particle spectrometer MEP-2 and space observatory RADIOASTRON (the size of the radiotelescope dish antenna  $D=10\text{m}$ , initial orbit  $390000\text{ km} \times 10000\text{ km}$ , inclination  $42.46^\circ$ , period  $8,86\text{ d}$ ).*

Amid significant results of the MEP-2 experiment, e.g., a new type of oscillations of energetic ions flux near the Earth's bow shock was revealed [2]. This kind of particle flux variability was possible to observe due to the high time resolution and wide energy range of MEP-2 spectrometer. The description and on-orbit operation of the PLASMA-F suite can be found in [1].

## 1.2. ESS processor on board of ROSETTA spacecraft at nucleus of comet 67P/Churyumov-Gerasimenko

Rosetta was launched on 2 March 2004 and after ten years and six billion kilometres of cruise flight over the Solar system, the spacecraft reached the comet and was captured in the orbit around the nucleus. On 12 November 2014, the lander module Philae performed the first successful landing in history on a comet.

The ESS processor unit (Electronic Support System) supported the lander module Philae separation from the main Rosetta orbiter and also provided bidirectional data communication between Philae and Orbiter during the descent phase and also during Philae operations on the comet nucleus surface. The ESS processor is mission critical hardware and was built from top-grade space qualified components. Its critical top-reliability was also secured by dual redundancy concept based on two identical systems. The ESS processor operated flawlessly during whole mission. It is installed on board of Rosetta-orbiter and is still fully operative, however, Philae on the nucleus surface is no longer active.

The Department of Space physics IEP SAS has contributed to the ESS construction in the frame of Scientific-technical cooperation agreement between IEP SAS and STIL NUIM, Maynooth, Ireland. The design, performance and operation of the ESS processor unit during the Rosetta mission is depicted in [3].

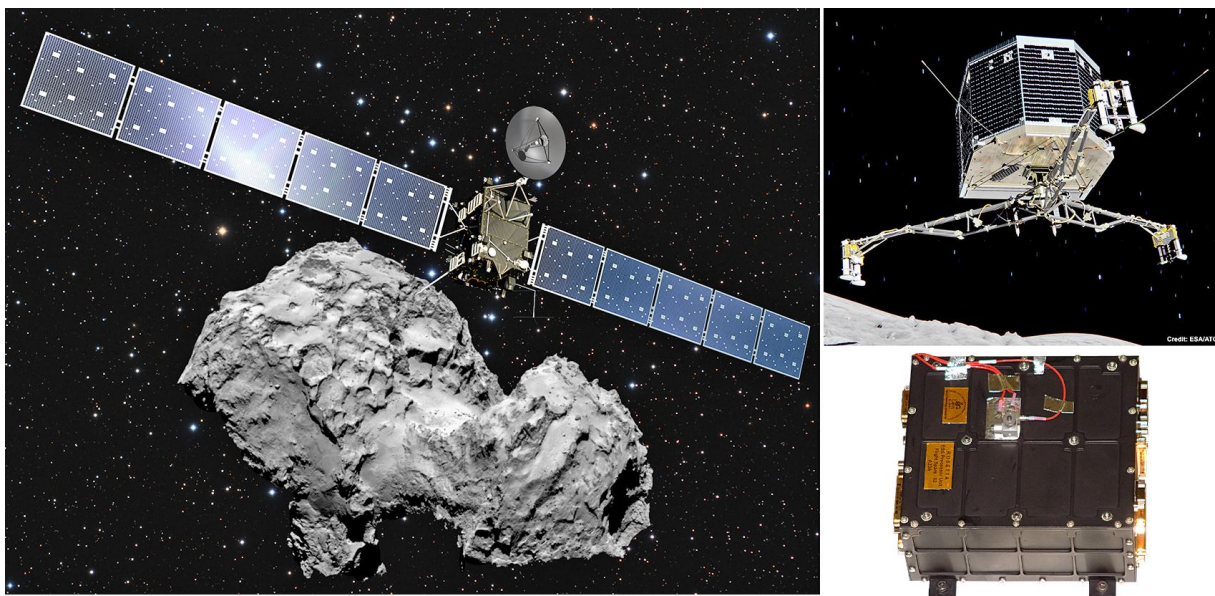


*Figure 1.2. ROSETTA at comet 67P/C-G, lander module Philae and the ESS processor unit that provided the communication between them.*

### 1.3. Experiment DOK-M for project RESONANCE (in development)

The experiment DOK-M is currently under development at IEP SAS in cooperation with Democritus University of Thrace, Xanthi, Greece and Institute for Space Research (IKI RAN), Moscow, for project RESONANCE.

RESONANCE is a magnetospheric space exploration mission conducted by IKI RAN and dedicated for advanced study of the wave – particle interactions in the Earth's magnetosphere. Earth's magnetosphere, as natural resonator for many types of electromagnetic waves, is a place where electromagnetic waves efficiently interact with charged energetic particles via cyclotron resonance.

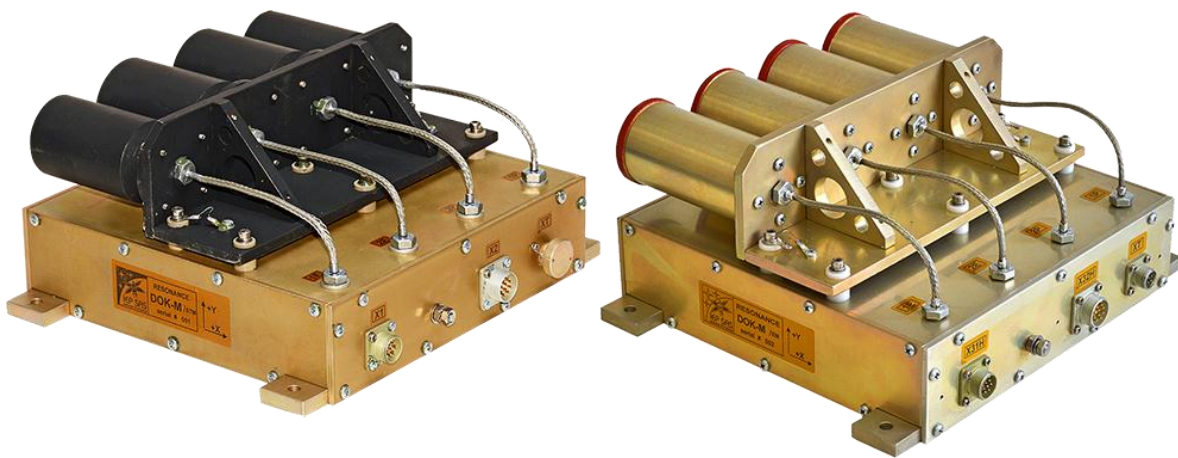


*Figure 1.3. The structural thermal model DOK-M/STM and engineering model DOK-M/EM are being tested at Space Research Institute, Moscow.*

Two identical models of the DOK-M will be installed on board of two satellites of the RESONANCE project. After some technical delays, the launch is presently scheduled for 2021.

### 1.4. Experiment PICAM for mission ESA-BepiColombo

IEP SAS contributes to ESA-BepiColombo mission to planet Mercury in cooperation with Space Technology Ireland (STIL) and Institute for Space Research of Austrian Academy of Sciences (IWF ÖAW). The delivery involves the mechanical structures of the PICAM (Planetary Ion Camera) instrument that were manufactured in Slovakia (mechanical components manufacture on 5-axis centre of Q-Products, Bratislava, space-qualified processing and integration and testing at IEP SAS, Košice). Overall 6 models (STM=Structural Thermal Model, PM=Prototype Model, EM=Engineering Model, QM=Qualification Model, FM=Flight Model, FS=Flight Spare model) were manufactured and delivered to IWF where full PICAM integration took place. After some delays due to

technical reasons, the launch of BepiColombo mission is expected in January-February 2017 from Kourou, French Guiana.

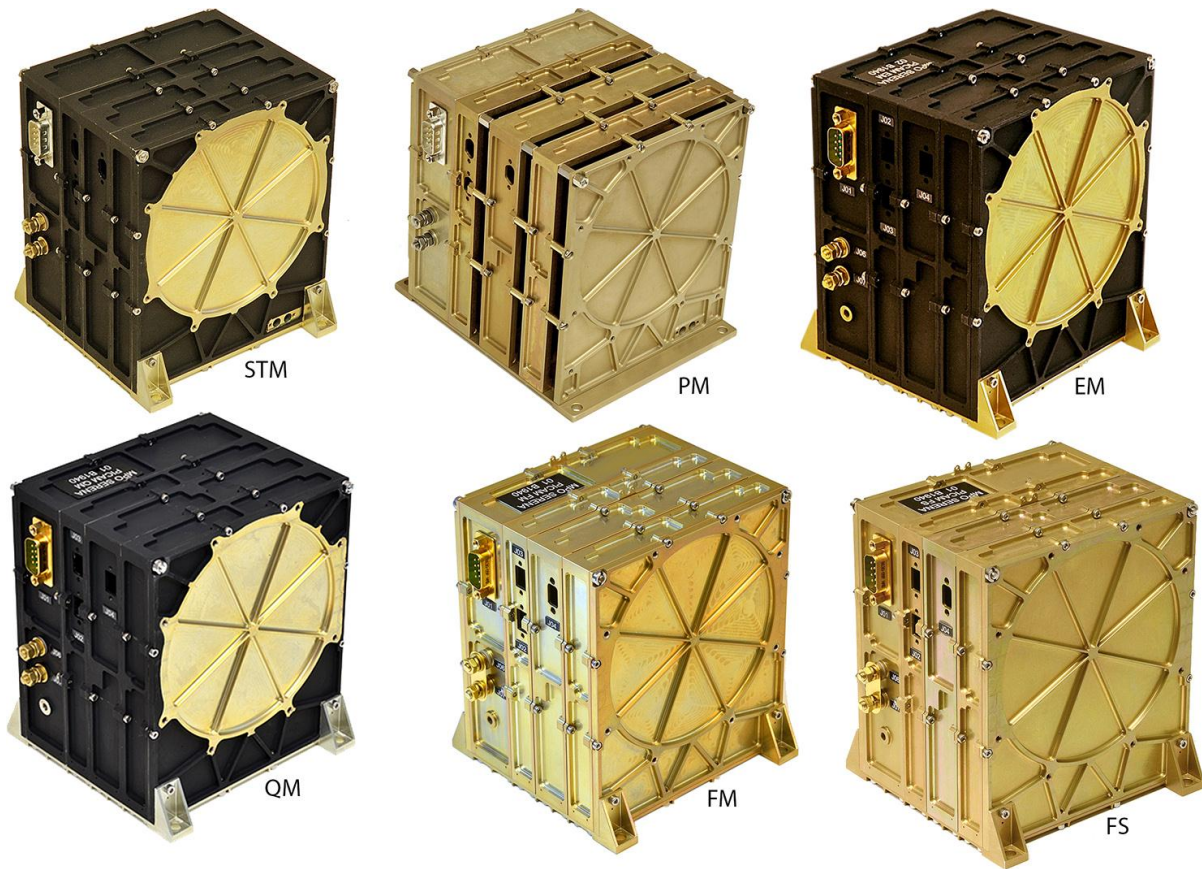


*Figure 1.4. The full set of PICAM electronic boxes manufactured in Slovakia for mission ESA-BepiColombo to Mercury (IEP-SAS and Q-Products). PICAM is a part of a complex space science suite SERENA for particle detection at planet Mercury.*

### **1.5. Experiment NAIS for Chinese mission MIT (Magnetosphere-Ionosphere-Thermosphere)**

IEP SAS contributes to development of experiment NAIS (Neutral Atom Imaging System) for Chinese MIT mission in cooperation with Chinese National Space Science Centre (NSSC), Beijing; Space Technology Ireland (STIL), Maynooth and Swedish Institute for Space Physics (IRF) in Kiruna. The high-energy part of the experiment, NAIS-H, is based on heritage of the neutral atom imager NUADU developed at IEP SAS for Double Star project. The NAIS-H development is in good progress, some technical configuration and simulation results are in [4].

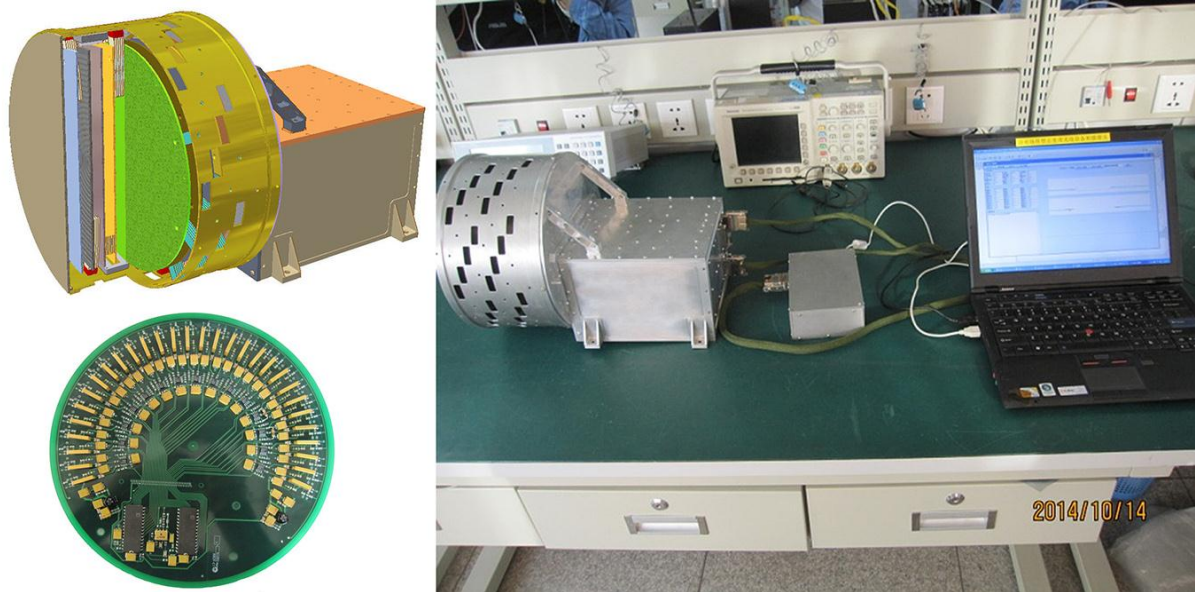


*Figure 1.5. The NAIS-H development is based on heritage of the neutral atom imager NUADU, developed at IEP SAS for Double Star mission.*

## **1.6. Participation of Slovakia in the project JEM-EUSO**

JEM-EUSO (Japanese Experiment Module – Extreme Universe Space Observatory) experiment will search for ultra-high energy cosmic rays (UHECR, with energy above  $10^{19}$  eV) by monitoring UV light produced in their interaction with atmosphere from International Space Station. Department of Space Physics IEP-SAS works in project frame mainly on two topics, on UV background model at the Earth night side and on pattern recognition methods for showers detection.

From the last year result we would like to mention four studies. A review of possibilities to study space weather effects in the frame of JEM-EUSO project has been prepared [5]. The analysis of UV background measurements from EUSO balloon flight in summer 2014 was realized [6]. Methods for UHECR showers recognition based on Hough method was applied to JEM-EUSO simulated data and results were published at ICRC conference [7]. The analysis of JEM-EUSO detector performance in version for Space-X Dragon spacecraft is in [8].

Wide description of the experiment was published in special issue of *Experimental Astronomy* dedicated to JEM-EUSO project [9]. The issue contains 15 articles focusing on all aspects of JEM-EUSO mission.

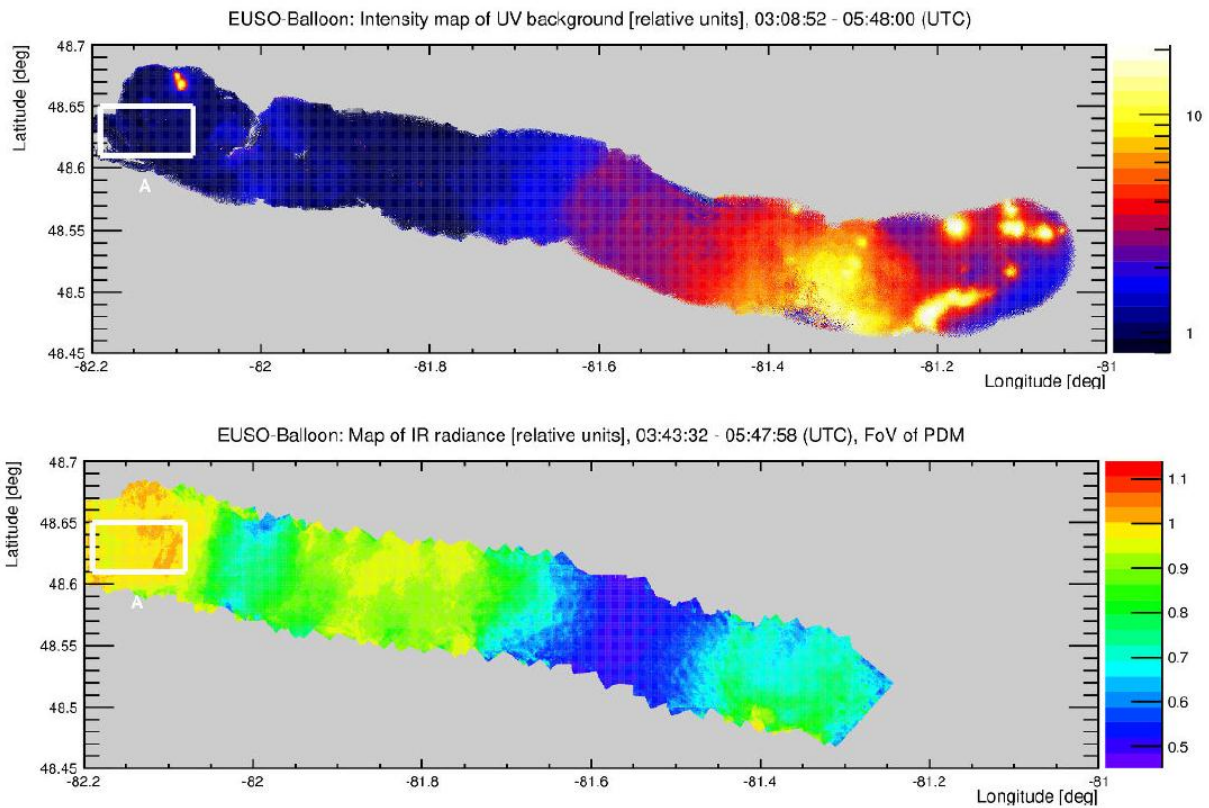


*Figure 1.6. Analysis of EUSO balloon measurements. The displayed values are relative to the mean value of IBG over reference area “A” (white box). Pixels with the lowest IBG and highest IR radiance correspond to clear atmosphere [6].*

## 1.7. Other experiments for space observations

Design, development and construction of the first Slovak satellite SKCUBE took place at the Žilina University in Žilina, Slovak Technical University in Bratislava, Technical University in Košice, several Slovak private companies and Slovak Organization for Space Activities (SOSA) laboratory within a partnership initiated by the SOSA. More information at (<http://www.skcube.sk/en>).

## References:

1. ZELENYI, L. M. – ZASTENKER, G. N. – PETRUKOVICH, A. A. – CHESALIN, L. S. – NAZAROV, V. N. – .... BALÁŽ, J. – KUDELA, K. – STRHÁRSKÝ, I. – SLIVKA, M.... PLASMA-F Experiment: Three Years of On-Orbit Operation. In *Solar System Research*, vol. 49, no. 7, pp. 580-603, 2015.
2. PETRUKOVICH, A. A. – INAMORI, T. – BALAZ, J. – KUDELA, K. – SLIVKA, M. – STRHARSKY, I. – GLADYSHEV, V. A. – SARRIS, T. – SARRIS, E. Oscillations of energetic ions flux near the Earth's bow shock, *J. Geophys. Res. Space Physics*, 120, doi:10.1002/2015JA021077, 2015.
3. McKENNA-LAWLOR, S. – RUSYNYAK, P. – BALAZ, J. – SCHMIDT, W. – FANTINATI, C. – KUECHEMANN, O. – GEURTS, K. Performance of the mission critical Electrical Support System (ESS) which handled communications and data transfer between the ROSETTA Orbiter and its Lander Philae while en route to and at comet 67P/Churyumov-Gerasimenko. *Acta Astronautica*, DOI:10.1016/j.actaastro.2015.12.015, 2015.
4. LU, L. – McKENNA-LAWLOR, S. – BALAZ, J. – SHI, J. – YANG C. – LUO, J. Technical configuration and simulation of the NAIS-H for the MIT mission. *Chinese Journal of Space Science.*, 2014, 34(3): pp. 341-351, doi:10.11728/cjss 2014.03.341
5. KUDELA, K. – BŁECKI, J. for the JEM-EUSO Collaboration, Possibilities of selected space weather and atmospheric studies in JEM-EUSO project? *Proceedings of Science PoS(ICRC2015)113*, 8 pages, presented at ICRC den Hague, August 2015, [http://pos.sissa.it/archive/conferences/236/113/ICRC2015\\_113.pdf](http://pos.sissa.it/archive/conferences/236/113/ICRC2015_113.pdf)
6. MACKOVJAK, S. – NEORONOV, A. – MORETTO, C. – BACHOLLE, S. – BOBIK, P. – PUTIS, M. – Del PERAL, L. – RODRIGUEY, F. M. – SHINOZAKI, K. – CATALANO, C. – SORIANO, J. F. – SAEZ CANO G. Night time measurement of the UV background by EUSO-Balloon, *Proceedings of 34th ICRC, Hague, 2015* <https://indico.cern.ch/event/344485/session/139/contribution/1302>
7. PASTIRČÁK, B. – BOBÍK, P. – PUTIŠ, M. – VRÁBEL, M. – VASILKO, J. – BERTAINA, M. – SHINOZAKI, K. – FENU, F. Pattern recognition study for different levels of UV background in JEM-EUSO experiment <https://indico.cern.ch/event/344485/session/139/contribution/1074>

8. SHINOZAKI, K. - SANTANGELO, A. – BAYER, J. – BERTAINA M. – BOBIK, P. – FENU, F. – GORODETZKY, P. – GUZMAN, A. – HAUNGS, A. – IWOTSCHNIK, E. – MEDINA TANCO, G. – MERNIK, T. – NERONOV, A. – OLINTO, A. – PASTIRCAK, B. – PUTIS, M. Evaluation of scientific performance of JEM-EUSO mission with Space-X Dragon option  
<https://indico.cern.ch/event/344485/session/139/contribution/682>
9. Experimental Astronomy, 2015, Volume 40, Issue 1, November 2015, Special Issue on the JEM-EUSO Mission, pp. 1 – 326.

## 2. SPACE PHYSICS, GEOPHYSICS AND ASTRONOMY

*I. Dorotovič, R. Gális, K. Kudela,  
J. Masarik, A. Ondrášková, M. Revallo, J. Rybák, J. Tóth*

Scientific studies in the space solar physics and X-ray astronomy, interplanetary matter and explorations of the comets, solar wind and its interactions with the Earth's magnetosphere, energetic particles including cosmic rays in the magnetosphere and in interplanetary space, atmosphere and ionosphere of the Earth, have been done in various institutes in Slovakia. The following short survey presents selected activities of the abovementioned directions and the obtained results.

The *Institute of Experimental Physics, SAS, Košice* (IEP SAS, its Department of Space Physics, <http://space.saske.sk>) in collaboration with the laboratories in abroad continued studies of the dynamics of low energy cosmic rays (CR) and of suprathermal cosmic particles, based on measurements in space. Papers/presentations related to very high energy CR are mentioned in Chapter 1 in connection with JEM-EUSO project. Collaboration list can be found at <http://jemeuso.riken.jp/en/members.html>.

Analysis of long term continual measurements by neutron monitor at high altitude laboratory of IEP SAS Lomnický štít (data in real time available at <http://neutronmonitor.ta3.sk>) along with other neutron monitor and muon telescope data (including the new installation SEVAN), yielded in (i) detailed description of quasi-periodicities of CR time series [9,10]; (ii) finding only marginal relation of cloud cover to CR at that mountain site over 30 years [5,7]; (iii) indicating possibilities and limitations of selected dosimetric measurements at altitude 2634 m asl [8]; (iv) estimates of the changing geomagnetic transmissivity of CR in the disturbed magnetosphere at selected neutron monitors [15]; (v) finding of important parameters of CMEs for the Forbush decreases in CR as well as for the geomagnetic activity [16]; (vi) indication of the influence of particles observed during GLE (ground level event) in December 2006 on the propagation of very low frequency electromagnetic waves on the night side of the magnetosphere [18].

Results on computations of secondary CR in the atmosphere over two solar activity cycles are published in [1]. Heliospheric propagation of CR using the HelMod code has been studied in [2]. Modulation of CR in the heliosphere according to observations by neutron monitors over solar cycles 21 – 24 was analyzed in [4].

The acceleration of particles connected with solar flares and with the plasma discontinuities in interplanetary space has been studied in [3]. Selected

solar flares with emission of high energy neutron and gamma rays as observed onboard CORONAS-F satellite (with use of detectors described in [12]) were analyzed in [11,13] and the physical processes behind have been discussed.

Dynamics of fluxes of energetic electrons and protons at low altitude orbit (CORONAS-F satellite, 2001-2005) during intervals characterized by variable geomagnetic activity is analyzed in [14,15].

Analysis of measurements by particle instrument MEP-2 on SPEKTR-R (<http://www.plasma-f.cosmos.ru/en/instruments>) yielded into finding a new type of suprathermal particle variations: in the foreshock region of the Earth as well as in the outer magnetosheath the oscillations of energetic ion fluxes are observed in broad energy range (up to ~ 400 keV) with the periods 10–30 s, often almost of monochromatic waveform and accompanied with magnetic oscillations [17]. That result lead to revisit the older measurements of similar type, namely on Interball-tail, with the aim to understand the process of formation the suprathermal ion oscillations.

Paper [6] presents empirically found relations (not of causal type) between space weather characteristics and human behaviour.

## References:

1. BOBIK, P. – PUTIS, M. – PASTIRCAK, B. – SHINOZAKI, K. – SANTANGELLO, A. – SZABELSKI, J. – BERTAINA, M. – FENU, F. Modeling of secondary cosmic ray spectra for 23 and 24 Solar Cycles, Proceeding of 34th ICRC, Hague, 2015, [http://pos.sissa.it/archive/conferences/236/512/ICRC2015\\_512.pdf](http://pos.sissa.it/archive/conferences/236/512/ICRC2015_512.pdf)
2. DELLA TORRE, S. – BOBIK, P. – BOSCHINI, M. J. – GERVASI, M. – GRANDI, D. – LA VACCA, D. – PENSOTTI, S. – PUTIS, M. – RANCOITA, P.-G. – ROZZA, D. – TACCONI, M. – ZANNONI, M. Cosmic Rays Propagation with HelMod: Difference between forward-in-time and backward-in-time approaches, Proceeding of 34th ICRC, Hague, 2015, [http://pos.sissa.it/archive/conferences/236/183/ICRC2015\\_183.pdf](http://pos.sissa.it/archive/conferences/236/183/ICRC2015_183.pdf)
3. FIROZ, K. A. – ZHANG, Q. M. – GAN, W. Q. – LI, Y. P. – RODRÍGUEZ-PACHECO, J. – MOON, Y.-J. – KUDELA, K. – PARK, Y.-D. – DORMAN, L. I. An interpretation of gle71 concurrent CME-driven shock wave, *Astrophysical Journal, Supplement Series*, 213 (2), art. no. 24, 2014.
4. CHOWDHURY, P. – KUDELA K. – MOON, Y.-J. Heliospheric modulation and periodicities of galactic cosmic rays during 21-24 solar cycles. Proc. 34th ICRC, Hague, 2015, [http://pos.sissa.it/archive/conferences/236/198/ICRC2015\\_198.pdf](http://pos.sissa.it/archive/conferences/236/198/ICRC2015_198.pdf)
5. KANCÍROVÁ, M. – KUDELA, K. Cloud cover and cosmic ray variations at Lomnický štít high altitude observing site, *Atmospheric Res.*, 149, pp. 66-173, 2014.
6. KANCÍROVÁ, M. – KUDELA, K. The Relationship between Suicide Incidents in Slovakia and the Czech Republic and Heliophysical Parameters: Empirical Results. *Astrobiol Outreach* 2: 116. doi: 10.4172/2332-2519.1000116, 2014.
7. KANCÍROVÁ, M, – KUDELA, K. – ERLYKIN, A. D. – WOLFENDALE, A. W. Relevance of long term time – series of atmospheric parameters at a mountain observatory to models for climate change. Proceedings of 34th ICRC, Hague, 2015, [http://pos.sissa.it/archive/conferences/236/060/ICRC2015\\_060.pdf](http://pos.sissa.it/archive/conferences/236/060/ICRC2015_060.pdf)
8. KUBANČÁK, J. – AMBROŽOVÁ, I. – BÜTIKOFER, R. – KUDELA, K. – LANGER, R. – DAVIDKOVÁ, M. – PLOC, O. – MALUŠEK, A. Liulin silicon semiconductor spectrometers as cosmic ray monitors at the high mountain observatories Jungfraujoch and Lomnický štít. *Journal of Instrumentation*, 9 (7), art. no. P07018, 2014.

9. KUDELA, K. – LANGER, R. On quasi-periodic variations of low-energy cosmic rays observed near earth. *Radiation Protection Dosimetry*, 164 (4), pp. 471-476, 2015.
10. KUDELA, K. – SABBAH, I. Quasi-periodic variations of low energy cosmic rays. (2015). *Science China Technological Sciences*, pp. 1-11. Article in Press, First online: 04 December 2015.
11. KURT, V. G. – YUSHKOV, B. Y. – KUDELA, K. – GALKIN, V. I. – KASHAPOVA, L. K. CORONAS-F observation of HXR and gamma-ray emissions from the solar flare X10 on 29 October 2003 as a probe of accelerated proton spectrum, *Contributions of the Astronomical Observatory Skalnaté Pleso*, 45 (1), pp. 42-59, 2015.
12. KUZNETSOV, S. N. – BOGOMOLOV, A. V. – GALKIN, V. I. – DENISOV, Yu. I. – PODOROLSKY, A. N. – RYUMIN, S. P. – KUDELA, K. – ROJKO, J. Scientific Set of Instruments "Solar Cosmic Rays". In *CORONAS-F SPACE MISSION: KEY RESULTS FOR SOLAR TERRESTRIAL PHYSICS*, ed. V.D. Kuznetsov, Astrophysics and Space Science Library, Springer, 400, pp. 289-299, 2014.
13. KUZNETSOV, S. N. – KURT, V. G. – YUSHKOV, B. Yu. – MYAGKOVA, I. N. – GALKIN, V. I. – KUDELA, K. Protons Acceleration in Solar Flares: The Results of the Analysis of Gamma-emission and Neutrons Recorded by the SONG Instrument Onboard the CORONAS-F Satellite. In *CORONAS-F SPACE MISSION: KEY RESULTS FOR SOLAR TERRESTRIAL PHYSICS*, ed. V.D. Kuznetsov, Astrophysics and Space Science Library, Springer, 400, pp. 301-325, 2014.
14. KUZNETSOV, S. N. – MYAGKOVA, I. N. – MURAVIEVA, E. A. – YUSHKOV, B. Yu. – STAROSTIN, L. I. – DENISOV, Yu. I. – KUDELA, K. Dynamics of the Relativistic Electrons Flux of the Earth Outer Radiation Belt Based on the MKL Instrument Data. In *CORONAS-F SPACE MISSION: KEY RESULTS FOR SOLAR TERRESTRIAL PHYSICS*, ed. V.D. Kuznetsov, Astrophysics and Space Science Library, Springer, 400, pp. 327-336, 2014.
15. KUZNETSOV, S. N. – DENISOV, Yu. I. – LAZUTIN, L. L. – MYAGKOVA, I. N. – MURAVIEVA, E. A. – YUSHKOV, B. Yu. – KUDELA, K. – BUČÍK, R. – SLIVKA, M. Dynamics of the Earth Radiation Belts During the Strong Magnetic Storms. In *CORONAS-F SPACE MISSION: KEY RESULTS FOR SOLAR TERRESTRIAL PHYSICS*, ed. V.D. Kuznetsov, Astrophysics and Space Science Library, Springer, 400, pp. 337-347, 2014.

16. PARNAHAJ, I. – BOBÍK, P. – KUDELA, K. Magnetospheric transmissivity for cosmic rays during selected recent events with interplanetary/geomagnetic disturbances. *Journal of Physics: Conference Series*, 632 (1), art. no. 012064, 2015.
17. PETRUKOVICH, A. A. – INAMORI, T. – BALÁŽ, J. – KUDELA, K. – SLIVKA, M. – STRHÁRSKÝ, I. – GLADYSHEV, V. A. – SARRIS, T. – SARRIS, E. Oscillations of energetic ions flux near the Earth's bow shock. *Journal of Geophysical Research A: Space Physics*, 120 (6), pp. 4700-4710, 2015.
18. ŽIGMAN, V. – KUDELA, K. – GRUBOR, D. Response of the Earth's lower ionosphere to the Ground Level Enhancement event of December 13, 2006. *Advances in Space Research*, 53 (5), pp. 763-775, 2014.

The activities of the *Department of nuclear physics and biophysics, Faculty of Mathematics, Physics and Informatics, Comenius University, Bratislava*, have been oriented mainly in the study of cosmic rays and their interaction with material objects.

Space research activities at the faculty are carried out at two departments, Department of nuclear physics and biophysics and Department of Astronomy, Physics of Earth and meteorology.

Department of Nuclear physics and biophysics concentrates its effort into two areas. First we finished building of new laboratory devoted to the measurements of very low radioactivity [1]. Part of the activities of this laboratory will be devoted to the studies of extraterrestrial material. During the last two years cosmogenic nuclides in Košice and Chelyabinsk meteorites were studied in [2,3].

For Košice meteorite results of nondestructive gamma-ray analyses of cosmogenic radionuclides (Be-7, Na-22, Al-26, Sc-46, V-48, Mn-54, Co-56, Co-57, Co-58, and Co-60) in 19 fragments of the Kosice meteorite were obtained [2,7]. The activities varied mainly with position of fragments in the meteoroid body, and with fluxes of cosmic-ray particles in the space affecting radionuclides with different half-lives. Monte Carlo simulations of the production rates of Co-60 and Al-26 compared with experimental data indicate that the pre-atmospheric radius of the meteoroid was 50 +/- 5 cm. In two Kosice fragments, He, Ne, and Ar concentrations and isotopic compositions were also analyzed. The noble-gas cosmic-ray exposure age of the Kosice meteorite is 5-7 Myr, consistent with the conspicuous peak (or doublet peak) in the exposure age histogram of H chondrites. One sample likely contains traces of implanted solar wind Ne, suggesting that Kosice is a regolith breccia. The agreement between the simulated and observed Al-26 activities indicate that the meteoroid was mostly irradiated by a long-term average flux of galactic cosmic rays of 4.8 particles cm<sup>-2</sup> s<sup>-1</sup>, whereas the short-lived radionuclide activities are more consistent with a flux of 7.0 protons cm<sup>-2</sup> s<sup>-1</sup> as a result of the low solar modulation of the galactic cosmic rays during the last few years before the meteorite fall.

On February 15, 2013, after the observation of a brilliant fireball and a spectacular airburst over the southern Ural region (Russia), thousands of stones fell and were rapidly recovered, bringing some extremely fresh material for scientific investigations. We undertook a multidisciplinary study of a dozen stones of the Chelyabinsk meteorite, including petrographic and microprobe investigations to unravel intrinsic characteristics of this meteorite [3]. We also study the short and long-lived cosmogenic radionuclides to characterize the initial meteoroid size and exposure age. Petrographic observations, as well as the mineral compositions obtained by electron microprobe analyses, allow us to confirm the classification of the Chelyabinsk meteorite as an LL5 chondrite. The

fragments studied, a few of which are impact melt rocks, contain abundant shock melt veins and melt pockets. It is likely that the catastrophic explosion and fragmentation of the Chelyabinsk meteoroid into thousands of stones was in part determined by the initial state of the meteoroid. The radionuclide results obtained show a wide range of concentrations of C-14, Na-22, Al-26, Mn-54, Co-57, Co-58, and Co-60, which indicate that the pre-atmospheric object had a radius  $>5\text{m}$ , consistent with other size estimates based on the magnitude of the airburst caused by the atmospheric entry and breakup of the Chelyabinsk meteoroid. Considering the observed Al-26 activities of the investigated samples, Monte Carlo simulations, and taking into account the Al-26 half-life (0.717Myr), the cosmic-ray exposure age of the Chelyabinsk meteorite is estimated to be  $1.2 \pm 0.2\text{Myr}$ . In contrast to the other radionuclides, C-14 showed a very large range only consistent with most samples having been exposed to anthropogenic sources of C-14, which we associate with radioactive contamination of the Chelyabinsk region by past nuclear accidents and waste disposal, which has also been confirmed by elevated levels of anthropogenic Cs-137 and primordial K-40 in some of the Chelyabinsk fragments.

Cosmogenic radionuclides produced by galactic cosmic rays (OCR) in meteorites during their motion in space are natural detectors of the OCR intensity and variations along the meteorite orbits. On the basis of measured and calculated contents of cosmogenic radionuclides in the freshly fallen Chelyabinsk and Kosice chondrites some peculiarities of generation of cosmogenic radionuclides of different half-lives in the chondrites of different orbits and dates of fall onto the Earth are demonstrated. Dependence of production rates of the radionuclides on the OCR variations in the heliosphere is analyzed [6]. Using radionuclides with different half-lives it is possible to compare the average OCR intensity over various time periods. The measurement and theoretical analysis of cosmogenic radionuclides in consecutively fallen chondrites provide a unique information on the space time continuum of the cosmogenic radionuclide production rates and their variations over a long time scale, which could be useful in correlative analyses of processes in the heliosphere. Some applications of cosmogenic radionuclide depth distribution in chondrites for estimation of their pre-atmospheric sizes are illustrated.

In the past we studied many factors influencing production rates of cosmogenic nuclides in meteorites. Last one factor that was not investigated in details is the shape of meteorite. Numerical simulations using the Los Alamos Code System (LCS) particle production and transport codes were done to investigate particle fluxes and production rates of cosmogenic nuclides Be-10, Al-26, and Co-60 in meteoroids of spherical, ellipsoidal, and cylindrical shapes [4]. The calculations show that fluxes of nuclear active particles and also production rates of cosmogenic nuclides are sensitive to the shape of the irradiated parent body.

Part of our investigations was devoted to the study of cosmic ray effects on the surface of Earth [5]. The depth-dependent attenuation of the secondary cosmic-ray particle flux due to snow cover and its effects on production rates of cosmogenic nuclides constitutes a potential source of uncertainty for studies conducted in regions characterized by frequent seasonal snow burial. Recent experimental and numerical modelling studies have yielded new constraints on the effect of hydrogen-rich media on the production rates of cosmogenic nuclides by low- and high-energy neutrons ( $<10^{-3}$  MeV and  $>10^2$  MeV, respectively). We present long-term neutron-detector monitoring data from a natural setting that we use to quantify the effect of snow cover on the attenuation of fast neutrons (0.1-10 MeV), which are responsible for the production of Ne-21 from Mg and Cl-36 from K. We use data measured between July 2001 and May 2008 at seven stations located throughout the Ecrins-Pelvoux massif (French Western Alps) and its surroundings, at elevations ranging from 200 to 2500 m a.s.l. From the cosmic-ray fluxes recorded during summer, when snow is absent, we infer an apparent attenuation length of  $148 \text{ g cm}^{-2}$  in the atmosphere at a latitude of similar to 45 degrees N and for altitudes ranging from similar to 200 to 2500 m a.s.l. Using snow water-equivalent (SWE) values obtained through snow-coring campaigns that overlap in time the neutron monitoring for five stations, we show that fast neutrons are much more strongly attenuated in snow than predicted by a conventional mass-shielding formulation and the attenuation length estimated in the atmosphere. We suggest that such strong attenuation results from boundary effects at the atmosphere/snow interface induced by the high efficiency of water as a neutron moderator. Finally, we propose an empirical model that allows calculating snow-shielding correction factors as a function of SWE for studies using Ne-21 and Cl-36 analyses in Mg- and K-rich minerals, respectively. This empirical model is of interest for studies with a focus on cosmic-ray exposure dating, particularly if the target rocks are made up of mafic to ultramafic units where seasonal snow-cover is a common phenomenon.

## References:

1. POVINEC, P. P. – MASARIK, J. – JESKOVSKY, M. – et al. Development of the Accelerator Mass Spectrometry technology at the Comenius University in Bratislava. *NUCL. INSTR. & METH.*, 361, 87-94, 2015.
2. POVINEC, P. P. – MASARIK, J. – SYKORA, I. – et al. Cosmogenic nuclides in the Kosice meteorite: Experimental investigations and Monte Carlo simulations. *METEORITICS & PLANETARY SCIENCE*, 50(5), 880-892, 2015.
3. POVINEC, P. P. – LAUBENSTEIN, M. – JULL, A. J. T. – et al. Cosmogenic radionuclides and mineralogical properties of the Chelyabinsk (LL5) meteorite: What do we learn about the meteoroid?, *METEORITICS & PLANETARY SCIENCE*, 50(2), 273-286, 2015.
4. MASARIK, J. – BENO, J. Effects of meteoroid shape on cosmogenic nuclide production processes. *METEORITICS & PLANETARY SCIENCE*, 50(2), 18-325, 2015.
5. DELUNEL, R. – BOURLES, D. L. – VAN DER BEEK, P. A. – et al. Snow shielding factors for cosmogenic nuclide dating inferred from long-term neutron detector monitoring. *QUATERNARY GEOCHRONOLOGY*, 24, 16-26, 2014.
6. LEYA, I. – MASARIK, J. On chlorine-36 in the early solar system. *METEORITICS & PLANETARY SCIENCE*, 49, SI 1, A234-A234, 2014.
7. ALEXEEV, V. A. – LAUBENSTEIN, M. – POVINEC, P. P. – et al. Variations of cosmogenic radionuclide production rates along the meteorite orbits. *ADVANCES IN SPACE RESEARCH*, 56(4), 766-771, 2015.
8. POVINEC, P. P. – TOTH, J. The Fall of the Kosice Meteorite. *METEORITICS & PLANETARY SCIENCE*, 50(5), 851-852, 2015.

*In the Department of Astronomy, Physics of the Earth and Meteorology, Faculty of Mathematics, Physics and Informatics, Comenius University, Bratislava,* the study of Schuman resonances (SR) continued. The precise determination of instantaneous frequency of SR modes, with the possibility of application to relatively short signal sequences, seems to be important for detailed analysis of SR modal frequency variations. Contrary to commonly used method of obtaining modal frequencies by the Lorentz function fitting of DFT spectra, the complex demodulation (CD) method in iterated form is employed in [1]. Results of iterated CD method applied on short and long measured sequences are compared. Results for SR signals as well as the comparison with Lorentz function fitting are presented. Decrease of frequencies of all first four SR modes from the solar cycle maximum to solar cycle minimum has been found using also the CD method.

The photometric program of asteroid observations continued at Astronomical and Geophysical Observatory in Modra, some programs with collaboration with Ondřejov Observatory. Important results were obtained as first triple Near Earth Object (primary + two satellites) was analysed and combination with Arecibo radar the basic characteristics were determined [2]. In the paper [3] the evolution of mutual orbits of asteroid 175706 and its satellite orbit with potential consequences for the entire binary asteroid population were studied.

The formation of the solar atmosphere transition region O IV and Si IV lines observable by the Interface Region Imaging Spectrograph (IRIS) is investigated for both Maxwellian and non-Maxwellian conditions characterized by a  $\kappa$ -distribution exhibiting a high-energy tail. The usefulness of the O IV ratios for density diagnostics independently of  $\kappa$  is investigated and it is found that the O IV 1404.78 Å/1399.77 Å ratio provides a good density diagnostics except for very low T combined with extreme non-Maxwellian situations [4]. SDO/AIA observations of an eruptive X-class flare of 2012 July 12, and comparison of its evolution with the predictions of a three-dimensional (3D) were numerically simulated. We focus on the dynamics of flare loops that are seen to undergo slipping reconnection during the flare. Processes are explained via 3D reconnection mechanisms resulting from the expansion of a torus-unstable flux rope. The AIA observations and the numerical model are complemented by radio observations showing a noise storm in the metric range. Dm-drifting pulsation structures occurring during the eruption indicate plasmoid ejection and enhancement of the reconnection rate. The bursty nature of radio emission shows that the slipping reconnection is still intermittent, although it is observed to persist for more than an hour [5]. We investigate the possibility of diagnosing the degree of departure from the Maxwellian distribution using single-ion spectra originating in astrophysical plasmas in collisional ionization equilibrium [6]. The calculated intensities of most of the Fe IX - Fe XIII EUV

lines show consistent behaviour with  $\kappa$  at constant temperature. Intensities of these lines decrease with  $\kappa$ , with the vast majority of ratios of strong lines showing little or no sensitivity to  $\kappa$ . Several of the line ratios, especially involving temperature-sensitive lines, show a sensitivity to  $\kappa$  that is of the order of several tens of per cent, or, in the case of Fe IX, up to a factor of two. Forbidden lines in the near-ultraviolet, visible, or infrared parts of the spectrum are an exception, with smaller intensity changes or even a reverse behaviour with  $\kappa$ .

In the frame of ESA projects several optical surveys campaigns were performed in cooperation with the Astronomical Institute of the University of Bern (AIUB) to improve the knowledge about the debris environment in the geostationary ring (GEO), the geostationary transfer orbit (GTO) region, and in the medium Earth orbit (MEO) region of the global navigation satellite constellations. For all these campaigns observation strategies, processing techniques and cataloguing procedures have been developed and successfully applied [7]. The results from the coverage and the orbit determination accuracy simulations performed within the recently completed ESA study “Assessment Study for Space Based Space Surveillance (SBSS) Demonstration System” (Airbus Defence and Space consortium). This study consisted in investigating the capability of a space based optical sensor (SBSS) orbiting in low Earth orbit (LEO) to detect and track objects in GEO (geosynchronous orbit), MEO (medium Earth orbit) and LEO and to determinate and improve initial orbits from such observations [8]. We simulated several observation scenarios for ground- and space-based sensor by assuming different observation and sensor properties. We will introduce the analyzed end-to-end simulations of the ground- and spacebased strategies in order to investigate the orbit determination accuracy and its sensitivity which may result from different values for the frame-rate, pixel scale, astrometric and epoch registration accuracies [9].

On 8 October 2011, the Draconid meteor shower (IAU, DRA) was predicted to cause two brief outbursts of meteors, visible from locations in Europe. For the first time, a European airborne meteor observation campaign was organized, supported by ground-based observations. Two aircraft were deployed from Kiruna, Sweden, carrying six scientists, 19 cameras and eight crew members. The flight geometry was chosen such that it was possible to obtain double-station observations of many meteors. The instrument setup on the aircraft as well as on the ground is described in full detail. The main peak from 1900-dust ejecta happened at the predicted time and at the predicted rate. The trajectory, velocity, deceleration and orbit of 35 double station meteors were measured. The magnitude distribution index was high. The light curve proved to be extremely flat on average, which was unexpected. Observations of spectra allowed us to derive the compositional information of the Draconids meteoroids and showed an early release of sodium, usually interpreted as resulting from fragile meteoroids [10]. Monitoring of meteor activity above the

Central Europe and Canary Islands by All-sky Meteor Orbit System (AMOS), autonomous video observatory for detection of transient events on the sky, is performed. Its hardware and software development and permanent placement on several locations in Slovakia allowed the establishment of Slovak Video Meteor Network (SVMN). The results from AMOS cameras - the SVMN database - as well as from two AMOS cameras on Canary Islands were presented [11]. We introduce the updated spectral All-Sky Meteor Orbit System (AMOS-Spec) and present its capability to measure the relative abundances of the main elements in meteoroids. Initial results from the spectroscopic observations are presented and are compared with independently measured meteoroid trajectories, heliocentric orbits and material strength parameters in data collected by the Slovak Video Meteor Network and the Central European Meteor Network. We aim to use this complex set of data to define the various meteoroid streams both dynamically and physically, and thus to identify the link between a meteoroid stream and its parent body [12]. The Kosice meteorite was observed on 28 February 2010 near the city of Kosice in eastern Slovakia and its mineralogy, petrology, and geochemistry are described. The characteristic features of the meteorite fragments are fan-like, mosaic, lamellar, and granular chondrules, which were up to 1.2 mm in diameter. The Kosice meteorite is classified as ordinary chondrite of the H5 type which has been slightly weathered, and only short veinlets of Fe hydroxides are present. Some fragments of the meteorite Kosice are formed by monomict breccia [13]. We propose a low-cost robotic optical survey aimed at 1-300 m Near Earth Objects (NEO) based on four state-of-the-art telescopes having extremely wide field of view. The small Near-Earth Asteroids (NEA) represents a potential risk but also easily accessible space resources for future robotic or human space in-situ exploration, or commercial activities. The survey system will be optimized for the detection of fast moving-trailed-asteroids, space debris and will provide real-time alert notifications. The successful demonstration of the system will promote cost-effective ADAM-WFS (Automatic Detection of Asteroids and Meteoroids -- A Wide Field Survey) systems [14].

## References:

1. ONDRÁŠKOVÁ, A. – ŠEVČÍK, S. The iterative complex demodulation applied on short and long Schumann resonance measured sequences. In *Contribution to Geophysics and Geodesy*, 44/4, pp. 313-328, 2014.
2. BECKER, T. M. – HOWELL – PRAVEC, P. – VILÁGI, J. – KORNOŠ, L. – GALÁD, A. – GAJDOŠ, Š. Physical modeling of triple near-Earth Asteroid (153591) 2001 SN263 from radar and optical light curve observations. *Icarus*, Volume 248, pp. 499-515.
3. SCHEIRICH, P. – PRAVEC, P. – GALÁD, A. – et al. The binary near-Earth Asteroid (175706) 1996 FG(3) – An observational constraint on its orbital evolution. *Icarus*, Volume 245, pp. 56-63.
4. DUDÍK, J. – Del ZANNA, G. – DZIFČÁKOVÁ, E. – MASON, H. E. – GOLUB, L. Solar transition region lines observed by the interface region imaging spectrograph: diagnostics for the O IV and Si IV lines. *The Astrophysical Journal Letters*, Volume 780, Issue 1, article id. L12, 7 pp., 2014.
5. DUDÍK, J. – JANVIER, M. – AULANIER, G. – Del ZANNA, G. – KARLICKÝ, M. – MASON, H. E. – SCHMIEDER, B. Slipping magnetic reconnection during an X-class solar flare observed by SDO/AIA. *The Astrophysical Journal*, Volume 784, Issue 2, article id. 144, 21 pp., 2014.
6. DUDÍK, J. – Del ZANNA, G. – MASON, H. E. – DZIFČÁKOVÁ, E. Signatures of the non-Maxwellian kappa-distributions in optically thin line spectra I Theory and synthetic Fe IX-XIII spectra. *Astronomy & Astrophysics*, Volume 570, id.A124, 23 pp., 2014.
7. SILHA, J. – SCHILDKNECHT, T. – HINZE, A. – VANANTI, A. – FLOHRER, T. Additional Optical Surveys for Space Debris on Highly Eccentric and Inclined MEO Orbits. *Proceedings of 65th International Astronautical Congress*, Toronto, Canada, 2014.
8. SILHA, J. – UTZMANN, J. – SCHILDKNECHT, T. – HINZE, A. – WAGNER, A. – FLOHRER, T. – WILLEMSSEN, P. – TESTON, F. Capability of a Space-based Space Surveillance System to Detect and Track Objects in GEO, MEO and LEO Orbits. *Proceedings of 65th International Astronautical Congress*, Toronto, Canada, 2014.
9. SILHA, J. – SCHILDKNECHT, T. – FLOHRER T. Improved Space Object Orbit Determination Using CMOS Detectors. *Proceedings of AMOS Conference*, Maui, Hawaii, 2014.

10. VAUBAILLON, J. – KOTEN, P. – MARGONIS, A. – TOTH, J. – et al. The 2011 Draconids: The First European Airborne Meteor Observation Campaign. *Earth, Moon, and Planets*, Volume 114, Issue 3-4, pp. 137-157, 2015.
11. TÓTH, J. – KORNOS, L. – ZIGO, P. – et al. All-sky Meteor Orbit System AMOS and preliminary analysis of three unusual meteor showers. *Planetary and Space Science*, Volume 118, pp. 102-106, 2015.
12. MATLOVIC, P. – RUDAWSKA, R. – TÓTH, J. – ZIGO, P. – KALMANCOK, D. Meteor spectra from AMOS video system. *Proceedings of the International Meteor Conference, Mistelbach, Austria, 27-30 August 2015*, Eds.: Rault, J.-L.; Roggemans, P., International Meteor Organization, pp. 105-107, 2015.
13. OZDÍN, D. – PLAVČAN, J. – HORÁČKOVÁ, M. – UHER, P. – PORUBČAN, V. – VEIS, P. – RAKOVSKÝ, J. – TÓTH, J. – KONEČNÝ, P. – SVOREŇ, J. Mineralogy, petrography, geochemistry, and classification of the Kosice meteorite. *Meteoritics & Planetary Science*, Volume 50, Issue 5, pp. 864-879, 2015.
14. VERES, P. – TÓTH, J. – JEDICKE, R. – TONRY, J. – DENNEAU, L. – WAINSCOAT, R. – KORNOS, L. – SILHA, J. Automatic detection of asteroids and meteoroids. A Wide Field Survey. *The Meteoroids 2013, Proceedings of the Astronomical Conference held at A.M. University, Poznan, Poland, Aug. 26-30, 2013*, Eds.: T.J. Jopek, F.J.M. Rietmeijer, J. Watanabe, I.P. Williams, A.M. University Press, 2014, pp. 307-314, 2014.

At the *Faculty of Science, UPJS Kosice*, the activities are completed by the results not included in our previous biennial reports.

At the *Department of Theoretical Physics and Astrophysics, Institute of Physics, Faculty of Science, P. J. Šafárik University in Košice*, the studies of X-ray emission of cataclysmic variables observed by mission *INTEGRAL* have been performed in past years. Since the results were not listed in earlier biennial reports, we indicate it below.

Cataclysmic variables (CVs) represent significant fraction of all *INTEGRAL* detections in hard X-ray/soft  $\gamma$ -rays [1, 2]. CVs are close binary systems consisting of a hot white dwarf (WD) and red main sequence star, which fills the volume of its inner Roche lobe and transfers matter to the vicinity of the WD. According to strength of WD magnetic field, this matter is creating an accretion disk or follows magnetic lines and falls onto the surface of the WD. Magnetic CVs are a small sub-set of all catalogued CV systems and fall into two categories: polars and intermediate polars (IPs). In a simple model of a column of gas impacting the WD atmosphere, a shock will form and hard X-ray/soft  $\gamma$ -ray emission will result from thermal bremsstrahlung cooling by free electrons in the hot post-shock region (PSR) with  $kT \approx (5 - 60)$  keV [2].

Publicly available observational data from *INTEGRAL/IBIS* were used to search for hard X-ray emission of all known IPs [1]. This observational material represents over 8 000 individual pointings obtained during almost 5 years (total exposure time over 23 Msec). We prepared the mosaics for all known IPs (65 in 2008) in (20 - 40) keV energy band. We were not able to find significant detection of the X-ray emission in the mosaics for 43 known IPs. On the other hand, in the 5 cases, namely AO Psc, TV Col, XY Ari, V1062 Tau and V2306 Cyg we can declare new, previously unreported detection of the hard X-ray emission in the (20 - 40) keV mosaics. Nevertheless, only 25% of all known IPs was detected and some IPs are not detectable even we have significant exposure time (more than 4 Msec) for these sources. This fact can be related with activity state of these close interacting binaries.

We used all available observations from *INTEGRAL/IBIS* to study possible long-term variability of a bright X-ray source V1223 Sgr in hard X-ray/soft  $\gamma$ -ray spectral bands [2]. *INTEGRAL/OMC* data were used to looking for long-term variability of this object in optical. The overall *INTEGRAL/IBIS* mosaics showed that V 1223 Sgr is detectable up to 80 keV. The light curves are displayed in Fig. 2.1 (left panel). It is clear that the fluxes especially in (15 - 25) keV and (25 - 40) keV bands are long-term variable with significant drop around  $MJD \approx 53\ 650$ . The optical light curve of V1223 Sgr based on available *INTEGRAL/OMC* data is showed in Fig. 2.1 (right panel). We can see that optical brightness of this source is long-term variable. Moreover these variations are correlated with the changes in (15 - 25) keV, (25 - 40) keV and (40 - 60)

keV spectral bands with correlation coefficients 0.81, 0.82 and 0.89, respectively. Significant part of optical emission from IPs is produced by a hot spot, where the matter from donor star interacts with outer rim of the accretion disk. X-ray emission is produced by interaction of the accreting matter with the WD surface. So, the emission in both optical and X-ray bands is related with mass transfer and therefore observed variations are probably caused by the changes in mass accretion rate [3].

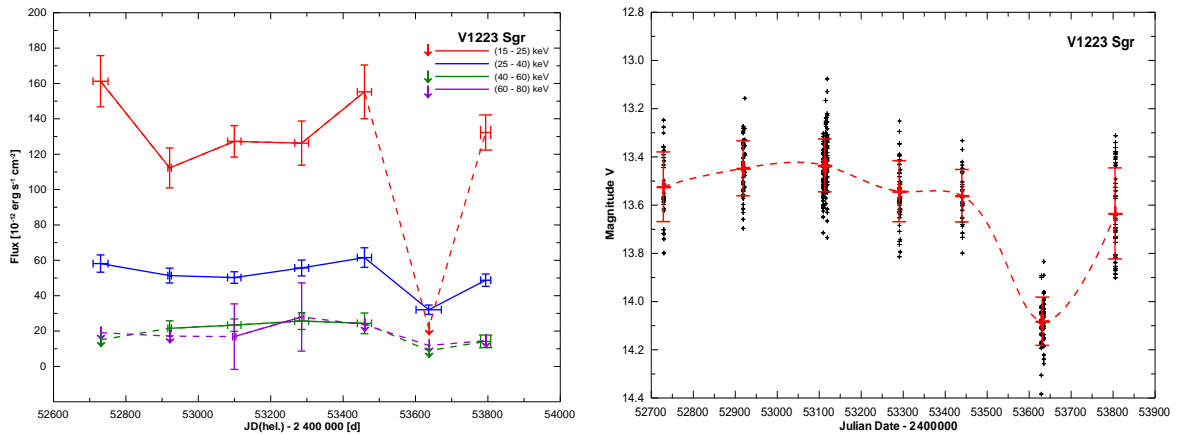


Figure 2.1. Left panel: *INTEGRAL/IBIS* light curves of V 1223 Sgr in corresponding energy bands. The arrows represent  $3\sigma$  upper limits. Right panel: *INTEGRAL/OMC* light curve of V 1223 Sgr in optical spectral band. The crosses represent average values of magnitude in the corresponding seasons.

The X-ray source V709 Cas was recognized as an IP following its detection in the *ROSAT* All Sky Survey. Our analysis of all available observational data from *INTEGRAL/IBIS* for V709 Cas showed that this source is detectable up to 100keV. The hard X-ray/soft  $\gamma$ -ray fluxes are not persistent, and the flux curves indicate that the brightness of this IP increased by a factor of  $\approx 2$  from MJD 52700 to MJD 53 700 in (15 - 25) keV energy band [4].

SS Cyg is an optically bright dwarf nova (DN) observed to undergo outbursts every  $\approx 40$  days, characterised by an increase in optical magnitude from  $V \sim 12$  to  $V \sim 8$ . The X-ray generation mechanism in DNe predicts a suppression of high energy emission during the regular optical outburst phases that typify these objects. Our analysis of all available observations of SS Cyg from *INTEGRAL/IBIS* showed that this source is detectable up to 100 keV [5]. The hard X-ray fluxes are not persistent and the flux curves confirm that the brightness increased by a factor  $\approx 2$  in (15 - 25) keV and (25 - 40) keV bands during optical quiescence of this X-ray source.

The broad-band (3 - 100) keV spectra of investigated IPs based on all available observation data from *INTEGRAL/JEM-X* and *INTEGRAL/IBIS* were well fitted by a thermal bremsstrahlung model with post-shock temperatures  $kT \approx (20 - 25)$  keV [2]. In the case of V2400 Oph (and possibly GK Per) there are

some evidences for emission excess around  $\approx 30$  keV, which can be caused by reflection of X-ray from an optically thick cold medium [5].

We investigated the possible short-term variability of V1223 Sgr in *INTEGRAL*/IBIS data [6]. We prepared unique method of folding particular phase interval on the base of proper time intervals from individual science windows. Our method applied the Good Time Intervals according to (orbital or other) phase bin and created the phase resolved mosaics (supposing sufficient exposure) of a periodic source. The phase diagram of V1223 Sgr in (15 - 25) keV band folded with orbital period 3.37 hrs showed that X-ray emission of this object is variable at short-time scales, too. This variability is probably related to the changes of visibility of the impact region at WD surface during its orbital motion.

IU Per is an eclipsing semi-detached binary with a pulsating component. Using our own ground-based, as well as *INTEGRAL* satellite photometric observations in the *B* and *V* passbands, we derived geometrical and physical parameters of this system [7]. We detected the short-term variations of IU Per in the residuals of brightness after the subtraction of synthetic light curves. Analysis of these residuals enabled us to characterize and localize the source of short-term variations as the pulsations of the primary component typical to  $\delta$  Scuti-type stars.

In years 2007 – 2009 Rudolf Gális work at *INTEGRAL* Science Data Centre (Versoix, Switzerland). He was responsible for scientific supervision on *INTEGRAL* operations (5 one-week Scientist on Duty shifts) and has been participated on the research of other X-ray sources (X-ray binaries, X-ray transients, and gamma ray burs) using observational data from *INTEGRAL* [8-11].

## References:

1. HUDEC, R. – ŠIMON, V. – MUNZ, F. – GÁLIS, R. New Results on Cataclysmic Variables Observed by INTEGRAL, Chinese Journal of Astronomy & Astrophysics Supplement, Vol. 8, pp. 259-264, 2008.
2. GÁLIS, R. – ECKERT, D. – PALTANI, S. – MÜNZ, F. – KOCKA, M. X-Ray Emission of Cataclysmic Variables Observed by Integral, Baltic Astronomy, Vol. 18, pp. 321-326, 2009.
3. HUDEC, R. – GÁLIS, R. – KOCKA, M. Lessons learned from ESA INTEGRAL: cataclysmic variables and blazars, Memorie della Societa Astronomica Italiana, v.81, 220 pp., 2010.
4. GÁLIS, R. – HRIC, L. – KUNDRA, E. – MÜNZ, F. Cataclysmic Variables - X-rays and Optical Activity in V1223Sgr and V709Cas, Acta Polytechnica, Vol. 51, No. 6, 13 pp., 2011.
5. GÁLIS, R. – HRIC, L. – KUNDRA, E. Hard X-ray and Optical Activity of Intermediate Polars, From Interacting Binaries to Exoplanets: Essential Modeling Tools, Eds. M. T. Richards and I. Hubeny, IAU Symposium, Volume 282, pp. 87-88, 2012.
6. HRIC, L. – KUNDRA, E. – GÁLIS, R. Mass Accretion in Intermediate Polar V1223 Sgr, Feeding Compact Objects: Accretion on All Scales, IAU Symposium, Vol. 290, pp. 225-226, 2013.
7. KUNDRA, E. – HRIC, L. – GÁLIS, R. Pulsation of IU Per from the Ground-based and 'Integral' Photometry, Baltic Astronomy, Vol. 22, pp. 111-122, 2013.
8. GÁLIS, R. – BECKMANN, V. – BIANCHIN, V. – GREBENEV, S. – McBRENN, B. – MEREGHETTI, S. – REVNIVTSEV, M. – SANCHEZ, C. – STRONG, A. – WESTERGAARD, N. J. SAX J2103.5+4545 in outburst, The Astronomer's Telegram, #1063, 2007.
9. SHAW, S. – KUULKERS, E. – MARKWARDT, C. B. – GÁLIS, R. X-ray activity of IGR J17379-3747 confirmed with INTEGRAL, The Astronomer's Telegram, #1711, 2008.
10. GOTZ, D. – PAIZIS, A. – MEREGHETTI, S. – BECKMANN, V. – BECK, M. – GÁLIS, R. – BORKOWSKI, J. GRB 080613: a long GRB detected with INTEGRAL, GRB Coordinates Network, Circular Service, 7871, 2008.
11. FIOCCHI, M. – NATALUCCI, L. – CHENEVEZ, J. – BAZZANO, A. – TARANA, A. – UBERTINI, P. – BRANDT, S. – BECKMANN, V. – FEDERICI, M. – GÁLIS, R. – HUDEC, R. Renewed Activity from the X-Ray Transient SAXJ 1810.8-2609 with Integral, The Astrophysical Journal, Volume 693, Issue 1, pp. 333-339, 2009.

In the *Earth Science Institute of the Slovak Academy of Sciences, Bratislava and Hurbanovo*, a number of issues concerning space weather were investigated (geomagnetic activity forecasting and geomagnetic storm modelling) and ground magnetic field measurements were performed.

The paper [7] deals with the relation of the southern orientation of the north-south component  $B_z$  of the interplanetary magnetic field to geomagnetic activity (GA) and subsequently a method is suggested of using the found facts to forecast potentially dangerous high GA. We have found that on a day with very high GA hourly averages of  $B_z$  with a negative sign occur at least 16 times in typical cases. Since it is very difficult to estimate the orientation of  $B_z$  in the immediate vicinity of the Earth one day or even a few days in advance, we have suggested using a neural-network model, which assumes the worse of the possibilities to forecast the danger of high GA - the dominant southern orientation of the interplanetary magnetic field. The input quantities of the proposed model were information about X-ray flares, type II and IV radio bursts as well as information about coronal mass ejections (CME). In comparing the GA forecasts with observations, we obtain values of the Hanssen-Kuiper skill score ranging from 0.463 to 0.727, which are usual values for similar forecasts of space weather. The proposed model provides forecasts of potentially dangerous high geomagnetic activity should the interplanetary CME (ICME), the originator of geomagnetic storms, hit the Earth under the most unfavorable configuration of cosmic magnetic fields. We cannot know in advance whether the unfavorable configuration is going to occur or not; we just know that it will occur with the probability of 31%.

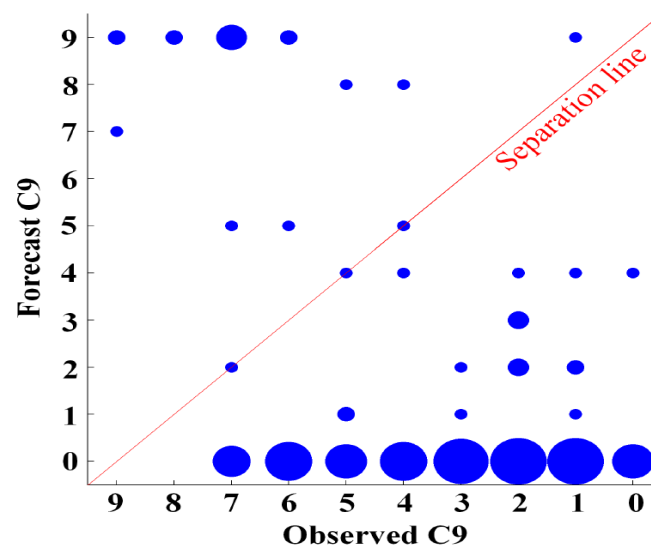


Figure 2.2. Diagrammatized contingency table describing successfulness of geomagnetic activity forecast in terms of the daily geomagnetic indices C9.

In [7], the daily geomagnetic indices C9 and one-hour means of north-south component of the IMF were studied. The method of ANN was employed to forecast geomagnetic activity. The model was proved to be able to classify two categories (yes/no) for occurrence of strong geomagnetic activity (with limiting value of C9 to be 7).

In [3,4,10,11], a model to forecast one-hour lead Dst index is proposed. Our approach is based on artificial neural networks (ANN) combined with an analytical model of the solar wind-magnetosphere interaction. Previously, the hourly solar wind parameters have been considered in the analytical model, all of them provided by registration of the ACE satellite. They were the solar wind magnetic field component Bz, velocity V, particle density n and temperature T. The solar wind parameters have been used to compute analytically the discontinuity in magnetic field across the magnetopause, denoted as [Bt]. This quantity has been shown to be important in connection with ground magnetic field variations. The method was published, in which the weighted sum of a sequence of [Bt] was proposed to produce the value of Dst index. The maximum term in the sum, possessing the maximum weight, is the one denoting the contribution of the current state of the near-Earth solar wind. The role of the older states is less important - the weights exponentially decay. Moreover, the terms turn to zero if  $B_z = 0$ . In this study, we set up a more comprehensive model on the basis of the ANNs. The model is driven by input time histories of the discontinuity in magnetic field [Bt], which are provided by the analytical model. At the output of such revised model, the Dst index is obtained and compared with the real data records. In this way we replaced those exponential weights in the published method with another set of weights determined by the neural networks. We retrospectively tested our models with real data from solar cycle 23. The ANN approach provided better results than a simple method based on exponentially decaying weights. Moreover, we have shown that our ANN model could be used to predict Dst one hour ahead. We assessed the predictive capability of the model with a set of independent events and found correlation coefficient  $CC = 0.74 \pm 0.13$  and prediction efficiency  $PE = 0.44 \pm 0.15$ . We also compared our model with the so called Dst-specification models. In those models, the Dst index was derived directly through an analytic or iterative formula or a neural network-based algorithm. We showed that the performance of our model was comparable to that of Dst-specification models.

In subsequent studies [9,12], the model developed in [3] is shown to distinguish between two classes of geomagnetic storms: those caused by coronal mass ejections (CMEs) and those caused by corotating interaction regions (CIRs). The results show that the model performance is better for the CME driven storms than for the CIR driven storms. At the same time, it appears that in the case of medium and weak storms the model performance is worse than in the case of intense storms.

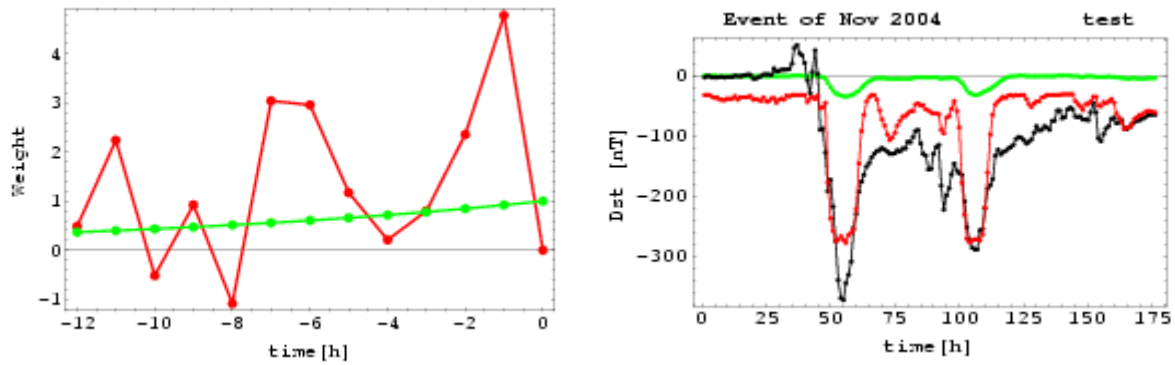


Figure 2.3. The weighting function measuring the importance of past solar wind parameters and the model of geomagnetic storm in terms of the Dst index (black – observational Dst, green – empirical model, red – neural network model).

In [2], geomagnetic response to solar activity is studied with focus on the causers such as CMEs and CIRs. A survey of the results for selected cases obtained over the last ten years is presented in [2]. Due to growing importance space weather topic brings together experts in various research fields and applications. To assure the proper use of space weather terminology among the Slovak experts in solar astrophysics and space geophysics a translated version of the comprehensive paper by R. Schwenn is presented in [5,6].

Along with theoretical studies, magnetic ground or repeat station surveys are performed to determine the geomagnetic field spatial distribution. Hurbanovo Geomagnetic Observatory of the Earth Science Institute of the SAS performs continuous monitoring and registration of the geomagnetic field components. The one-minute mean values of all components of the geomagnetic field as well as the records acquired with the one-second sampling interval are available. K-indexes characterizing the geomagnetic activity in the middle latitudes are computed regularly. The data are published on the CD-ROMs prepared in the frame of INTERMAGNET. Information about the geomagnetic activity is also published on the web site of the observatory, [www.geomag.sk](http://www.geomag.sk). The level of the geomagnetic activity is reported to public media (TV), too.

The members of the Hurbanovo Geomagnetic Observatory staff regularly perform field measurements at the observation points of the national magnetic repeat station network, which is a part of the European repeat station network. The measurements are coordinated by the MagNetE Group. Measurements of the magnetic declination are performed regularly at selected Slovak airports

The knowledge of the distribution of the geomagnetic field elements over a country is important for many practical as well as scientific reasons. Such distributions result from magnetic surveys. The surveys need to be repeated periodically: two-year period has been agreed for repeat stations by the MagNetE Group. This periodicity enables to find out information about the magnetic secular variations. The report in [13,14,15] presents the results of the

joint repeat and ground station survey which was carried out in Slovakia in the year 2014. The measurements were performed at 12 observation points; 3 stabilized repeat stations were supplemented by 8 temporary ground survey points. First degree polynomial models of the distributions of the geomagnetic field elements were derived. The differences between the current and the previous repeat station surveys are shown too. In addition, a note about the method of calculating azimuths of reference marks is appended. The note concerns a typing error in the listing of a computer code that has been printed in a manual that is widely used within the geomagnetic community. Fixing this inconspicuous error is recommended in order to obtain correct values of magnetic declination.

Records of historical measurements of the geomagnetic field are invaluable sources to reconstruct temporal variations of the Earth's magnetic field. In [1,8], old observatory records with different origins are collected. The gathered records are integrated into a database together with corresponding metadata, such as the used measurement instruments and methods. This information allows an assessment of quality and reliability of the historical observations. The combination of compilations of historical measurements with high quality archeo- and paleomagnetic data in a single database enables a reliable joint evaluation of all types of magnetic field records from different origins.

## References:

1. ARNEITZ, P. – HEILIG, B. – VADASZ, G. – VALACH, F. – DOLINSKÝ, P. – HEJDA, P. – FABIAN, K. – HAMMERL, Ch. – LEONHARDT, R. Historical records of the geomagnetic field. In Geophysical Research Abstracts, EGU General Assembly 2014, vol. 16, EGU2014-6550, 2014.
2. HEJDA, P. – BOCHNÍČEK, J. – VALACH, F. – REVALLO, M. Geomagnetic response to solar activity: summary for the last ten years and analysis of selected cases, Geophysical Research Abstracts, Vol. 16, EGU2014-6003, 2014, EGU General Assembly 2014. (poster)
3. REVALLO, M. – VALACH, F. – HEJDA, P. – BOCHNÍČEK, J. A neural network Dst index model driven by input time histories of the solar wind-magnetosphere interaction. In Journal of Atmospheric and Solar-Terrestrial Physics 110-111 9–14, 2014, <http://dx.doi.org/10.1016/j.jastp.2014.01.011>
4. REVALLO, M. – VALACH, F. – HEJDA, P. – BOCHNÍČEK, J. Modelovanie silných geomagnetických búrok 23. slnečného cyklu. 22. celoštátny slnečný seminár, Nižná nad Oravou, 26.-30. mája 2014, Zborník na CD-ROM, (in Slovak).
5. VALACH, F. – DOROTOVIČ, I. Kozmické počasie zo slnečnej perspektívy: predstavenie slovenského prekladu prehľadového článku profesora Rainera Schwenna, 22. celoštátny slnečný seminár, Nižná nad Oravou, 26.-30. mája 2014, Zborník na CD-ROM, (Prednáška in Slovak).
6. VALACH, F. – DOROTOVIČ, I. (prekladatelia). Kozmické počasie: Slnečná perspektíva, Preklad prehľadovej práce SCHWENN, Rainer. 2006: Space Weather: The Solar Perspective. Pôvodner publikované v Living Rev. Solar Phys., [online], 3, 2. Preklad uverejnený ako príloha v Zb. ref. 22. celoštátny slnečný seminár, Nižná nad Oravou 2014 [CD-ROM], počet strán 73, (in Slovak).
7. VALACH, F. – BOCHNÍČEK, J. – HEJDA, P. – REVALLO, M. Strong geomagnetic activity forecast by neural networks under dominant southern orientation of the interplanetary magnetic field. In Advances in Space Research, Volume 53, Issue 4, pp. 589–598, 2014, <http://dx.doi.org/10.1016/j.asr.2013.12.005>
8. LEONHARDT, R. – ARNEITZ, P. – EGLI, R. – FABIAN, K. – HEILIG, B. - KOVÁCS, P. - VALACH, F. - DOLINSKÝ, P. - HEJDA, P. Historical magnetic records and the past geomagnetic field evolution. In MagNetE 2015, Budapest 16-18 september : abstracts. Budapest : Geological and Geophysical Institute of Hungary, 2015, p. 22.

9. REVALLO, M. – VALACH, F. – HEJDA, P. – BOCHNÍČEK, J. Modeling of CME and CIR driven geomagnetic storms by means of artificial neural network. In Contributions to Geophysics and Geodesy, 2015, vol. 45, no. 1, pp. 53-65. (2015 - SCOPPUS). ISSN 1335-2806. [http://gpi.savba.sk/GPIweb/ogg/ikohut/CGG/45/1/Revallo-et-al\\_CGG-45-1\\_web.pdf](http://gpi.savba.sk/GPIweb/ogg/ikohut/CGG/45/1/Revallo-et-al_CGG-45-1_web.pdf)
10. REVALLO, M. – VALACH, F. – HEJDA, P. – BOCHNÍČEK, J. Modeling of geomagnetic storms by means of an analytical model and artificial neural networks. In 26th IUGG general assembly 2015, Praha, 22. jún-2. júl 2015. - Praha: The Czech Academy of Sciences, 2015.
11. REVALLO, M. – VALACH, F. – HEJDA, P. – BOCHNÍČEK, J. Modeling of severe geomagnetic storms of solar cycle 23 by means of artificial neural networks. In Geophysical Research Abstracts, vol. 17, EGU2015-12927, 2015. ISSN 1029-7006. <http://meetingorganizer.copernicus.org/EGU2015/EGU2015-12927.pdf>
12. REVALLO, M. – VALACH, F. – HEJDA, P. – BOCHNÍČEK, J. Two classes of geomagnetic storms modeled by means of artificial neural networks. In 11th slovak geophysical conference, 8.-9. september, 2015 : abstracts [elektronický zdroj]. Bratislava: Slovak University of Technology, Faculty of Civil Engineering, Department of Theoretical Geodesy, 2015, p. 59. Názov z vytlačeného dokumentu.
13. VÁCZYOVÁ, M. – VALACH, F. The accuracy of the reduction of magnetic surveys – dependence on the distance from the magnetic observatory. In 11th slovak geophysical conference, 8.-9. september, 2015 : abstracts [elektronický zdroj]. Bratislava : Slovak University of Technology, Faculty of Civil Engineering, Department of Theoretical Geodesy, 2015, p. 61. Názov z vytlačeného dokumentu.
14. VALACH, F. – VÁCZYOVÁ, M. – ŠOLTIS, T. – VAJKAI, M. Report on the magnetic survey in Slovakia for the 2014.5 epoch. In MagNetE 2015, Budapest 16-18 september : abstracts. Budapest : Geological and Geophysical Institute of Hungary, 2015, p. 31.
15. VALACH, F. – VÁCZYOVÁ, M. – ŠOLTIS, T. – VAJKAI, M. The results of the magnetic repeat station survey in Slovakia for epoch 2014.5. In 11th slovak geophysical conference, 8.-9. september, 2015 : abstracts [elektronický zdroj]. Bratislava : Slovak University of Technology, Faculty of Civil Engineering, Department of Theoretical Geodesy, 2015, p. 62. Názov z vytlačeného dokumentu.

In the *Slovak Central Observatory (SCO)* in Hurbanovo (<http://www.suh.sk>), a number of activities related to space research were performed. We observed sunspots (the Wolf number data were submitted to the SIDC in Brussels, Belgium and to the SONNE Netz in Germany) and prominences (images are published at the website of the Observatory). We performed also spectrographic observations of the solar spectrum (variations of selected spectral lines during a solar activity cycle) using a horizontal solar telescope with spectrograph, we registered solar radio bursts using a solar radio spectrometer CALLISTO [1], and impact of solar flares on the Earth's ionosphere using a SID monitor. The research activities comprise study of the:

- modified coronal index (MCI) and the modified homogeneous data set (MHDS) of coronal intensities based on satellite EUV measurements,
- time-latitude distribution of prominences,
- asymmetry of the north and south hemispheric solar activity,
- rotation of the solar corona,
- temporal evolution of magnetic field and intensity properties of photospheric pores,
- oscillations of the cross-sectional area and the intensity of magnetic waveguides located in the lower solar atmosphere,
- impact of the solar activity on the tree growth of pine trees.

One researcher from the SCO is the national ISWI (International Space Weather Initiative, <http://iswi-secretariat.org>) coordinator for the Slovak Republic and since September 2014 has been appointed also as a Scientific Discipline Representative of the SCOSTEP for the field of solar physics.

We continued to publish at the website of the SCO data on the modified coronal index (MCI) and the modified homogeneous data set (MHDS) of coronal intensities based on satellite EUV measurements as a replacement of ground-based coronagraphic observations at Lomnický Štít.

In [2] we published a method that allows one to successfully substitute the ground-based observations by satellite observations and, thus, continue with the publication of the Homogeneous data Set (HDS, Fig. 2.4). For this purpose, the observations of the Extreme-ultraviolet Imaging Telescope (EIT), onboard the Solar and Heliospheric Observatory (SOHO) satellite, were exploited. Among other data the EIT instrument provides almost daily 28.4 nm (Fe xv) emission-line snapshots of the corona. The Fe xiv and Fe xv data (4051 observation days) taken in the period 1996 – 2008 have been compared and good agreement was found. The method to obtain the individual data for the HDS follows from the correlation analysis described in this article. The resulting data, now under the name of Modified Homogeneous Data Set (MHDS), are identical up to 1996 to those in the HDS. The MHDS can be used further for studies of the coronal solar activity and its cycle. These data are available at <http://www.suh.sk>.

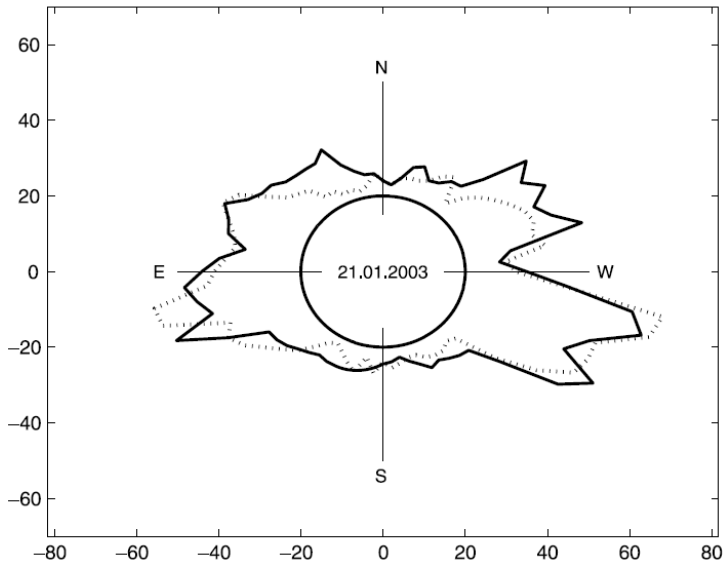


Figure 2.4. Comparison between the resulting radial intensity diagram from the MHDS (solid line) and the HDS (dashed line).

It seems that prominences occur randomly across the surface of the Sun. This applies only to heliographic latitudes of  $\pm 40^\circ$ , and even this is not valid everywhere. In higher latitudes is clearly observable the so-called polar branch of prominences (Fig. 2.5 and 2.6) as it has been investigated in [3]. It is an interesting indicator of the magnetic polarity reversal.

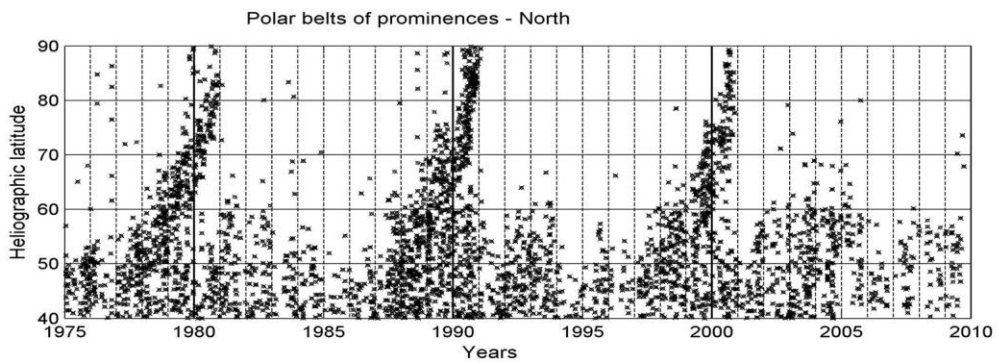


Figure 2.5. Polar branches of prominences near the North Pole of the Sun.

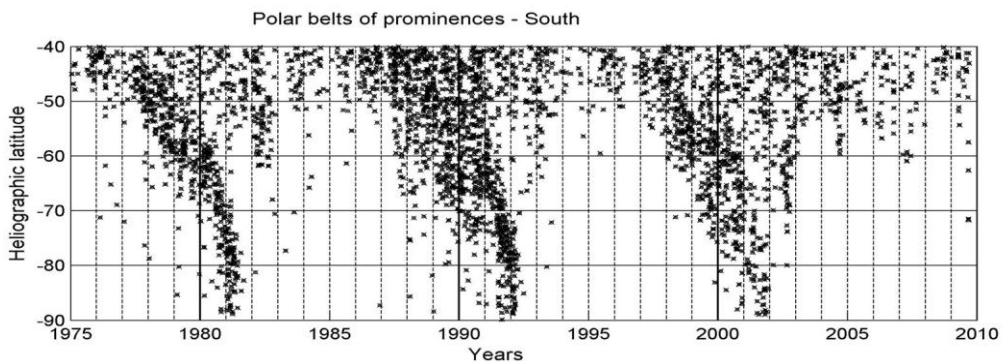


Figure 2.6. Polar branches of prominences near the South Pole of the Sun.

Evolution of the area of bright chromospheric plages and the corresponding north-south (N-S) asymmetry of this area, as measured in the period of 1975 – 2008 (solar cycles 21 – 23) from the Ca II K3 spectroheliograms registered in the Observatório Astronómico da Universidade de Coimbra (Portugal), was used in [4] to study dynamic asymmetry and conditional volatility of plage region areas. The classical ARMA model has proven to be insufficient to describe the time variations seen in the data because of the strong conditional variability. We found that the data are well fitted by ARMA mixed with power-  $\delta$  TGARCH error models. We also detected dynamic asymmetry in the plage region areas observed in the two hemispheres when two different temporal models were obtained to fit them. This statistical modeling of time series, taking into account new and different characteristics of the solar activity, will be very useful in subsequent forecast developments.

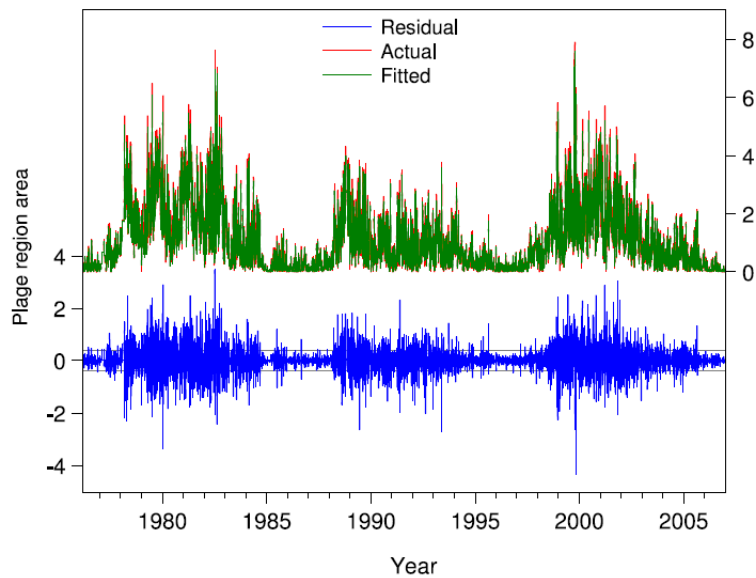


Figure 2.7. The daily northern hemisphere time series after model fitting. The red curve shows the completed data, while the green curve shows the fitted model. The blue curve indicates the residuals.

In [5] we focused on the analysis of data for the ring width of two pine tree species: samples of six maritime pines (*Pinus pinaster*), grown in the north of Portugal, and one sample of Scots pine (*Pinus sylvestris*), grown in the south of Slovakia. A negative impact of solar activity (SA) represented by the sunspot number (SSN) was observed on the growth of these pine trees. Furthermore, it was found that it is the latewood width (LWW) that is affected whereas earlywood width (EWW) is not affected.

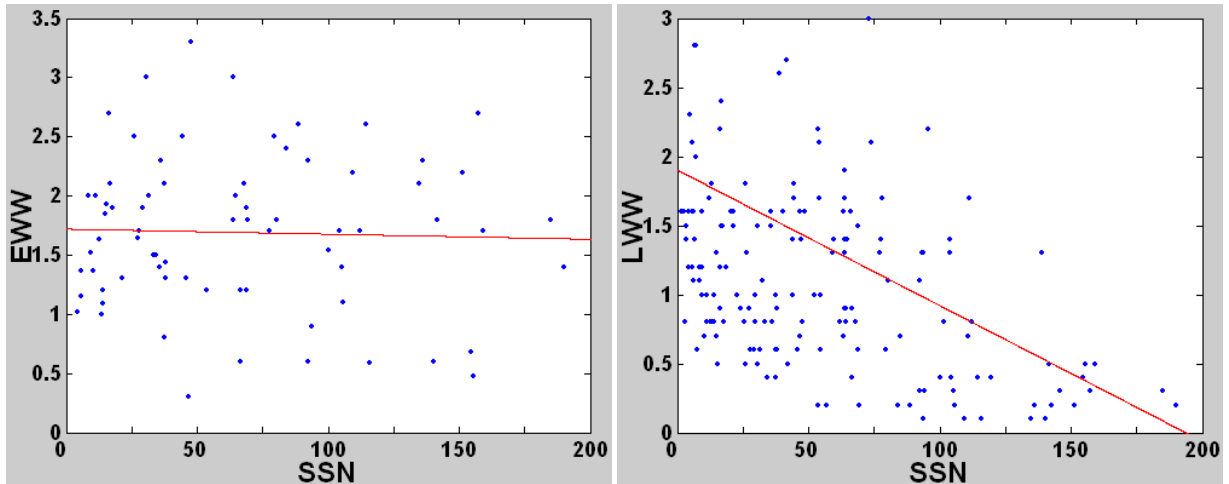


Figure 2.8. Bivariate fit of the EWW (left panel) and the LWW (right panel), respectively, of the maritime pine by the solar (sunspot) activity (yearly SSN).

In collaboration with the Computer Intelligence Group (CA3) of the CTS/UNINOVA (Caparica (Portugal)) has been developed in previous years a software tool for automatic tracking of solar activity features (sunspots and coronal bright points - CBPs) using a hybrid algorithm combining PSO (Particle Swarm Optimization) and Snake algorithms for detecting and tracking of a feature, and determining the differential rotation of the Sun [6]. In the period of 2014 – 2015 we tested the algorithm on further selected datasets of solar images recorded by the instruments AIA and HMI onboard the *Solar Dynamics Observatory* (SDO) satellite and. In [7] we reported results of our tests with our evolutionary computation based algorithm for calculating solar differential rotation by automatic tracking of coronal bright points. It will be necessary to automatize also the identification of SA features due to huge amount of SDO data. Collaboration with the research group of the Kyoto University (Japan) in the processing of solar images recorded in the Hida Obs. and the by the instruments of the future SOLAR-C satellite is envisaged in [11].

We aimed in [8] to identify properties of the observed magneto-acoustic waves and study the background properties of magnetic structures within the lower solar atmosphere. In [9] we used two series of high-resolution intensity images with short cadence of two isolated magnetic pores captured by the Dutch Open Telescope (DOT) and Rapid Oscillations in the Solar Atmosphere (ROSA) instruments, resp. Combining wavelet analysis and empirical mode decomposition (EMD), we searched for characteristic periods within the cross-sectional (i.e., area) and intensity time series. Several oscillations have been identified within these two magnetic pores. Their periods range from 3 to 20 minutes. Both wavelet analysis and EMD enables us to find the phase difference between the area and intensity oscillations. From these observed features, we conclude that these oscillations can be classified as slow MHD sausage waves.

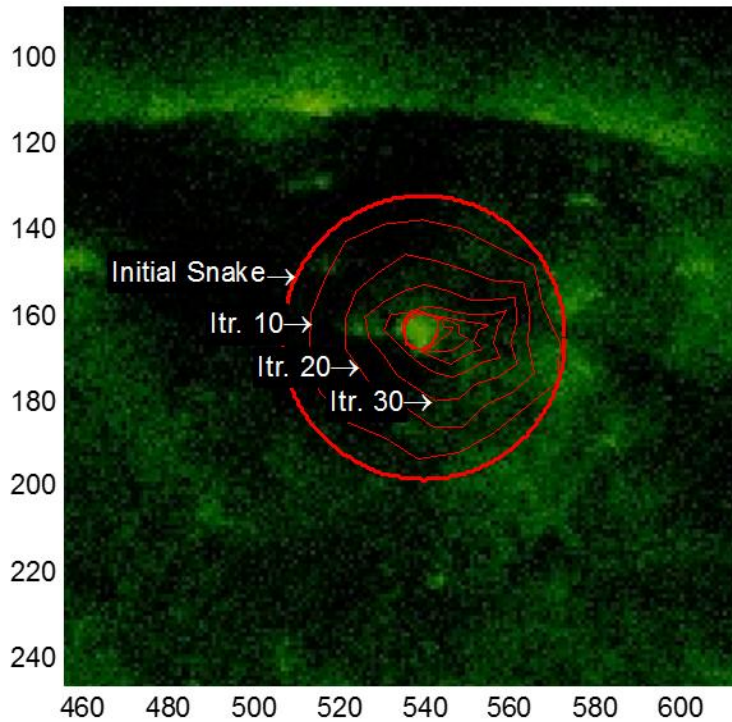


Figure 2.9. Detection process of a selected CBP (2010-10-5). Initial contour around the region of interest is evolved to precisely delineate the CBP boundaries. The outer contour is the initial snake and the inner contours are the transitional contours of every 10 iterations of the PSO-Snake detection algorithm. In the final stage contours converge and do not change much through iterations.

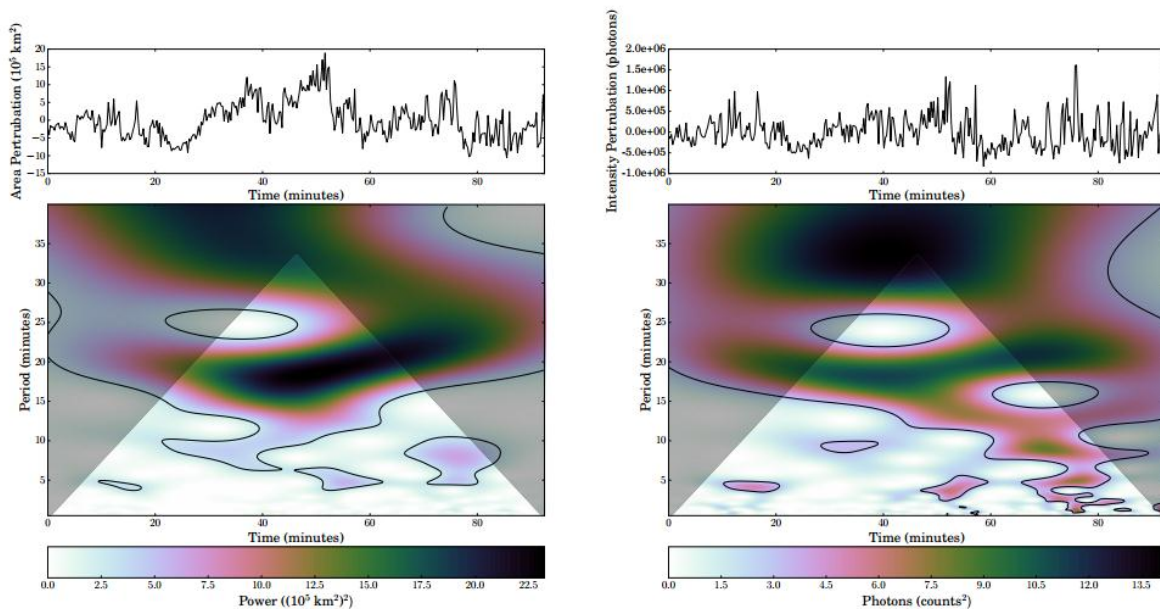


Figure 2.10. Evolution of the area of the pore (Upper panels). The corresponding wavelet power spectrum for a white noise background. The cone of influence is marked as the shaded region and the contour lines show the 95% confidence level (Lower panels).

We described in [10] conditions of pore formation in relation to the configuration and intensity of magnetic field, using observations of the

SDO/HMI instrument. We analyzed the temporal evolution of the area and brightness of the pores (time step of 15 minutes), their statistics, and in parallel a time-sequence of the line-of-sight magnetic field intensity and its correlation with the area and brightness. Positions of the magnetic field maxima precede the visible positions of the pore in the direction of rotation for the positive polarity and lag behind it for the negative polarity.

The SCO organised in the year 2014 the 22<sup>nd</sup> National Solar Physics Meeting with participation from abroad. The goal of the Meeting was to present new results of solar physics and from the field of the Sun-Earth connections, to provide overview of present status in selected fields of solar physics and geophysics. A separate space was devoted to the presentation of research results of undergraduate and PhD students of university and academic departments and also to results of scientific and popularisation activities of Astronomical Observatories in the Slovak Republic and the Czech Republic. Invited talks, short contributions and posters covered the following fields: physical phenomena in the solar atmosphere, solar activity, total solar eclipses, space weather and geoactivity.

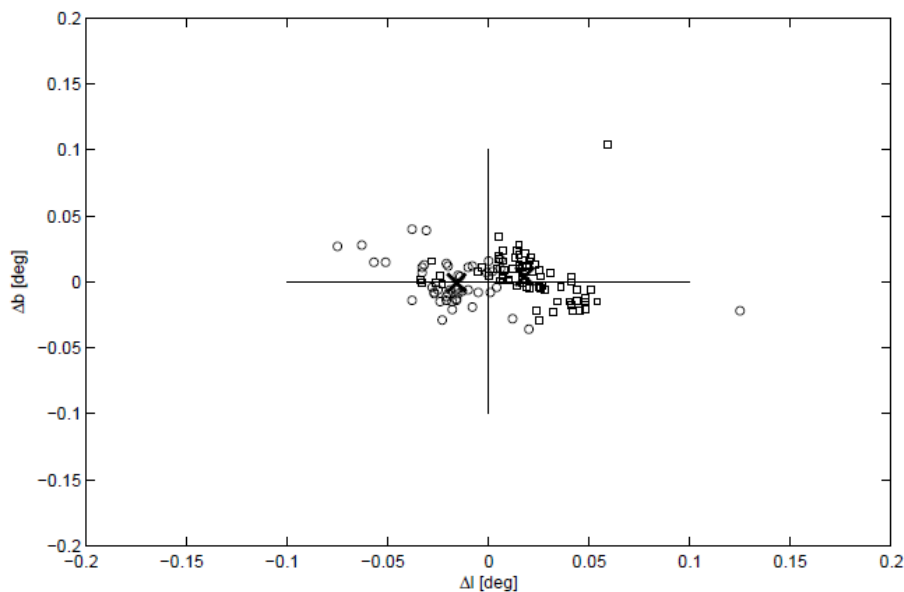


Figure 2.11. Differences between positions of intensity minima and magnetic maxima of pores in the  $(\Delta l, \Delta b)$  coordinates. The magnetic field maxima precede the pore positions for positive polarity (squares) and vice versa (circles). The cross at  $\Delta l = -0.02^\circ$  indicates centroid position of the magnetic field maxima for negative polarities and the cross at  $\Delta l = 0.02^\circ$  indicates centroid position of the magnetic field maxima for positive polarities.

The SCO was co-organizer of the Coimbra Solar Physics Meeting 2015 “Ground-based Solar Observations in the Space Instrumentation Era”, <http://www.mat.uc.pt/~cspm2015/>. The main organizer was the University of Coimbra (Observatório Geofísico e Astronómico da Universidade de Coimbra - OGAUC) and the meeting covered various aspects of solar dynamic and

magnetic phenomena which are observed over the entire electromagnetic spectrum. Emphasis was placed on instrumentation, observing techniques, and solar image processing techniques, as well as theory and modelling. The long-term (cyclic) evolution of solar magnetism and its consequence for the solar atmosphere, eruptive phenomena, solar irradiation variations, and space weather, was also in focus. One researcher from the SCO was member of SOC and LOC of the meeting and also the editor of Proceedings of the CSPM-2015.

## References:

1. DOROTOVIČ, I. – PINTÉR, T. (2014). Solar Radio Spectrometer CALLISTO in Hurbanovo - first results. *Sun and Geosphere*, Volume 9, No. 2, 105-107.
2. DOROTOVIČ, I. – MINAROVJECH, M. – LORENC, M. – RYBANSKÝ, M. (2014). Modified Homogeneous Data Set of Coronal Intensities. *Solar Physics*, Vol. 289, Issue 7, 2697-2703. doi: 10.1007/s11207-014-0501-2.
3. PINTÉR, T. – RYBANSKÝ, M. – DOROTOVIČ, I. (2014). The polar belts of prominence occurrence as an indicator of the solar magnetic field reversal. In 'Nature of Prominences and their role in Space Weather', Proceedings of the International Astronomical Union, IAU Symposium, B. Schmieder, J.-M. Malherbe, and S. Wu (eds.), Volume 300, 456-457. doi: 10.1017/S1743921313011538.
4. GONÇALVES, E. – MENDES-LOPES, N. – DOROTOVIČ, I. – FERNANDES, J. – GARCIA, A. (2014). North and South Hemispheric Solar Activity for Cycles 21 - 23: Asymmetry and Conditional Volatility of Plage Region Areas. *Solar Physics*, Vol. 289, Issue 6, 2283-2296. doi: 10.1007/s11207-013-0448-8.
5. DOROTOVIČ, I. – LOUZADA, J.L. – RODRIGUES, J.C. – KARLOVSKÝ, V. (2014). Impact of Solar Activity on the Growth of Pine Trees – Case Study. *European Journal of Forest Research*, Published online in February 2014. doi: 10.1007/s10342-014-0792-8.
6. DOROTOVIČ, I. – SHAHAMATNIA, E. – LORENC, M. – RYBANSKÝ, M. – RIBEIRO, R.A. – FONSECA, J.M. (2014). Sunspots and Coronal Bright Points Tracking using a Hybrid Algorithm of PSO and Active Contour Model. *Sun and Geosphere*, Volume 9, No. 2, 81-84.
7. SHAHAMATNIA, E. – DOROTOVIČ, I. – FONSECA, J.M. – RIBEIRO, R.A. (2016). An evolutionary computation based algorithm for calculating solar differential rotation by automatic tracking of coronal bright points. *J. of Space Weather and Space Climate*, Vol. 6, A16. doi: 10.1051/swsc/2016010 (accepted in 2015).
8. DOROTOVIČ, I. – ERDÉLYI, R. – FREIJ, N. – KARLOVSKÝ, V. – MÁRQUEZ, I. (2014). Standing sausage waves in photospheric magnetic waveguides. *Astronomy and Astrophysics*, Volume 563, A12. doi: 10.1051/0004-6361/201220542.

9. FREIJ, N. – DOROTOVIČ, I. – MORTON, R.J. – RUDERMAN, M.S. – KARLOVSKÝ, V. – ERDÉLYI, R. (2016). On the Properties of Slow MHD Sausage Waves within Small-scale Photospheric Magnetic Structures. *The Astrophysical Journal*, Volume 817, Issue 1, article id. 44. doi: 10.3847/0004-637X/817/1/44 (accepted in 2015).
10. DOROTOVIČ, I. – RYBANSKÝ, M. – SOBOTKA, M. – LORENC, M. – BARANDAS, M. – FONSECA, J.M. (2016). Temporal Evolution of Magnetic Field and Intensity Properties of Photospheric Pores. In *Ground-based Solar Observations in the Space Instrumentation Era, Proceedings of the CSPM-2015, University of Coimbra, Coimbra, Portugal, 5-9 October 2015*, I. Dorotovic, C. E. Fischer, M. Temmer (eds.), ASP Conf. Series, Vol. 504, 37 (accepted in 2015 / in press).
11. UENO, S. – SHIBATA, K. – ICHIMOTO, K. – NAGATA, S. – DOROTOVIČ, I. – SHAHAMATNIA, E. – RIBEIRO, R.A. – FONSECA, J.M. (2016). Roles of Ground-based Solar Observations of Hida Observatory toward the Solar-C Era. In *Ground-based Solar Observations in the Space Instrumentation Era, Proceedings of the CSPM-2015, University of Coimbra, Coimbra, Portugal, 5-9 October 2015*, I. Dorotovič, C. E. Fischer, M. Temmer (eds.), ASP Conf. Series, Vol. 504, 309 (accepted in 2015 / in press).

The activities of *the Astronomical Institute of the Slovak Academy of Sciences (AISAS)*, Tatranská Lomnica ([www.astro.sk](http://www.astro.sk)), related to COSPAR, were devoted to research in solar and stellar physics using different satellite observations, mainly in the UV, XUV and X-ray spectral regions. Stellar data of the IUE, FUSE, INTEGRAL, XMM-Newton, Kepler satellites, and the HST were used for research of various variable stars [1-6]. Data of the current SOHO mission, Hinode, SDO, and RHESSI satellites were used for solar research mostly focused on solar prominences [7-11]. Hereby we present an example of the results obtained by the AISAS staff, information on an education activity of the AISAS and information on the WAMIS proposal cooperation [12,13].

Within the research of the stellar astrophysics, we used observations carried out with the space observatories, the Far Ultraviolet Spectroscopic Explorer (FUSE), Hubble Space Telescope (HST), International Ultraviolet Explorer (IUE) and X-ray Multi-Mirror Mission (XMM-Newton) to model the spectral energy distribution (SED) of supersoft X-ray sources (SSS). On the basis of these observations we developed a method of multiwavelength modelling the SED of SSSs (Fig. 2.12). We showed that the multiwavelength approach overcomes the problem of the mutual dependence between the temperature, luminosity and amount of absorption, which appears when only the X-ray data are fitted. Thus, the method provides an unambiguous solution. It is essential in determining physical parameters of SSSs [1]. Application of the method to the recurrent symbiotic nova RS Oph showed that the luminosity of this object was super-Eddington during the whole outburst – from the explosion to the end of the supersoft X-ray phase. This required a high accretion rate from the surrounding disk resulting in the ejection of collimated high-velocity mass outflow. The high accretion rate could be a result of a focusing the wind from the cool giant in RS Oph towards the orbital plane. This then allowed the white dwarf to accrete the wind at very high rate [2,3].

The Astronomical Institute organised in the year 2014 the lecture course – Magnetohydrodynamics in astrophysics – given for the undergraduate and PhD students from Slovakia by Dr. Petr Jelínek of the Institute of Physics and Biophysics (Faculty of Science, University of South Bohemia, České Budějovice, Czech republic) on August 18-22, 2014 at AISAS at Tatranska Lomnica. The course of lectures provided insights to basic plasma physics, motion of charged particles in the magnetic field, cosmic electrodynamics, fluid description of plasma, magnetohydrodynamics, oscillations and waves in plasma, magnetoacoustic waves in plasma, plasma in astrophysics, MHD dynamo, solar wind, cosmic rays and to reconnection of the magnetic field. More details about the course of lectures can be found at the dedicated web page - <https://www.ta3.sk/~koza/mhd/mhd.htm>.

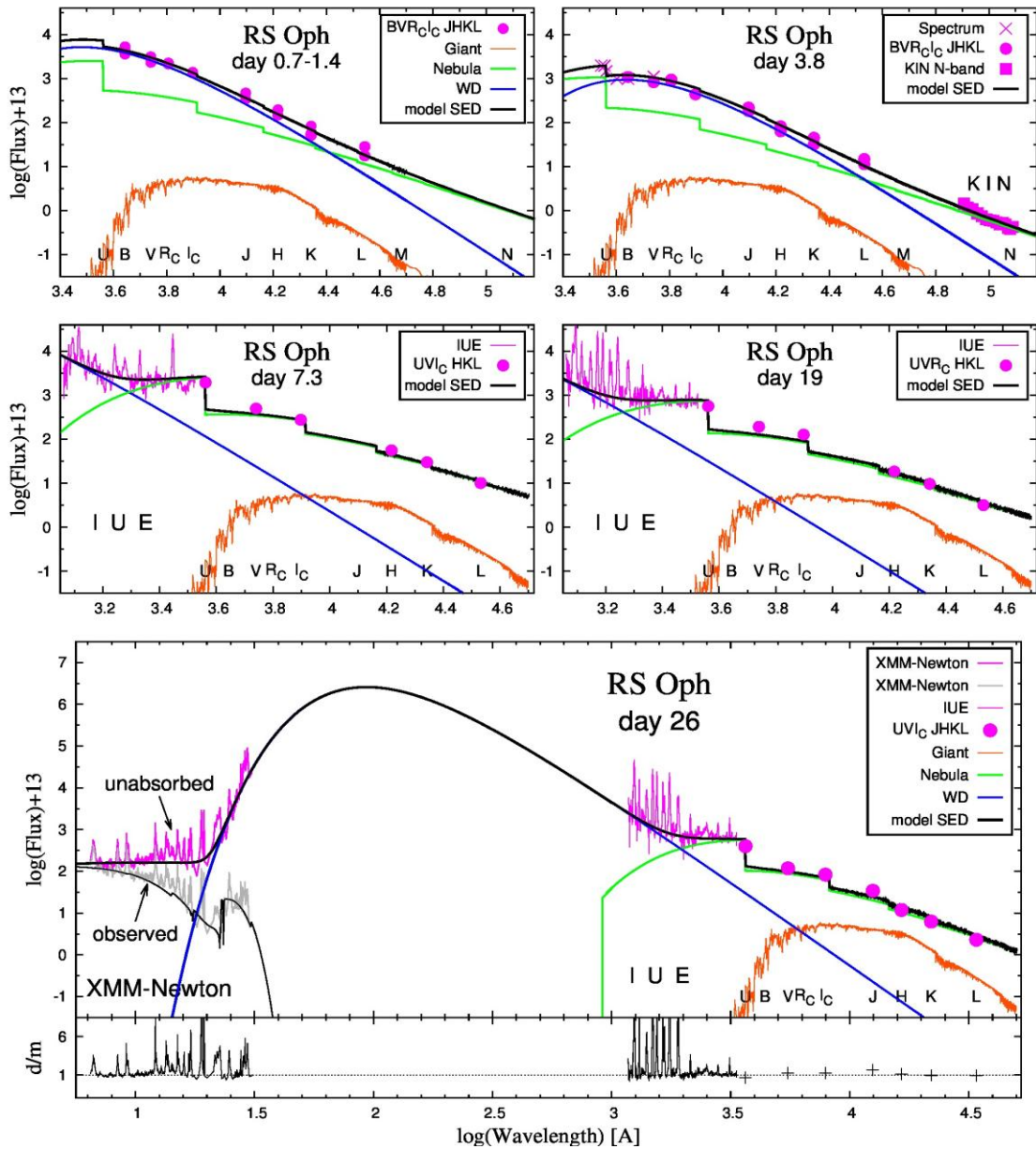


Figure 2.12. A comparison of the measured SED (in magenta) and model SED (black solid line) of RS Oph from day 1 after its explosion to day 26. Data-to-model ratios ( $d/m$ ) are plotted for the day-26 SED to judge the reliability of the fit. The blue, green and orange lines denote components of radiation from the SSS, nebula and giant, respectively. Fluxes are in units  $\text{erg s}^{-1} \text{cm}^{-2} \text{\AA}^{-1}$ .

In the years 2014-2015 AISAS has become involved in the proposal which has been submitted twice for consideration of an award by NASA (NASA H-TIDeS LCAS program). The proposal called “Waves and Magnetism in the Solar Atmosphere (WAMIS)” is led by Yuan-Kuen Ko (Naval Research Lab, Washington, USA) (PI), and its AISAS part by J. Rybak (Co-I). The team has received a negative agency decision due to NASA budget limitations although the proposal has been ranked high. The project is a long duration balloon-born

20 cm aperture coronagraph designed to obtain continuous measurements of the strength and direction of coronal magnetic fields within a large field-of-view over at least weeks at the spatial and temporal resolutions required to address several outstanding problems in coronal physics [12,13]. The WAMIS investigation, comprising a balloon-borne infra-red coronagraph and polarimeter to observe Fe XIII forbidden transitions and the He I line, should enable breakthrough science and enhance the value of data collected by other observatories on the ground (e.g. ATST, FASR, SOLIS, COSMO) and in space (e.g. Hinode, STEREO, SDO, SOHO and IRIS), and will advance technology for a future orbital missions.

Besides of this, the AISAS staff was involved (or leading) in the last two years in 4 coordinated observing campaigns focused on observations of several aspects of the solar activity. The integral part of the campaigns were also measurements performed by the space-born instruments on different satellites, e.g. SUMER/SoHO, EIS/Hinode. The measurements were coordinated with the ground-based instruments including the AISAS owned CoMP-S instrument at the Lomnický Peak Observatory.

## References:

1. SKOPAL, A. Multiwavelength modelling the SED of supersoft X-ray sources. I. The method and examples. In *New Astronomy*, 2015, vol. 36, pp. 116-127.
2. SKOPAL, A. Multiwavelength modeling the SED of supersoft X-ray sources. II. RS Ophiuchi: From the explosion to the SSS phase. *New Astronomy*, 2015, vol. 36, pp. 128-138.
3. SKOPAL, A. Multiwavelength modeling the SED of supersoft X-ray sources III. RS Ophiuchi: The supersoft X-ray phase and beyond. *New Astronomy*, 2015, vol. 34, pp. 123-133.
4. SEKERÁŠ, M. – SKOPAL, A. Mass-loss rate by the Mira in the symbiotic binary V1016 Cygni from Raman scattering. *The Astrophysical Journal*, 2015, vol. 812, article no. 162, pp. 1-8.
5. SKOPAL, A. – CARIKOVÁ, Z. Wind mass transfer in S-type symbiotic binaries I. Focusing by the wind compression model. *Astronomy and Astrophysics*, 2015, vol. 573, article no. A8, pp. 1-5.
6. SKOPAL, A. – DRECHSEL, H. – TARASOVA, T. N. – KATO, T. – FUJII, M. – TEYSSIER, F. – GARDE, O. – GUARRO, J. – EDLIN, J. – BUIL, C. – ANTAO, D. – TERRY, J.-N. – LEMOULT, T. – CHARBONNEL, S. – BOHLSSEN, T. – FAVARO, A. – GRAHAM, K. Early evolution of the extraordinary Nova Delphini 2013 (V339 Del). *Astronomy and Astrophysics*, 2014, vol. 569, article no. A112, pp. 1-14.
7. SCHWARTZ, P. – GUNÁR, S. – CURDT, W. Non-LTE modelling of prominence fine structures using hydrogen Lyman-line profiles. *Astronomy and Astrophysics*, 2015, vol. 577, article no. A92, pp. 1-10.
8. SCHWARTZ, P. – HEINZEL, P. – KOTRČ, P. – FÁRNÍK, F. – KUPRYAKOV, Yu. A. – DELUCA, E. E. – GOLUB, L. Total mass of six quiescent prominences estimated from their multi-spectral observations. *Astronomy and Astrophysics*, 2015, vol. 574, article no. A62, pp. 1-18.
9. SCHWARTZ, P. – JEJČIČ, S. – HEINZEL, P. – ANZER, U. – JIBBEN, P. R. Prominence visibility in HINODE/XRT images. *The Astrophysical Journal*, 2015, vol. 807, article no. 97, pp. 1-9.
10. GUNÁR, S. – SCHWARTZ, P. – DUDÍK, J. – SCHMIEDER, B. – HEINZEL, P. – JURČÁK, J. Magnetic field and radiative transfer modelling of a quiescent prominence. *Astronomy and Astrophysics*, 2014, vol. 567, article no. A123, pp. 1-16.

- 11.SU, Y. – GÖMÖRY, P. – VERONIG, A. – TEMMER, M. – WANG, T. – VANNINATHAN, K. – GAN, W. – LI, Y.P. Solar magnetized tornadoes: rotational motion in a tornado-like prominence. *The Astrophysical Journal Letters*, 2014, vol. 785, article no. L2, pp. 1-6.
- 12.STRACHAN, L. – KO, Y.-K. – MOSES, J. D. – LAMING, J. M. – AUCHERE, F. – CASINI, R. – FINESCHI, S. – GIBSON, S. – KNOELKER, M. – KORENDYKE, C. – MCINTOSH, S. – ROMOLI, M. – RYBÁK, J. – SOCKER, D. – TOMCZYK, S. – VOURLIDAS, A. – WU, Q. Waves and magnetism in the solar atmosphere (WAMIS). In *Polarimetry: From the Sun to Stars and Stellar Environments : Proceedings of IAU Symposium vol. 305*. Edited by K.N. Nagendra, Stefano Bagnulo, Rebecca Centeno and Maria Jesus Martinez Gonzalez. - Cambridge : Cambridge University Press, 2015, pp. 121-126.
- 13.KO, Y.-K. – MOSES, J. D. – LAMING, J. M. – STRACHAN, L. – BELTRAN, S. T. – TOMCZYK, S. – GIBSON, S. E. – AUCHERE, F. – CASINI, R. – FINESCHI, S. – KNOELKER, M. – KORENDYKE, C. – MCINTOSH, S. W. – ROMOLI, M. – RYBÁK, J. – SOCKER, D. G. – VOURLIDAS, A. – WU, Q. Waves and Magnetism in the Solar Atmosphere (WAMIS). *Frontiers in Astronomy and Space Sciences : Stellar and Solar Physics*, 2016, vol. 3, article no. 1, pp. 1-13.

Research on radiation-resistant microbes was performed at the *Slovak Organization for Space Activities* in collaboration with Department of Earth Sciences of University College London UK with focus on implications for potential habitability of life on Mars [1].

**References:**

1. MUSILOVA M. – WRIGHT, G. – WARD, J. M. – DARTNELL, L. R. Isolation of Radiation-Resistant Bacteria from Mars Analog Antarctic Dry Valleys by Preselection, and the Correlation between Radiation and Desiccation Resistance. *Astrobiology*, 15, 12, 2015.

### 3. MATERIAL RESEARCH IN SPACE

*J. Lapin*

Material research in space of the *Institute of Materials and Machine Mechanics of the Slovak Academy of Sciences* (IMMS SAS) has been connected with the international project entitled "Gravity dependence of CET in peritectic TiAl alloys (acronym GRADECET)" in the framework of the ELIPS-4 programme of ESA. The international consortium of the project consists of seven partners: Access e.V. - project coordinator (Aachen, Germany), Ecole des Mines de Nancy (Institut Jean Lamour, SI2M, Nancy, France), Deutsches Zentrum für Luft- und Raumfahrt (Institut für Materialphysik im Weltraum, Köln, Germany), Trinity College Dublin, School of Engineering, Mechanical and Manufacturing Engineering (Dublin, Ireland), Wigner Reserch Centre for Physics, (Hungarian Academy of Sciences, Budapest, Hungary), Snecma Safran Group (Villaroche, France), and Institute of Materials and Machine Mechanics (Slovak Academy of Sciences, Bratislava, Slovak Republic). Project GRADECET is divided into three distinguished phases: (i) extensive ground based preparatory phase aiming at producing all necessary data and technical solutions for space mission, (ii) space mission using sounding rocket MAXUS and (iii) ground based evaluation of samples prepared at microgravity and hypergravity conditions. Four peritectic TiAl based alloys with nominal compositions Ti-43.5Al-5Nb-0.2C-0.2B, Ti-44.5Al-5Nb-0.2C-0.2B, Ti-46.5Al-5Nb-0.2C-0.2B and Ti-47Al-5Nb-0.2C-0.2B (at.%) are evaluated in the frame of the project. These alloys are candidates for near net shape casting of light-weight structural components, like aero-engine blades and turbocharger wheels for automotive engines.

Several processing technologies are capable of producing parts from TiAl alloys, among them; investment casting, electron beam melting or EBM, and forging with advanced machining, the latter using pre-shaped cast feedstock. Accordingly, the materials properties in the liquid state and the solidification behaviour of TiAl alloys with respect to morphology, microsegregation and texture formation are current research topics with wide impact on future alloy development and process engineering. One possible event in casting of TiAl alloys is columnar to equiaxed transition (CET). The CET occurs during columnar growth when equiaxed grains begin to form, grow, and subsequently stop the columnar growth. Normally either a columnar or equiaxed grain structure is desired in industry applications, so that consistent mechanical properties are achieved throughout the casting. During solidification, the CET leads to a change of the grain structure within castings and hence to a change of their mechanical properties. While the CET phenomenon and various equiaxed nucleation models have been discussed in literature only a few investigations

focus on TiAl alloys. This is due to the experimental difficulties presented by handling the highly reactive melt and also because solidification patterns are easily lost, i.e., being overrun by solid state transformations. Another experimental difficulty arises where unwanted radial temperature gradients lead to radial columnar growth instead of equiaxed growth at the expected location of CET. For most TiAl castings, solidification with equiaxed grains is targeted, aiming to achieve isotropic properties throughout the cast component. Therefore, understanding the CET in microgravity, ground based gravity and hypergravity conditions is of a great importance from fundamental and industrial point of view to accelerate further development and industrial applications of these light weight high-temperature structural alloys. The participation of IMMM SAS in the project is financially supported by the Slovak Academy of Sciences (SAS) in the frame of international cooperation of SAS with ESA.

Microgravity solidification experiments offer a unique opportunity to minimise the effects of convection (thermal and solutal) and subsequently phenomenon associated with convection like sedimentation and macro-segregation on structure of castings. ESA's next sounding rocket mission, MAXUS-9, which is funded by ESA through the European Programme for Life and Physical Science in Space (ELIPS) with the sounding rocket and launch services provided to ESA by an industrial joint venture between EADS Astrium and the Swedish Space Corporation.

For ground based experiments, Bridgman type furnace at IMMS SAS has been redesigned to achieve CET in selected TiAl alloys using power down technique. The new design of the furnace allows performing CET experiments on cylindrical samples under controlled solidification conditions. The CET experiments were conducted in dense high purity  $Y_2O_3$  crucibles under an argon atmosphere. The power down technique consisted of: (i) heating of the sample to a temperature at a constant heating rate, (ii) stabilization at the temperature, (iii) partial displacement of the sample from the hot zone of the furnace into the crystallizer, (iv) temperature decrease at constant cooling rates and (v) furnace cooling of the sample to room temperature. Figure 3.1 shows section images of the etched and polished samples from Ti-45.5Al-4.7Nb-0.2C-0.2B (at.%) alloy, where sample I was cooled at  $15^\circ C min^{-1}$ , sample II was cooled at  $20^\circ C min^{-1}$ , sample III was cooled at  $30^\circ C min^{-1}$ , and sample IV was cooled at  $50^\circ C min^{-1}$ . In each sample the predominant growth pattern(s) of the primary  $\beta$ -phase was identified and the transition between each region is given by a solid white line in the figure. Regions marked 'U' were unmelted during the procedure, regions marked 'C' had axial columnar growth, regions marked 'R' had radial equiaxed growth.

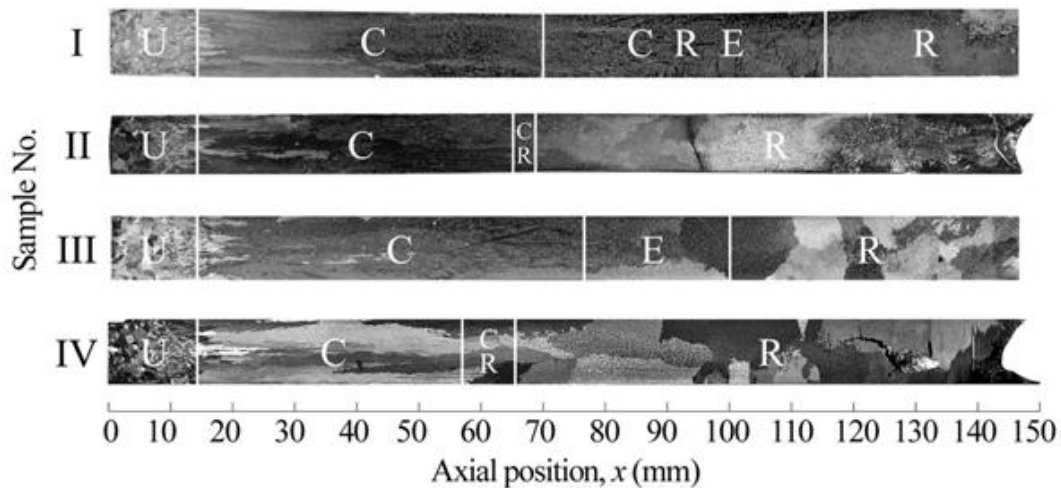


Figure 3.1. Images of etched and polished samples (numbered I–IV) with primary  $\beta$ -phase microstructure regions identified as follows: U – unmelted, C – axial columnar, R – radial columnar, and E – equiaxed.

The Bridgman Furnace Front Tracking Model (BFFTM), tailored specifically for the experimental furnace set-up (in terms of heat transfer coefficients) and the applied growth conditions by Mooney et al. [1, 2], was used to interpret the experimental results. The BFFTM simulated the conditions at the dendrite tip, namely, undercooling ( $\Delta T_{\text{tip}}$ ), growth rate ( $V_{\text{tip}}$ ), and temperature gradient ( $G_{\text{tip}}$ ), throughout the solidification process. The evolution of dendrite tip growth rate, and corresponding tip undercooling, are plotted against front position in Figures 3.2 and 3.3, respectively. Figure 3.4 shows dendrite tip growth rate plotted against temperature gradient at the dendrite tip. This graph is frequently used in CET modelling when a Hunt analysis is performed. Each plot on the graph is a locus of temperature gradient and growth rate evolution at the columnar tips. Each plot in Figure 3.4 should be interpreted by following the loci (all of which start on the x-axis) initially travelling from left to right before looping around in a clockwise direction, and continuing from right to left in the general direction towards the y-axis of the graph.

The BFFTM highlights an important consideration for CET experiment designers who intend to use the power-down method. High cooling rates lead to a situation where the heater temperature is less than that of the liquid in the sample. This subsequently leads to an unfavourable heat flow pattern that promotes radial columnar growth, thereby ‘choking’ undercooled liquid ahead of (axial) columnar grains and preventing the possibility of CET. Even though the radial temperature gradients in the case presented here were relatively small, the axial temperature gradient had to be reduced to a low value for CET and, ultimately, the axial and radial gradients reached a similar order of magnitude.

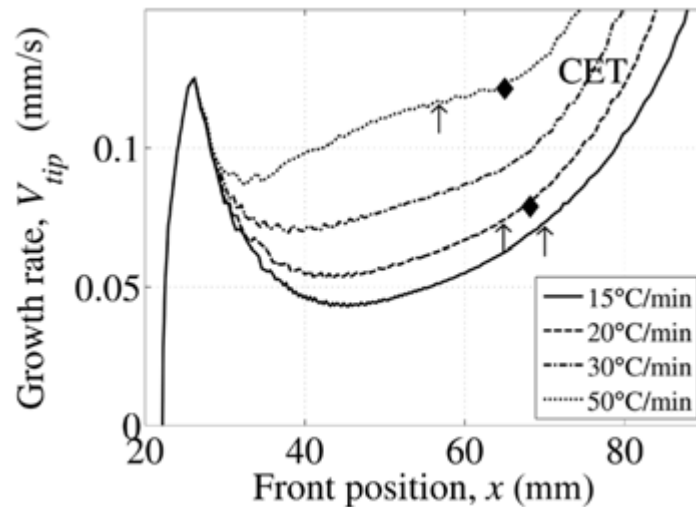


Figure 3.2. Dendrite tip growth rate versus front position.

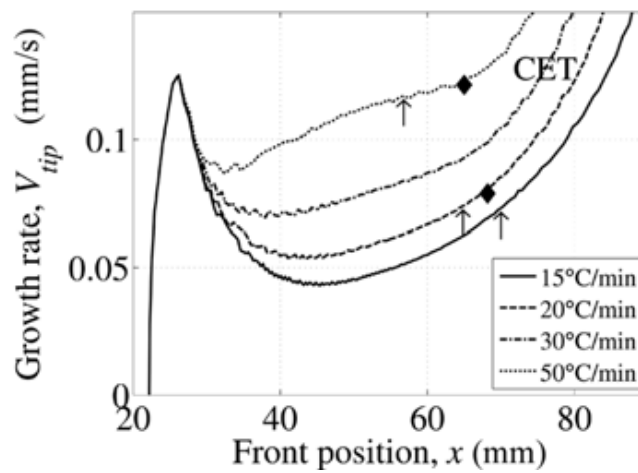


Figure 3.3. Dendrite tip undercooling versus front position.

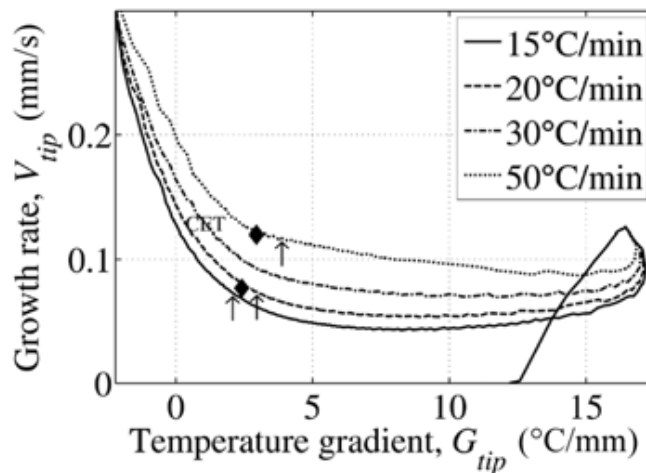


Figure 3.4. Dendrite tip growth rate versus temperature gradient.

## References

1. MOONEY, R. P. – MCFADDEN, S. – GABALCOVÁ, Z. – LAPIN, J. (2014). An experimental-numerical method for estimating heat transfer in a Bridgman furnace. *Applied Thermal Engineering*, 67, pp. 61-71.
2. MOONEY, R. P. – HECHT, U. – GABALCOVÁ, Z. – LAPIN, J. – MCFADDEN, S. (2015). Directional solidification of a TiAl alloy by combined Bridgman and power-down technique. *Kovove Mater.*, 53, pp. 187–197.

## 4. REMOTE SENSING

*I. Barka, T. Bucha, J. Feranec, Z. Klikušovská, M. Kopecká, Z. Kováčiková,  
J. Nováček, R. Pazúr, M. Rusnák, I. Sačkov, J. Sládek, M. Sviček*

**Selected activities of four institutions are included in this report (for 2014-2015):**

**Institute of Geography, Slovak Academy of Sciences (IG SAS) in Bratislava**

Remote sensing activities at the IG SAS involved:

### *Urban Atlas project*

IG SAS has continued its participation in the Urban Atlas (UA) 2012 – a joint project of the European Commission Directorate General (EC DG) for Regional Policy and EC DG for Enterprise and Industry with the support of the European Space Agency (ESA) and the European Environment Agency (EEA) in the context of Global Monitoring for Environment and Security (GMES)/ Copernicus Land (GIO Land) activities. The main input datasets for UA 2012 are the UA 2006 datasets and/or the Very High Resolution (VHR SPOT 5 with 2.5 m resolution) satellite images of the reference year 2012. 200 large urban zones (LUZs) were interpreted at the IG SAS during 2014-2015. The Figure 4.1 shows obtained results on the example of LUZ Bratislava.

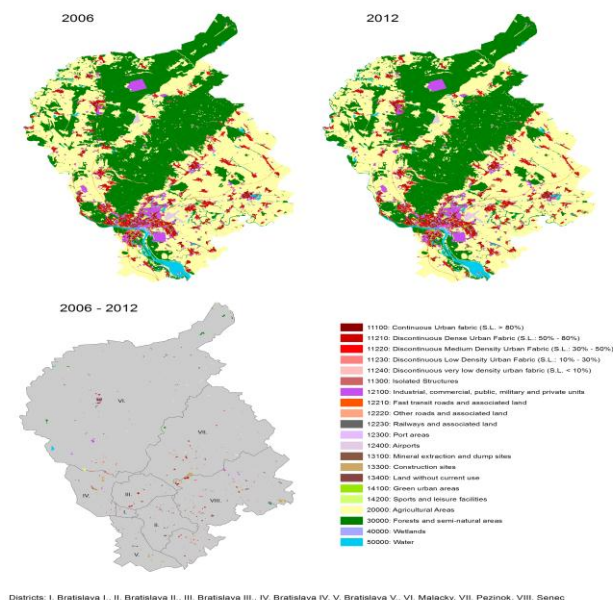


*Figure 4.1. The spatial distribution of UA classes of LUZ Bratislava for the years 2006, 2012 and their changes in 2006-2012.*

## *Monitoring of the Dynamics of Built-up Areas*

The aim of the monograph *Monitoring of the Dynamics of Built-up Areas* recently published by the IG SAS is to present topical trends in monitoring of built-up areas on various levels of spatial and thematic resolution using remote sensing data. Identification and quantification of recent changes in urbanised landscape, possibilities of their visualisation, and comparison of the available data sources in the assessment of the dynamics of built-up areas is demonstrated on study areas selected with special focus on Slovakia.

Individual chapters present analyses of the state and dynamics of built-up areas based on different databases (e.g., CORINE Land Cover – CLC, UA, High Resolution Layer Imperviousness) derived from satellite data. Assessment of changes in built-up areas at European level applying CLC databases is focused on the LU/LC changes connected with transformation of agricultural areas, forest and semi-natural areas into urbanised areas (land cover flow urbanisation – LCFU). CLC databases were also used for the assessment of urbanised landscape at the level of individual administrative regions (NUTS 3 level) in Slovakia. Fig. 4.2 present change of agricultural land, forest, wetland and water areas, (CLC classes 21, 22, 23, 24, 31, 32, 33, 41, 51, and 52) into urbanised areas (11, 12, 13, and 142) in administrative regions of Slovakia in 2000-2012. In 2000-2006 the overall increase of built-up areas was 3299.5 ha. Similar trend in the development of built-up areas in Slovakia also continued in 2006-2012 and the increase of built-up areas in all regions of the country was more intensive than in the previous period reaching in total 7405.4 ha.

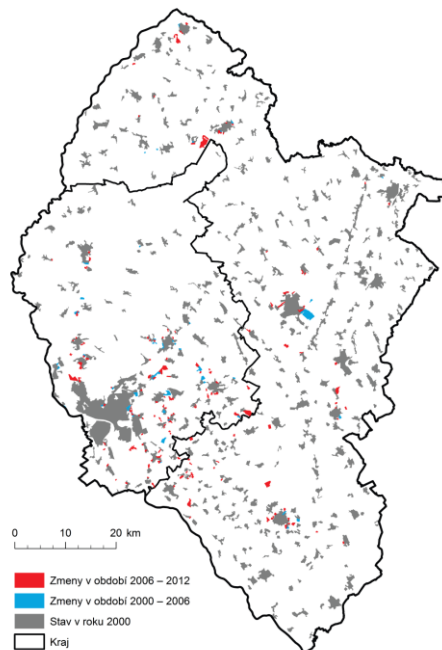


*Figure 4.2. Increase of artificial areas in Trnava and Bratislava regions in 2000-2012 based on CLC data.*

CLC data layers play important role in the monitoring of urban fabric at European to national levels. The detailed analysis of LUZ Bratislava applying the UA change map is an example of more detailed approach suitable for documenting changes of LC at the level of regions, particularly the metropolitan regions (LUZ) of selected European cities and their hinterlands. The basic information about the land cover/land use of urbanized areas in selected European cities is retrieved from the high-resolution satellite images. UA data were employed here in also in a reclassified (simplified) binary form, in order to evaluate fragmentation of landscape of LUZ Nitra and its changes. The Landscape fragmentation tool (LFT v2.0) is used to map the landscape fragmentation in Nitra district. The results indicate significant increase of landscape fragmentation in the period 2006-2012 (Fig. 4.3). Non-fragmented core areas decreased by 1.1%.

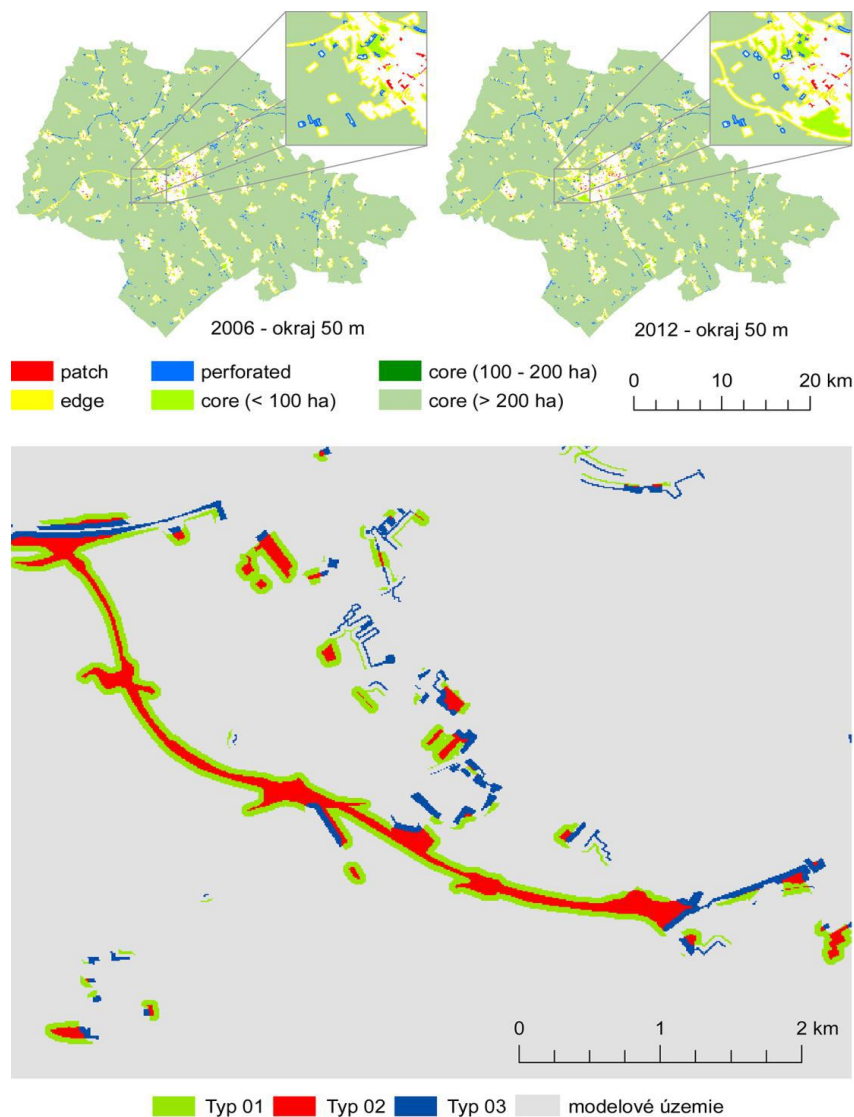


Figure 4.3. Changes in landscape fragmentation in Nitra district based on Urban Atlas data.

## Application of UAV technologies

UAV technologies generally allow financially and time-effective mobile mapping and detailed capture of spatial phenomena at large scales and can be considered as a bridge between the classical field mapping and using aerial photographs. IG SAS continues with monitoring of avulsion channel near the Stropkov (formed during flood events in year 2010). Carrier Hexakopter XL was used for obtaining 3 sets of images in monitoring campaigns in year 2012 and 2014 (April and July). Datasets cover area with approximately dimension 250 m (width) and 420 m (length). For spatial referencing were used 13 – 21 ground control points (GCP) and Agisoft PhotoScan software for imagery data processing (Fig. 4.4). Overall, been successfully processed 78 (in year 2012) images, respectively 259 (in 4/2014) and 375 (in 7/2014) and bank cliff retreat in the period of 24 months about 7.5 m was identified.

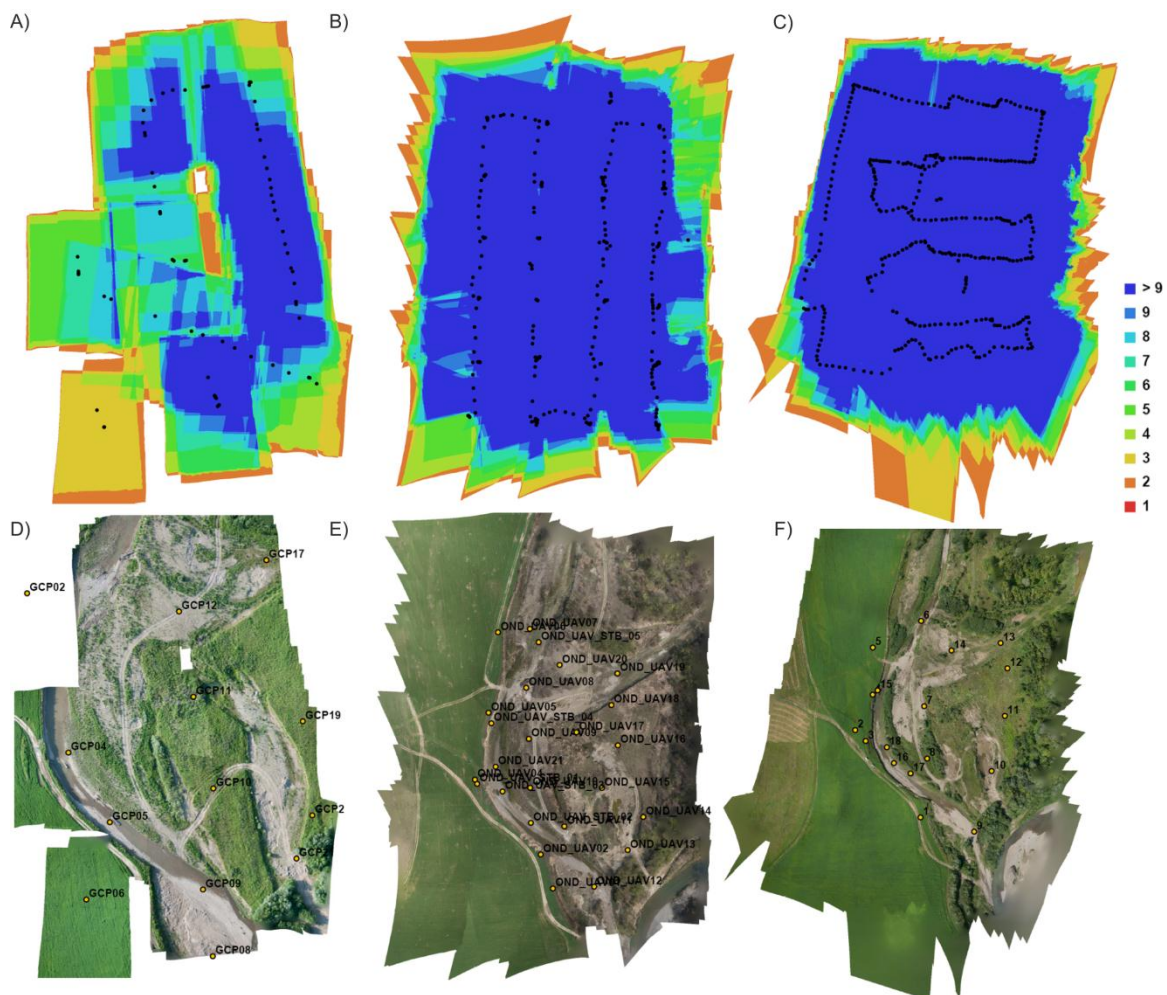


Figure 4.4. Images overlap in 2012 (A), in April 2014 (B) and June 2014 (C) and GCPs distribution on the orthophotos from 2012 (D), April 2014 (E) and June 2014 (F).

Monitoring of slope deformation in Svätý Anton village in central Slovakia started in 2014 (Figures 4.5). Compared to terrestrial LIDAR scanning, data acquisition of landslide area (approx. 200 x 170 m) based on UAV

(Unmanned Aerial Vehicle) takes about 8 minutes. The point cloud (approx. 60 mil. points), 3D mesh, shaded relief and orthophoto are results of aerial mapping. Precise mapping allows to use dataset as a base for creating DTM or DEM and subsequently for computation of morphometric parameters.

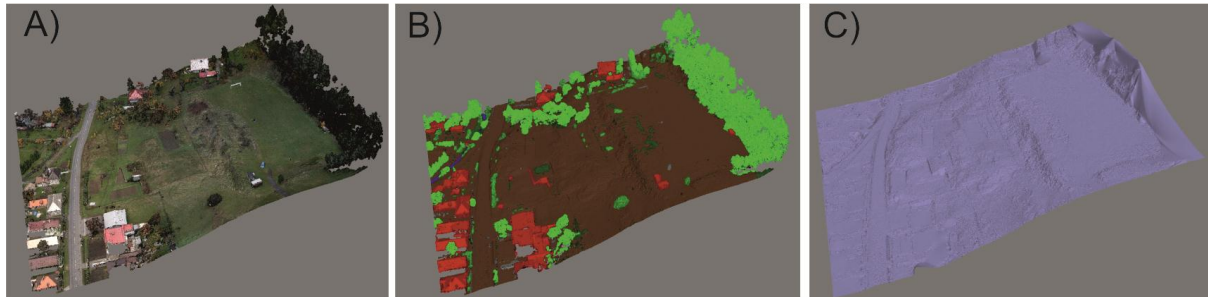


Figure 4.5. Dense point cloud (A), point cloud classes (B, 54 607 748 points creates the point cloud) and solid model of digital terrain model from TIN (C).

One of the latest campaigns started in October 2015 and focused on the braided-wandering Belá River in northern Slovakia, where channel narrowing and incision is evident (Fig. 4.6). Small hydropower plant bypassing the main channel was constructed and several landslides occurred in the places where river undercut Pleistocene terraces. Datasets cover area of the river in the length 1.3 km and for data processing were used more than 1700 images in Agisoft PhotoScan software (Figure 4.6). Orthophoto and digital terrain model was generated in pixel resolution 5 cm.

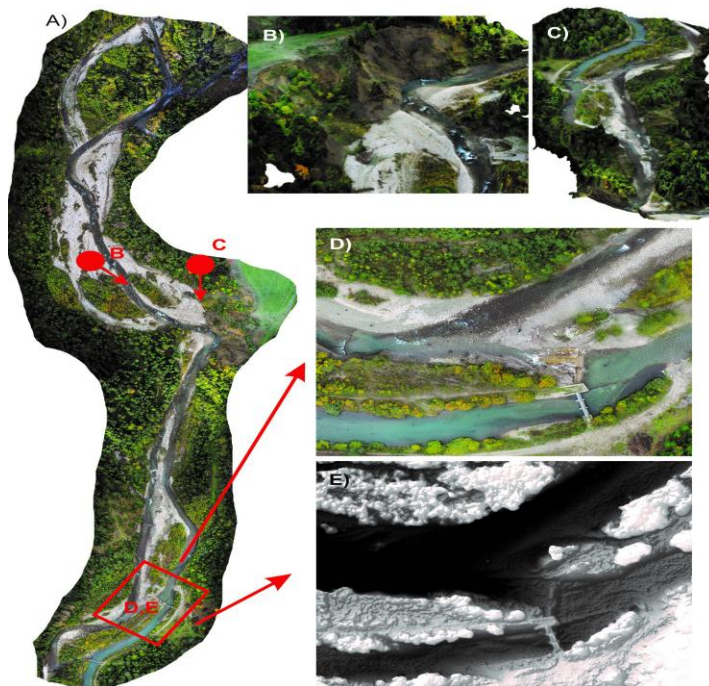


Figure 4.6. Orthophoto of 1,3 km long river reach (Belá) near Vavrišovo (A) and photorealistic 3D model of surface (view B, C). Details of orthophoto (D) and digital surface model (E) with pixel resolution 5 cm.

## **Slovak Environmental Agency (SEA) in Banská Bystrica**

Activities of the SEA were concentrated on the solution of **Copernicus** programme and **GIO Land** project:

### ***Copernicus***

Programme Copernicus (until the end of 2012 the name of the programme was G.M.E.S) is European programme for Earth Observation. In the years 2014 and 2015 programme Copernicus entered its operational stage. The work on EU level was concentrated on cooperation with Copernicus Committee, Copernicus Security board, GMES User forum and newly established Copernicus Ground segment task force and commenting on the EU level technical and legislative documents regarding the programme. In February 2015 the Slovak Republic signed a Cooperating state contract with ESA. With this Slovak Republic entered second stage of the procedure of accession for ESA. In June 2015 first Slovak organizations entered the ESA PECS call.

At the national level Slovak national Copernicus working group was established in May 2014. The group aim is the coordination of programme Copernicus related activities on national level and dissemination of information related to programme Copernicus. The group was established by the Ministry of Environment of the Slovak Republic. The members are from Ministry of Education, Science, Research and Sport, Ministry of Interior, Slovak Hydro-meteorological Institute and Slovak Environment Agency. Ministry of Interior of the Slovak Republic provide a contact for Copernicus Emergency service for Slovak users. With the start of ESA Sentinel Data HUB and Sentinel 1 and 2 data availability Slovak Environment Agency distribute Sentinel 1 and 2 satellite images for Slovak Republic on demand.

### ***GIO land monitoring***

Slovak Environmental Agency (SEA) joined the activities in project “Initial Operations (GIO) Land Monitoring 2011 – 2013 in the framework of regulation (EU) No 911/2010”. Project was coordinated by European Environmental Agency (EEA). The contract between SEA and EEA was signed in October 2012. Works on tasks of the national level were continued in period 2013-2014.

### ***CORINE land cover – part***

CORINE land cover inventory 2012 (CLC2012) was verified and was finished on September 2014. Final products of CLC2012 (revised CLC2006, status CLC2012 and change layer CHA2006-2012) were uploaded on CDR (Central data repository). All of the time horizons CLC data are available for free through web feature services (WFS) and web map services (WMS). WFS

were started in 2015 on geoserver SEA (<http://maps.geop.sazp.sk/web/>). Satellite mosaics that were used for interpretation are available too.

#### *High resolution layers – part*

All of the high resolution layers were verified by Slovak verification team. Enhancement layers for Forest HRL were prepared in 2013 and were accepted in 2014. Enhancement layers for HRLs were prepared and accepted in 2014. The products HRL without HRL grassland are available through official Copernicus web site (<http://land.copernicus.eu/>).

### **National Agricultural and Food Centre – Soil Science and Conservation Research Institute (SSCRI) in Bratislava**

Remote sensing oriented projects and activities of the SSCRI:

#### ***Remote sensing control of area-based subsidies in agriculture (2014-2015)***

The subsidies play a key role in agriculture sector and contribute to the prosperity of agricultural subjects. The subsidies to agriculture sector represent major part of European budget and that's why there is taken an emphasis to the control.

On the following figure the distribution of the control sites can be seen. The Slovak Administration has chosen six control sites in 2014 defined by 228 km<sup>2</sup> in DUNA, 225 km<sup>2</sup> in KEMA, 400 km<sup>2</sup> in KOZA, 458 km<sup>2</sup> in LIMA, 693 km<sup>2</sup> in MONA and 513 km<sup>2</sup> in TONA. For the 2015 campaign the Slovak Administration decided to have also six control sites defined by 389 km<sup>2</sup> in ALFA, 761 km<sup>2</sup> in BETA, 790 km<sup>2</sup> in GAMA, 211 km<sup>2</sup> in JOTA, 160 km<sup>2</sup> in KAPA and 320 km<sup>2</sup> in ZETA (Figure 4.7). They cover approximately 5.4 % of the applications in 2014 and 7.4 % of the applications in 2015.

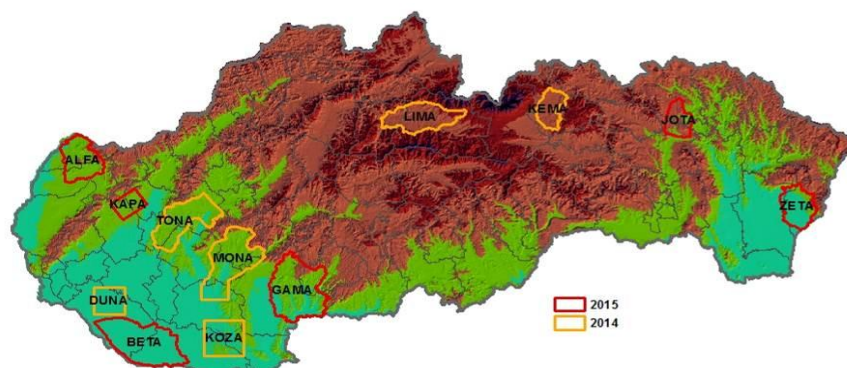


Figure 4.7. Localization of the controlled sites in campaigns 2014 and 2015.

In control procedure a set of high resolution (HR) multispectral images as SPOT 6, SPOT 7 and UK-DMC 2 were used for precise identification of grown crop (Figure 4.8). Two HR acquisition windows were used: HR-1 and HR+1. To control the cultivated area and the usage Very High Resolution (VHR) images from WorldView 2 and 3, GeoEye1 and WorldView 1 and KOMPSAT 3 as back-up images were used per each site (Figure 4.9). Features which have to be excluded from the parcels like field path, straw stacks, midden, etc. are well recognisable on these images.

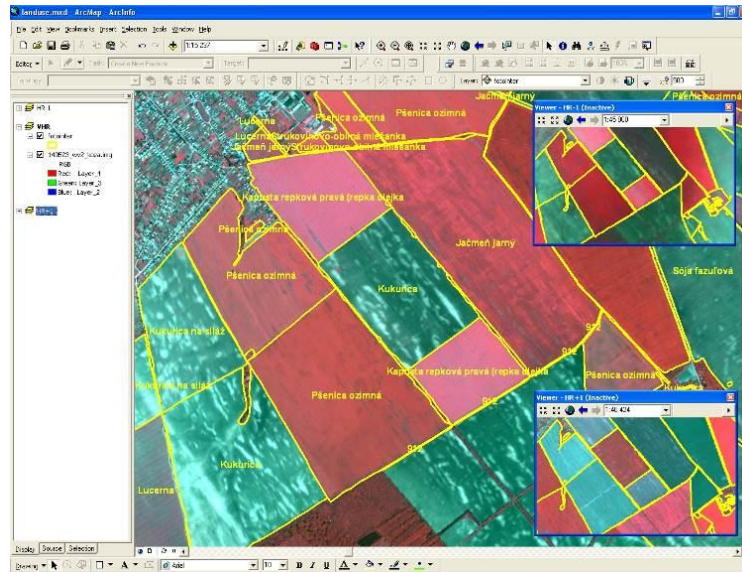


Figure 4.8. Example of land use check on HR images from different acquisition windows.

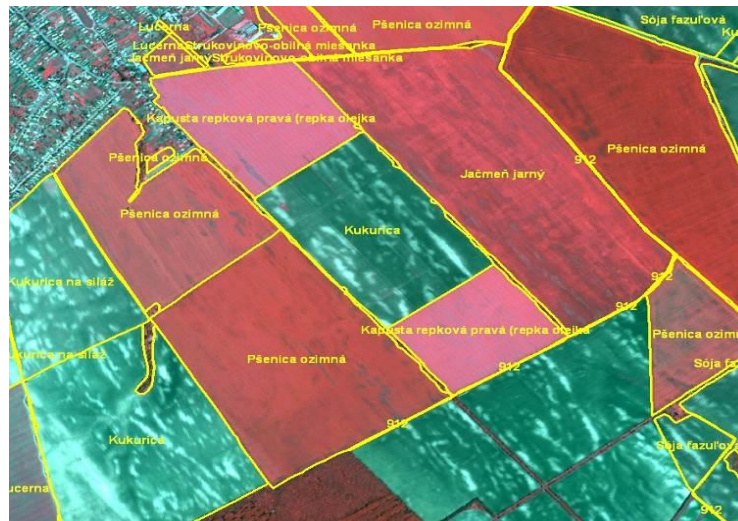


Figure 4.9. Example of boundary check on WorldView 2 image (VHR).

The CAPI has been adjusted to the annual conditions of the regulations of subsidy schemes. Approximately 61,750 graphical annexes were printed and delivered to the farmers where they indicated the agricultural parcels they cultivate.

In 2014 campaign the total number of applicants was 17,751 the number of dossiers controlled with remote sensing was 964. The total area controlled was 110,267.80 hectares, with 3903 reference parcels. There were 13,345 agricultural parcels to control (in 2 schemes), on average 14 parcels/farmer and 114.39 hectare/dossier. According to the final diagnosis, which summarizes the diagnoses of the conformity and completeness tests at dossier level, 439 (45.54%) dossiers were accepted for Single area payment scheme, 403 (41,80%) for Complementary National Direct Payment scheme and no dossier for Special Areas Of Conservation and Special Protection Areas (for birds) (Figure 4.10).

In 2015 campaign the total number of applicants was 18,422, the number of dossiers controlled with remote sensing was 1374. The total area controlled was 113,968.66 hectares, with 3661 reference parcels. There were 19,906 agricultural parcels to control (in 11 schemes), on average 14 parcels/farmer and 82.95 hectare/dossier. According to the final diagnosis, which summarizes the diagnoses of the conformity and completeness tests at dossier level, 554 (40.32 %) dossiers were accepted for Single area payment scheme, 3 (0.22 %) for payment for agri-environment – climate action, 20 (1.46 %) for area facing natural constraints, 545 (39.67%) for Complementary National Direct Payment scheme, 1 (0.07 %) for payments on organic farming, 2 (0.15 %) for payment for agricultural practices beneficial for the climate and the environment, 2 (0.15 %) for coupled direct payments for vegetables with high labour inputs, 1 (0.07 %) for coupled direct payments for vegetables with very high labour inputs and no dossier for coupled direct payments for tomatoes and hops and no dossier too for Special Areas of Conservation (Figure 4.10).

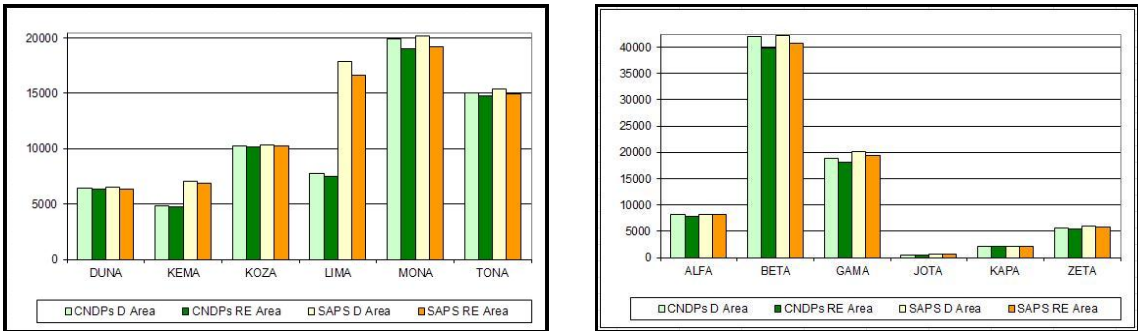


Figure 4.10. Declared and retained area (ha) for schemes CNDPs and SAPS per site.

**Remote sensing within crop yield and crop production forecasting (2014-2015)**

*Monitoring of Crop Conditions and Crop Monitoring*

Regional monitoring of natural crop conditions aims to study the influence of weather (coupled with soil) on crop growth and crop development during current vegetation season.

Day and night land surface temperature and also NDVI (Normalized Difference Vegetation Index) are derived from NOAA's AVHRR sensor (Figures 4.11 and 4.12).

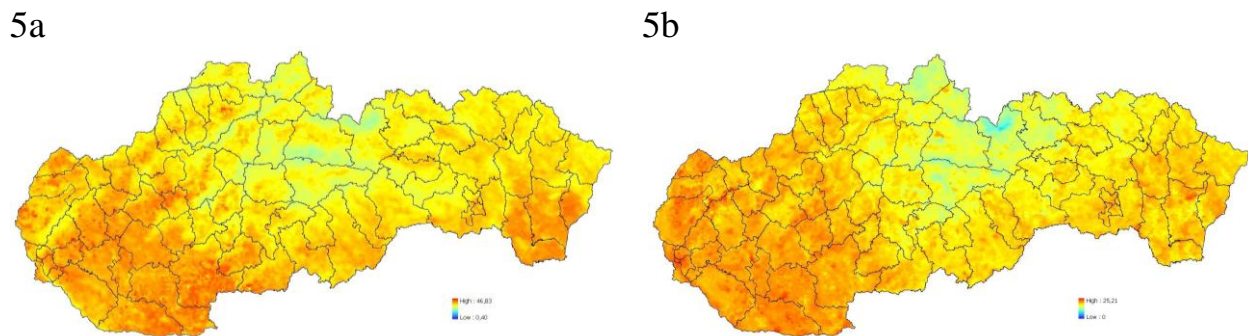


Figure 4.11. Day (5a) and night land surface temperature average (5b) in the third decade of July 2015.

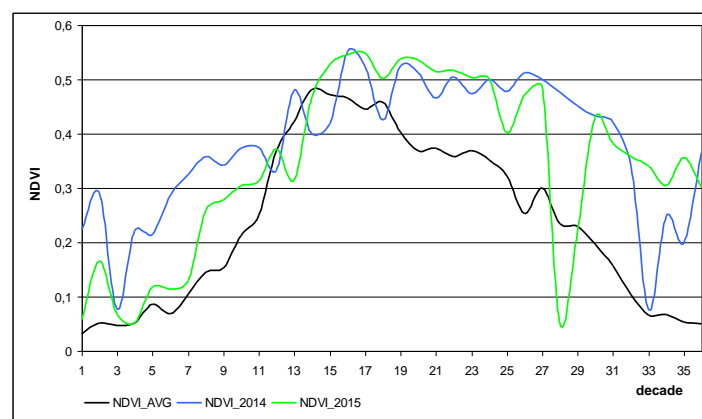


Figure 4.12. Comparison of NDVI development in 2014, 2015 and NDVI long term average.

### Crop yield forecasting

The aim of the crop yield and crop production forecasting is to provide the most likely, scientific, as precise as possible and independent forecast for main agricultural crop yields for Ministry of Agriculture and Rural Development of the Slovak Republic and for the public.

National Crop Yield and Crop Production Forecasting System has been created on SSCRI and is based on three different principles which are applied to specify vegetation indexes as biomass development stage and biomass development:

- Remote Sensing method – method of interpretation of vegetation indicators (as NDVI or DMP- Dry matter development) from satellite images (mainly from low resolution satellite sensors as NOAA AVHRR and SPOT Vegetation satellite system);

- Bio-physical modelling (WOFOST model) and simulation of vegetation indexes (mainly TWSO – Total Dry Weight of Storage Organs and TAGP - Total Above Ground Production). In WOFOST, weather and phenological data, soil hydro-physical data and crop physiological data are utilized as model key inputs;
- Integrated assessment method, which means the implementation of specific meteorological and vegetation indicators in the statistical analysis, assesses the impact of weather on the projected harvest. Integrated estimate summarizes a wider range of disparate indicators and indices that are currently for the purposes of forecasting yields and consequently the production of crops used.

The crop yield and crop production forecasting is carried out for main agricultural crops – winter wheat, spring barley, oil seed rape, grain maize, sugar beet, sunflower and potatoes. The forecasts are reported six times per year – in the half of May, June and July for “winter and spring crops” and in the end of July, August and September for “summer crops”. The forecast results are interpreted at national level as well as at NUTS3 and NUTS4 level. The example of crop yield forecasting in 2015 can be seen in the Figure 4.13.

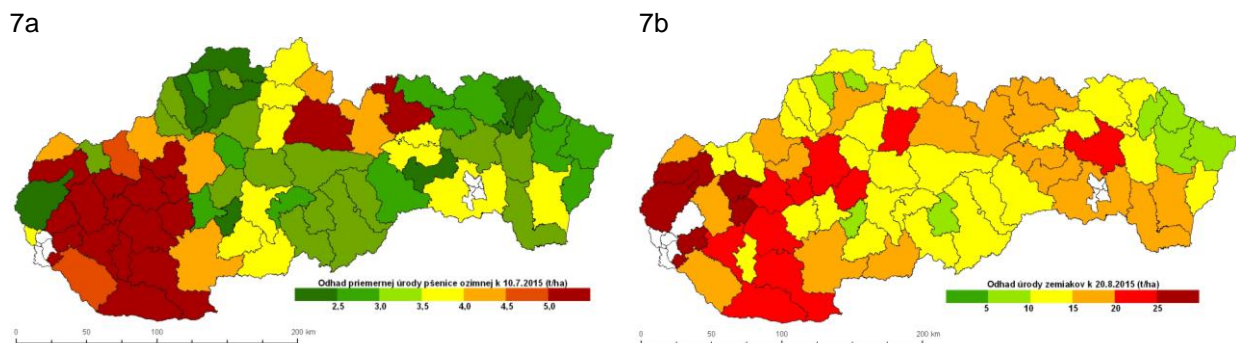


Figure 4.13. Example of crop yield forecasting with remote sensing in first decade of July in 2015 for winter wheat (7a) and in the second decade of August for potato (7b).

### National Forest Centre (NLC) in Zvolen

Remote sensing research activities of the NLC were aimed at tree basic topics:

- Applications of airborne laser scanner technology in the forest management
- Satellite-based observation of forest decline.
- Forest management for enhancing hydrological role of forest

## *Applications of airborne laser scanner technology in the forest management*

### *Airborne laser scanning platform (ALS)*

Remote sensing research activities related to the airborne laser scanning (ALS) over the years 2014-15 were solved based on four projects i) Centre of excellence “Decision support in forest and country (ITMS:26220120069), ii) Innovative methods of inventory and monitoring of the Danube floodplain forests using 3-D Remote Sensing technology (HUSK/1101/1.2.1/0141), iii) Systems of optimal forest management for enhancing the hydrological role of forests in preventing the floods in Bodrog river catchment (HUSKROUA/1101/262), iv) Innovative methods of close-to-nature forest management (APVV-0439-12).

The common goal of research projects was to develop the algorithm usable in the frame of forest inventory and transportation survey based on ALS data. For all study areas situated in different ecosystems condition (from monoculture to natural forest) were taken needed aerial (multispectral images and point clouds) and ground data (field reference data contained the measured positions and dimensions more than 10,000 trees).

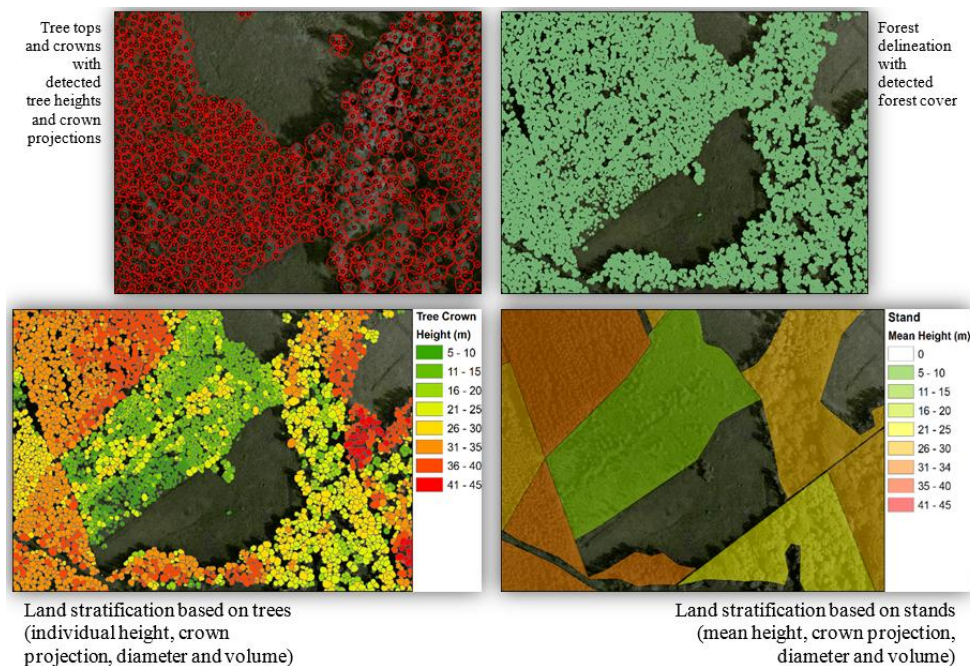


Figure 4.14. Results of reFLex algorithm for forest inventory based on ALS.

### *Algorithm for forest inventory based on ALS*

The proposal of algorithm is implemented in reFLex (remote Forest Land explorer) software, which was developed by the National Forest Centre (Slovakia). The objective of such implementation is to develop an application, which is easy to use in forestry practice (Sačkov et al., 2014):

The input file is a classified point cloud that contains ground and vegetation classes. The initial procedures are applied to transform the point cloud to a regular mesh and to reduce the number of points in the input file (Point cloud tiling; Height restriction). These operations produce a point cloud that is further used for an iterative search for treetops and tree crowns (Finding the local maxima; Geo-Dendrometric test; Delineation of tree crowns). Finally, the outputs of all procedures are exported to point and polygon vector files in the ESRI shp format (Figure 4.14).

#### *Algorithm for transportation survey based on ALS*

For the purposes of the automated evaluation of the forest roads, the algorithm developed for skidding distance calculation was performed in ArcGIS 10.1 software (Esri). Skidding distance is a combination of winch distance (the distance from the forest stand up to the skidding road), and hauling distance (the distance along the road, from the place where the winch distance ends up to the hauling place).

The algorithm is created from connected operations which are aggregated into three steps (Sačkov, Smreček, Tuček, 2014):

Step 1a: The goal of this step is winch distance calculation. The input source is DTM with spatial resolution and the forest road layer. For each cell of DTM raster layer, the distance over the terrain to the forest road was iteratively calculated. The result was the raster layer, which was converted into a vector point layer.

Step 1b: The goal of this step is hauling distance calculation. The input source is DTM with spatial resolution and the forest road network with hauling places. Forest road was derived from ALS data, and the hauling places were taken from the terrain survey. Using the map algebra was assigned the value of DTM to every cell of roads. Thereafter for each cell of forest road raster layer, the distance over the terrain to the hauling place was iteratively calculated. The result was the raster layer, which was converted into a vector point layer.

Step 2: The goal of this step is skidding distance calculation. The input source is layers from steps 1a and 1b. In these layers, the nearest points were identified and then the same identifier (ID) was assigned to them. Based on the added identifier, the layers were connected and then the distance calculated in steps 1a and 1b was summed. The resulting vector point layer was converted into the raster layer. After overlapping this raster layer with the layer representing the forest stands, using the zonal statistics tools, the skidding distance for every forest stand was calculated. After joining the resultant table with the vector layer representing forest stands, the output of step 2 was created (Figure 4.15).

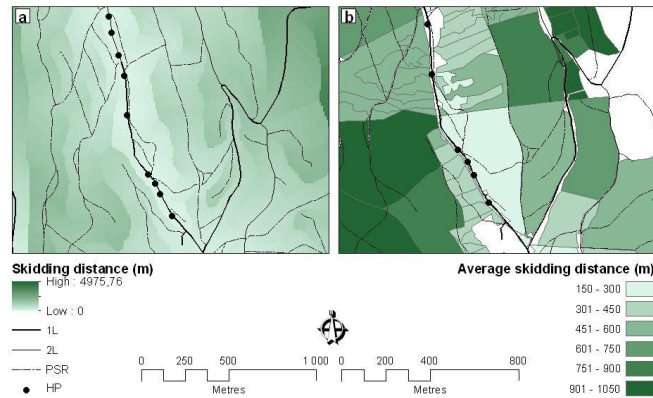


Figure 4.15. Map of skidding distance: (a) Skidding distance – raster layer; (b) Average skidding distance – vector layer. Note: 1L, 2L – Hauling roads of category 1L and 2L; PSR – Permanent skidding road; HP – Hauling place.

### Satellite-based observation of forest decline

The activities were focused on further development of the web service STALES [www.nlcsk.org/stales](http://www.nlcsk.org/stales) (Figure 4.16). The system is proposed to inform forest owners and forest state administration about the actual condition of forest stands and its changes. Up to know there have been added satellite images from all over Slovakia from 1990, 1996, 1998, 2000, 2003, 2006, 2007, 2008, 2009, 2010, 2011, 2012, 2013, 2014 and 2015.

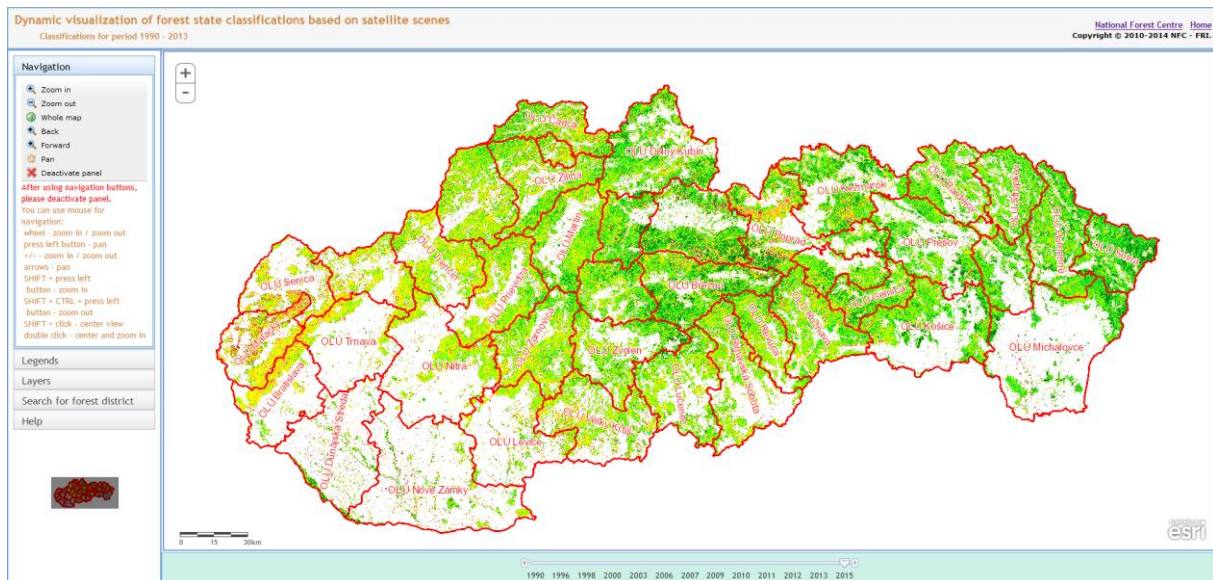


Figure 4.16. Web service <http://www.nlcsk.org/stales/> – map application for dynamic visualization of forest health condition classifications from Landsat.

The individual images were created nationwide mosaic, from which we derived forest damage to each of those years. The service is based on Landsat satellite images in spatial resolution of 30 x 30 meters. Mosaics are created from

the composition of Landsat bands in false colours, i.e. 4/5/3 - near-infrared, mid-infrared and red band.

Mapping applications are prepared so that boundaries of forest districts are visible at the scale of 1:100 000 and the boundaries of forest compartments at the scale of 1:20 000. STALES has been gradually extended to reach into the current form when service consists of 4 map applications:

Map application 1 - visualisation of satellite scenes and forest health condition

Map application 2 - a comparison of satellite scenes from different time periods

Map application 3 - dynamic visualization of actual and historical satellite scenes

Map application 4 - dynamic visualization of forest health condition classifications

The English version started operated in March 2015.

### **Forest management for enhancing hydrological role of forest**

Evaluation of the forest cover changes in transboundary region of Slovakia and Ukraine was complemented within project “HYDROFOR: Systems of optimal forest management for enhancing the hydrological role of forests in preventing the floods in Bodrog river catchment (HUSKROUA/1101/262)”. Evaluation was based on the Landsat satellite imagery (granules 026/185 and 026/186) as the main data source used. The main reason for data source selection was the long time series of Landsat satellite scenes and free-of-charge access. Period 1990-2013 was covered. The time series of Landsat scenes were processed and analysed. Tree cover maps (at the beginning and end of the period) were developed by classifications of satellite scenes, using training areas in both Slovakia and Ukraine. Database of forest stands, maintained by NFC, was utilized for definition of training areas. Maps of positive and negative changes (forest gain and loss) were developed as well. Results showed, that within 4 main sub-watersheds of the study area (watersheds of rivers Ondava, Laborec, Uh and Latorica), tree cover gain ranged between 3.1 and 4.3%, tree cover loss from 1.2 to 2.1%. Moreover, loss of tree cover was caused mainly by planned felling of forest stands and tree cover will be restored again. As a result, the total share of tree cover in the whole catchment raised from 49% to 51.1% within period 1990-2013. Output maps were published using Hydrofor web map application (<http://www.forestportal.sk/sites/hydrofor>) (Figure 4.17). Map of tree species composition was derived as well, showing distribution of the main tree species within Bodrog river catchment. The RS output were used as inputs for proposal of flood prevention measures.

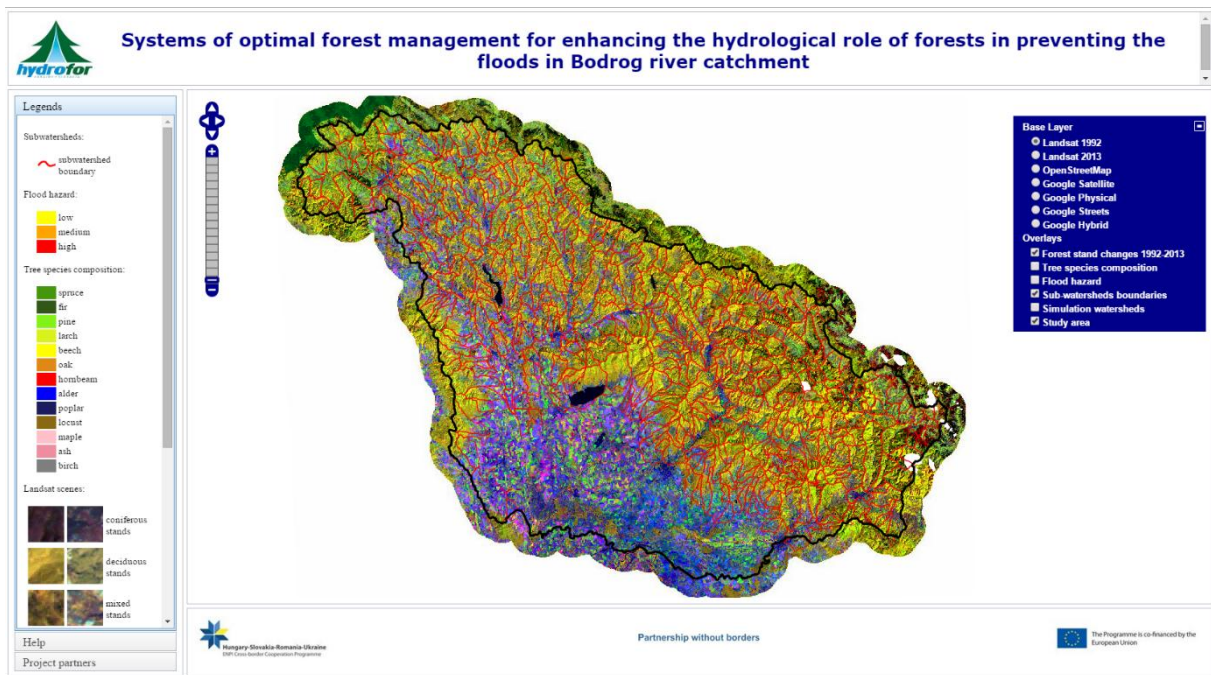


Figure 4. 17. Hydrofor project web map application with published outputs.

## 5. SPACE METEOROLOGY

*J. Kaňák, L. Okon, L. Méri, M. Jurašek, K. Hrušková, M. Zvolenský*

### 5.1 Evaluation of EUMETSAT Super Rapid Scan experiments

Convection Working Group of EUMETSAT and ESSL (European Severe Storm Laboratory) proposed first 2.5-minutes experiment using new MSG-3 satellite on 11-12 September 2012. On the base of successful results delegates of working groups STG-SWG and STG-OPSWG of EUMETSAT recommended to EUMETSAT Secretariat to carry out additional four experiments in 2013 during summer season using older MSG-1 satellite. These experiments were planned according severe weather forecasts provided by ESSL. After successful realization of all scheduled experiments huge amount of experimental data was obtained. Because of technical limitations of MSG SEVIRI imager for 2.5-minutes continuous measurements number of questions appeared:

- **While calibration of SEVIRI sensors during experiment could not run, what is their stability during the whole experiment period?**
- **Because of MSG satellite and scan mechanism mechanical construction constrains (15-minutes scan reduced to 2.5-minutes scan) how stable is the image geometry?**
- **Because of Sun sensor malfunctions on the satellite MSG-1 how precise is East-West and overall image rectification during the whole experiment?**

To answer these questions we decided to perform number of image sequence consistency checks.

#### Calibration stability tests

Tests were done by comparison of mean brightness temperature differences of measured scene with different satellites (MSG-1, 2, 3) which were operated in parallel.

Analyses of all experiments showed that shapes of calibration curves are very similar with evident diurnal changes, as it is shown on Figures 5.1 and 5.3. Position of maximum of each curve depends on angular distance between satellites and season (September, May, June, and July). Maximum temperature difference was observed during the day, minimum during the night. We consider the anisotropy of atmosphere and diurnal changes of brightness temperatures of scanned scene by different satellites as the most common features responsible for these differences.

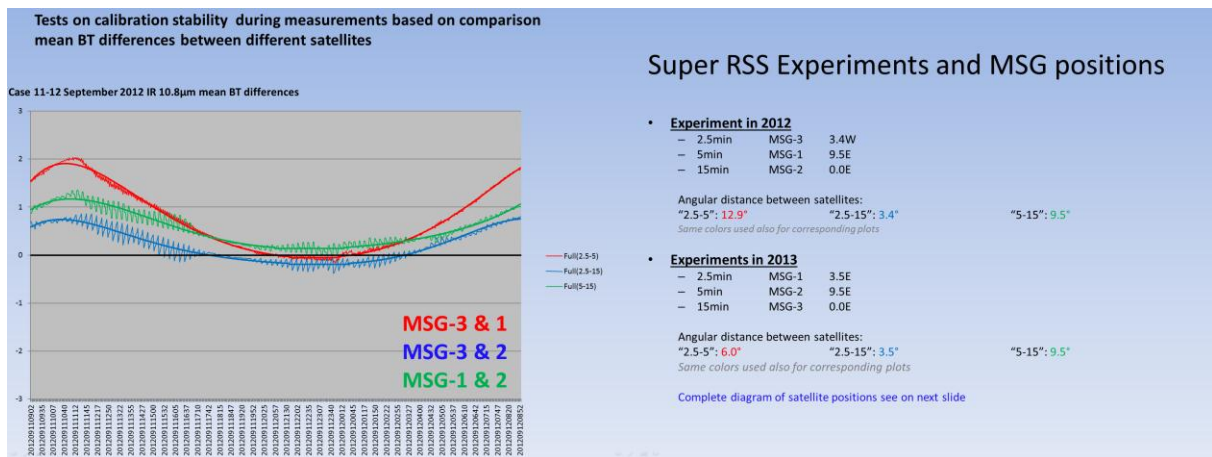


Figure 5.1. Comparison of BT differences (left panel) between couples of MSG satellites (right panel), which observed the same scene during all Super Rapid Scan experiments.

Bearing in mind anisotropy effects and maximum deviations of IR BT differences we can consider IR BT values of 2.5-minutes RSS consistent enough with similar IR BT values of 5 and 15 minutes scans. Calibration stability tests showed that all standard algorithms which are using IR BT values (e.g. NWC SAF, Land SAF and severe storms detection applications) can be applied to experimental dataset without any doubts.

## Image drift calculations

Image drift tests were done by two different methods. First method was based on correlation between two consecutive images of image sequence; second method used precise calculations of position of land surface features over clear sky areas. Results of both methods will be discussed in evaluation part of this report.

Correlation between two consecutive images in 2.5-minutes image sequence is usually high because of small temporal changes of scan scene (short steps in cloud displacement). But in case of some satellite or scan mechanism anomalies correlation decreases significantly and can indicate some defections of image rectification process.

Clear area mask we created for clear air regions identified over the image scene during daytime period of RSS experiment. Daily average, minimum and maximum from HRV and IR imagery was calculated. Then more RGB combinations (HRV max, HRV avg, IR min, HRV max, HRV max, IR max ...) were tested. Finally RGB (*HRV maximum, HRV average, IR maximum*) combination was selected for visual identification of clear air areas (cloudy free areas). Visual identification was done manually in Photoshop-like editor. Results of identified clear air areas are shown in Figure 5.2 in dark-green color.

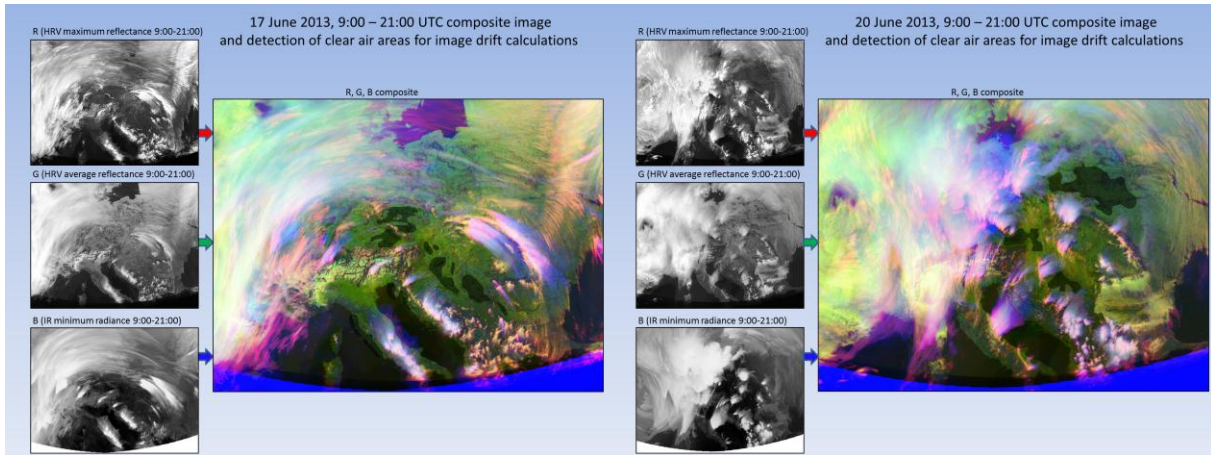


Figure 5.2 Examples of composite images used for separation of cloud free and cloudy areas (clear area mask preparation) before application of image drift calculations: Left for 17 June 2013 experiment, right for 20 June 2013 experiment.

Image drift calculations were based on definition of object's mass center, where for an object in a gray scale image, its *center of mass* is the point around which the gray of the object is equally distributed. In our case mass center coordinates were calculated for each image time slot over the areas defined by clear air area mask, using formula:

$$\mathbf{R} = \frac{1}{M} \sum_{i=1}^n m_i \mathbf{r}_i$$

Values of HRV pixel albedo and/or IR BT were used instead of  $m_i$  weights and pixel coordinates (x, y) represented vector  $\mathbf{r}_i$ . Mass center coordinates were calculated separately for  $x_i$  and  $y_i$  in EW and NS directions and for each timeslot ( $i=9:00$  to  $21:00$  UTC with step 2.5 minutes). Then relative image shift between consecutive time slots was calculated as:

$$\Delta x_i = x_i - x_{i-1} \quad \Delta y_i = y_i - y_{i-1} \quad \text{and} \quad \Delta R_i = \sqrt{(\Delta x_i)^2 + (\Delta y_i)^2}$$

Finally extremes in image shifts were estimated calculating changes of second order:

$$\Delta^2 R_i = \Delta R_i - \Delta R_{i-1}$$

## Evaluation of results

### a) Anisotropy effects

In the analysis of calibration stability mostly special effects, resulting from the anisotropy of the atmosphere were observed particularly in the visible, but also in the infrared part of the spectrum. These effects are manifested regularly on daily base as changes in average values of radiance, brightness temperature and albedo. Course of these changes were slightly different for different experiments and corresponded to different inclination of the Earth's axis from season to season, as it is shown on Figure 5.3. Significant effects were

only observed during the Sun set or Sun rise close to the terminator (twilight, rapid changes of surface temperature).

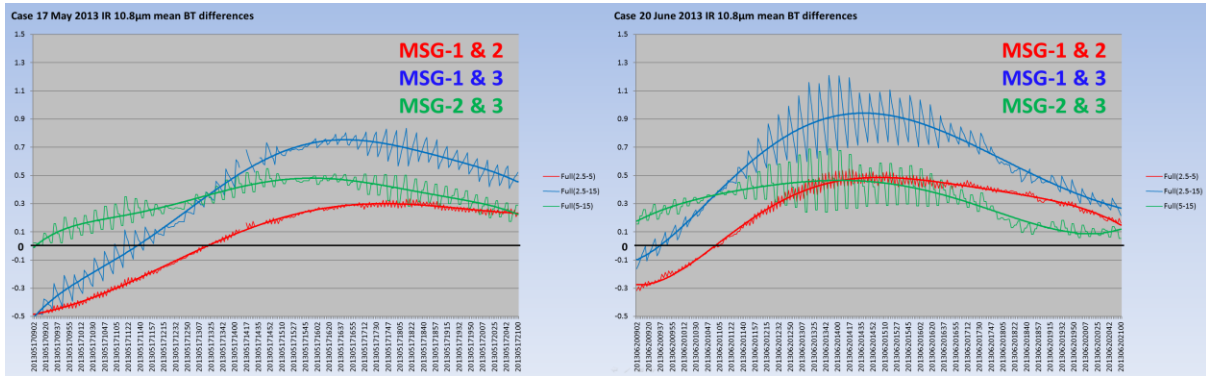


Figure 5.3. Tests on calibration stability of sensors based on comparison of mean brightness temperature differences between different satellite couples – MSG 1 & 2, MSG 1 & 3, MSG 2 & 3. Case 17 May 2013 is on the left, case 20 June 2013 on right.

### b) Regular and irregular image shifts

Calculation of the correlation between two successive frames showed regular periodical oscillations of the correlation values with a period of 30 minutes in case of 20 June 2013 (Figure 5.4 right panel). In other cases from 2013 these periodic oscillations were recognised only with the effort because they were often disturbed by irregular drifts of higher order (Figure 5.4 left panel). Similar oscillations were not observed during first experiment from 11 September 2012, which was done by new MSG-3 satellite. We suppose that periodical 30-minutes oscillations relate to technical status of MSG-1 satellite after 11 years of operations. The reason of discontinuities is wobbling of image in EW direction, namely the minimum of correlation is related to the fast jump of image in direction from West to East.

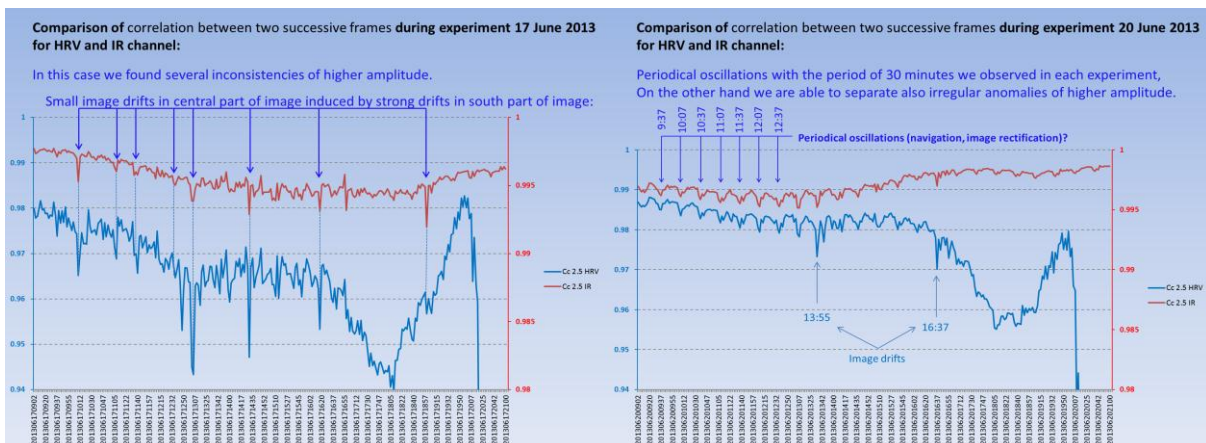


Figure 5.4 Results of consecutive image correlation and detection of inconsistencies in image sequence, which correspond to significant satellite wobbling. On the left panel case 17 June 2013 four significant shifts were detected, while the case 20 June 2013 on right panel was very stable, only periodical 30-minutes oscillations resulting from satellite scan mechanism performance were observed. Red lines correspond to IR, blue lines to VIS imagery.

Explanation of irregular drifts was possible by detailed analyses of cloud-free areas movement. By visual inspection of imagery we found out that extreme shifts of cloud-free area mass centres were detected in the same timeslots when extreme line shifts were observed in southern part of the image. In spite of the fact that cloud-free areas were selected northerly to avoid these parts of image (affected by return point of scan mechanism), we were able to detect 1 or 2 pixel drifts in average over central parts of images.

### c) Comparison of image drifts in different experiments

Detailed monitoring of mass center movement of cloudless parts of the image showed that the experiments from 11 September 2012, 17 May 2013, 20 June 2013 and 29 July 2013 provided very stable imagery with an average positional accuracy of 0.1 to 0.2 pixels. Only in the experiment from 17 June 2013 we have identified several more pronounced short-term image displacements with amplitude of 2 pixels per timeslot (Figure 5.5 left panel). These shifts are evident also in the visual observation of high-speed video sequence of cloud-free areas.

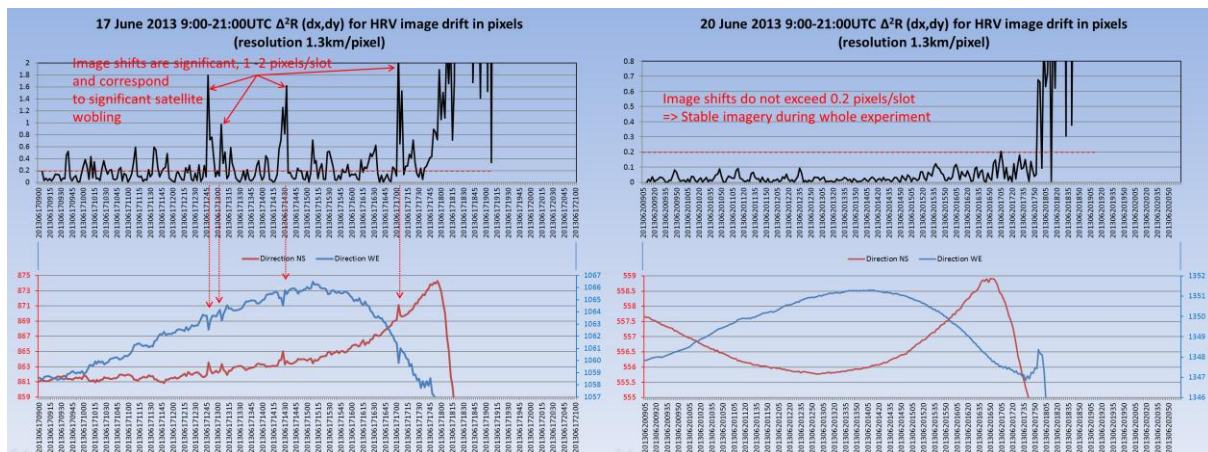


Figure 5.5. Image drifts magnitudes in pixels. Red line represents drift in North-South, blue line in West-East direction, and black represents combined drift. Only during 17 June 2013 experiment (left panel) image drifts were significant. Imagery during 20 June 2013 experiment (right) was very stable.

### d) Overall evaluation of experiments

Finally, the experimentally obtained 2.5-minutes super RSS data by MSG satellites are of high quality in terms of the calibration stability and georeferencing, apart from a few timeslots of 17 June 2013, notably slots 10:10, 11:07, 11:40, 12:47, 13:05, 14:30, 16:17, 16:57 and 19:06. Also the slot 14:15UTC from 17 May 2013 shows noticeable image shift of value 0.4 pixel per slot. Image quality is partially lower also in the south part of scanned area which is affected by return point of scan mechanism, but this region was excluded from checks performed by this study.

### e) Meteorological consequences of results evaluation

From meteorological point of view small scale features of severe storms, namely overshooting tops observed in standard scan mode of MSG 15-minute imagery, exhibit random behaviour with observing time below scan time interval. But also in shorter scan intervals (5-minutes RSS and 2.5-minutes super RSS) this random behaviour retains observable (Figure 5.6).

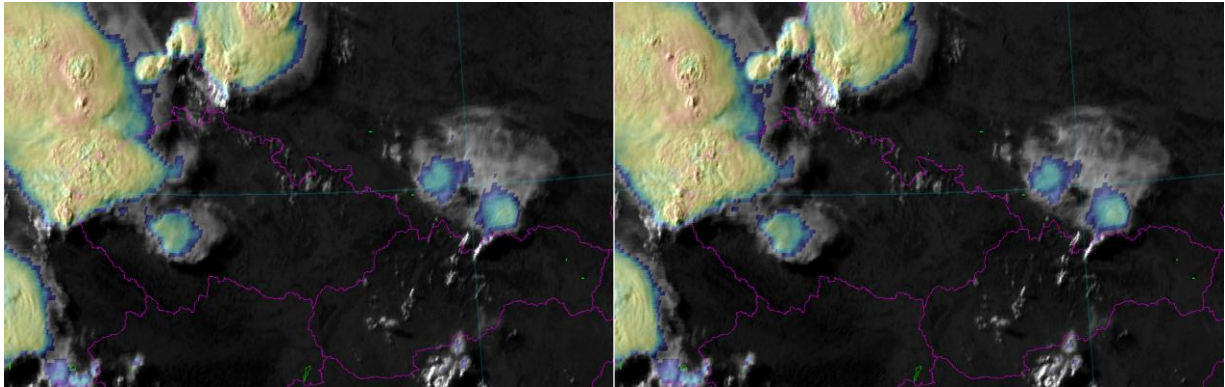


*Figure 5.6. Couple of images from 20 June 2013 super rapid scan experiment. Left is from 16:37:30 UTC, right from 16:40:00 UTC.*

Strong convection over Germany and west borders of Czech Republic exhibited overshooting tops over cloud anvils. It is evident from these two images that cloud top features of storms were changed in such a small time period of 2.5 minutes.

This is the reason why study of image calibration, navigation and rectification is important. Identification of high image quality is important for confident usage of experimental data in any other studies. Next shortening of scan time intervals should refer in future also to higher space resolution, which is promising by next generation of geostationary satellites in the frame of MTG program.

## **5.2 Project H-SAF of EUMETSAT, Phase CDOP2 – SHMÚ validation activities**

Within the H-SAF project precipitation product validation has to be fulfilled by means of ground based weather radars. This implicates the needs to quantify the radar data quality before using these data for validation. Indeed, the radar observations are conditioned by several uncertainty sources that need to be properly evaluated and compensated for, before using the related rainfall products as benchmark for any satellite-based precipitation estimates. To accomplish this task it is necessary to manage the raw radar data, possibly adopting the same processing chain. This is to summarize the proposed data quality scheme and provide practical information to be used for the implementation phase. Such study was done in cooperation with H-SAF leading entity (DCP Italy) and based on this study SHMÚ in 2015 participated actively in practical realization of this task in a form of visiting scientist activity (VSA) titled “Common Radar Rainfall Rate Estimation and Quality Control Procedure for Ground-validation of the H-SAF rainfall products”.

In the frame of this VSA SHMÚ delivered complete standard programming package which contain following functionality:

- Main tool to produce surface rainfall intensity radar product
- Tool to create static clutter maps
- Tool to calculate partial radar beam blockage
- Tool to calculate averaged vertical profile of reflectivity (VPR)
- Set of tools to manage hdf5 radar data format

The package contains full set of configuration files and documentation (product user manual), all standardized according EUMETSAT documentation regulations.

SHMÚ continued also in standard validation of HSAF operational products and hydrological validation. For hydrological validation of satellite products it is necessary to perform integration of precipitation intensities in time. We used various approaches related to specific product:

### **Approach for product H03:**

Precipitation intensities are averaged from four 15-minutes measurements (hh:12, hh:27, hh:42 and hh:57) of MSG satellite. Quality of output is highest when all 4 inputs are available, and lowest, when only 1 input is available. When no input is available, no data is assigned to selected timeframe (hour). Output of this procedure is 1-hour cumulated precipitation field over HSAF H03 domain.

#### **Approach for product H04:**

Precipitation intensities are averaged from two 30-minutes measurements (hh:00 and hh:30). Quality of output is highest when 2 inputs are available, and is lowest, when only 1 input is available. When no input is available, “no data” flag is assigned to selected timeframe (hour). Output of this procedure is 1-hour cumulated precipitation field over HSAF H04 domain.

#### *Integration of cumulated precipitation in space as input into hydrological models:*

For products H03, H04 and H05 procedure for common integration in space is used. This integration is based on summing all grid points of the product, which are geographically lying inside the test river sub catchment. Averaged value of all pixels is calculated and is considered as input to hydrological runoff model.

It is assumed that in case of small catchments (this is the case of Slovak H-SAF test catchments) it is not necessary to use space-distributed runoff models. But in case of application H-SAF products to small-scale events spatial distribution can be useful. For such purposes special sub-catchments mask can be used for integration of precipitation per each sub-catchment. Hydro validation was done for following products: H03, H04, H05 (precipitation products), H08 and H14 (soil moisture products), over the river catchments Kysuca, Nitra and Hron.

Amount (volume) and time distribution of precipitation are still the main limitation of satellite precipitation products. Satellite product overestimates convective precipitation, on the other hand lack of rainfall from November 2014 to April 2015. The consequence, from hydrological point of view, is inaccurate simulation of rainfall-runoff process with respect to runoff timing, rate and volume.

Lack of winter precipitation derived by satellite product generally is still problematic. Processes of snow accumulation and snow-melt runoff are very important for hydrological regime of Slovak river basins.

Monthly updating procedure contributes to improving of results achieved. Model is calibrated only on ground raingauge data. Model calibration based on satellite data should increase performance of the model during validation of satellite product.

SHMÚ worked in 2015 also on improvement of satellite data upscaling methods used in process of comparison satellite and radar data. Example is shown in Figure 5.7 for product H01 (precipitation from microwave conical scanners. Advantage of satellite data is evident from the image – right panel, where bigger area is covered by signal in comparison to limited radar network coverage. Extension of precipitation and absolute precipitation intensities captured by satellite and radar are in good agreement. Microwave satellite measurements are often used for calibration or morphing of IR MSG cloud data

into precipitation fields. Advantage of MSG satellite is the regular 15-minute time step from which accumulated precipitation is summed and used as input into hydrological run off models.

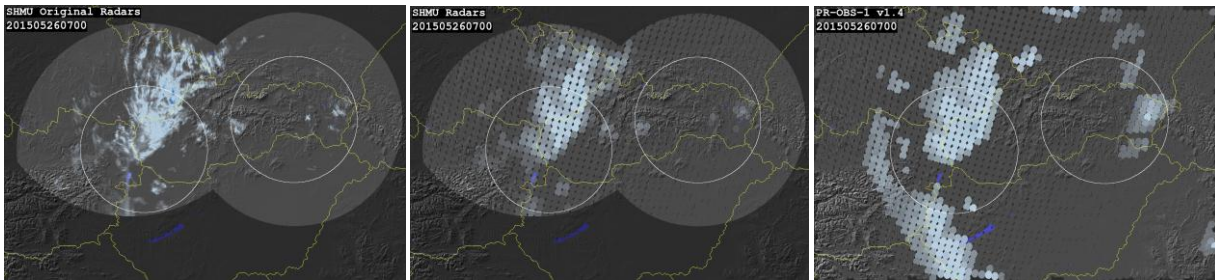


Figure 5.7. Left: Original radar data resolution as measured by SHMU radar network. Middle: Radar data upscaled into satellite native grid. Right: Satellite data from microwave conical scanner.

In 2015 we added new functionalities into common validation software: decoding of all parameters coded inside BUFR-formatted product files, like precipitation intensity, phase (liquid, frozen or mixed), percentage confidence for these values, quality index and sea/land/coast mask. Example of decoded data is shown in Figure 5.8.

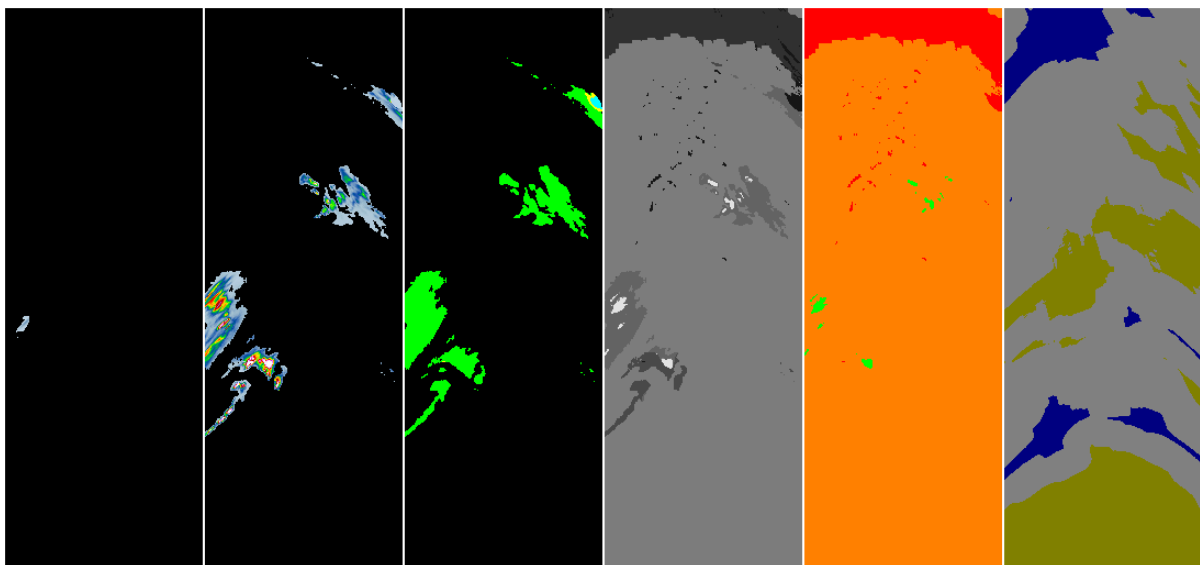
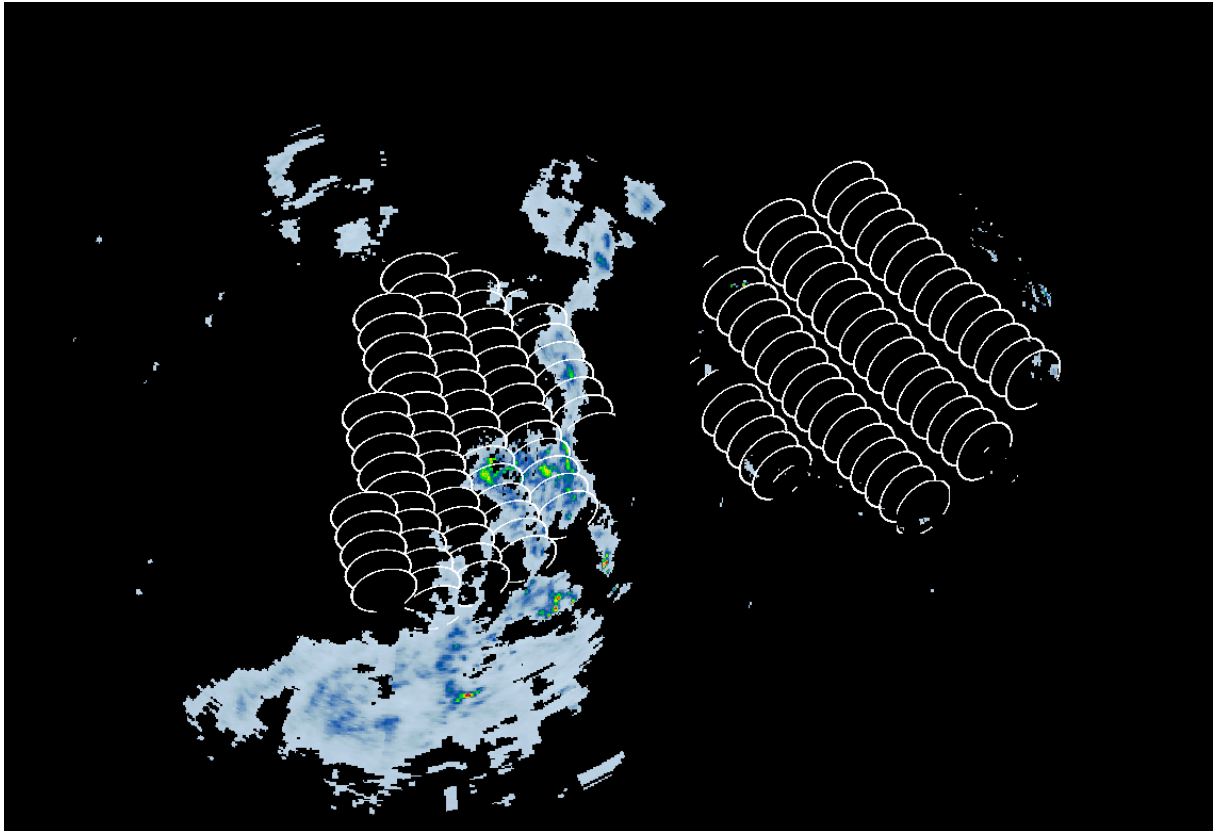


Figure 5.8. Processed productH01now allow us to use all parameters of satellite product in validation procedure. Columns represent satellite overpass over central Europe and contain following parameters from left to right: radar precipitation, satellite precipitation, cloud phase, percent of confidence, quality index, and land/sea/coast mask.

Additionally this software was enhanced with configuration file which enable us to use the same validation procedure for different products H01, H02, H03, H04 and H05. Some additional work is foreseen for optimization and unification of source codes which is planned in next few months.

Very important part of software is devoted to physically correct upscaling algorithms, which differs because of different scanning modes – conical scan in case of H01, cross-track scan in case of H02, regular grid in geo-satellite view projection in case of H03, H04 and H05 products. Example of correct matching of radar pixels in 1 km resolution with H01 satellite fields of view is shown in Figure 5.9.



*Figure 5.9. Radar precipitation field overlaid with satellite data footprints (ellipses) calculated exactly according satellite path, scan swath and Gaussian spread of sensor sensitivity.*

### 5.3 Detection of severe storms by overshooting tops monitoring

Special method for detection of overshooting tops (OT) over severe convective clouds was developed at SHMÚ in past years. This method is based on localization of shadows cast on the cirrus anvil of the storm. Because OTs occurs mainly in afternoon hours, Sun elevation is optimal for such purposes. But many of storms remain to late evening hours; therefor also IR detection method must be used commonly. SHMÚ closely cooperate in this field with ČHMÚ (Czech Republic) and NASA Langley Research Center (United States). Geometrical scheme of SHMÚ method is shown on Figure 5.10. This method requires special interactive visualisation tool, which also was developed at SHMÚ. Calculations are done automatically, but there is necessity of “human eye” visual inspection of satellite imagery.

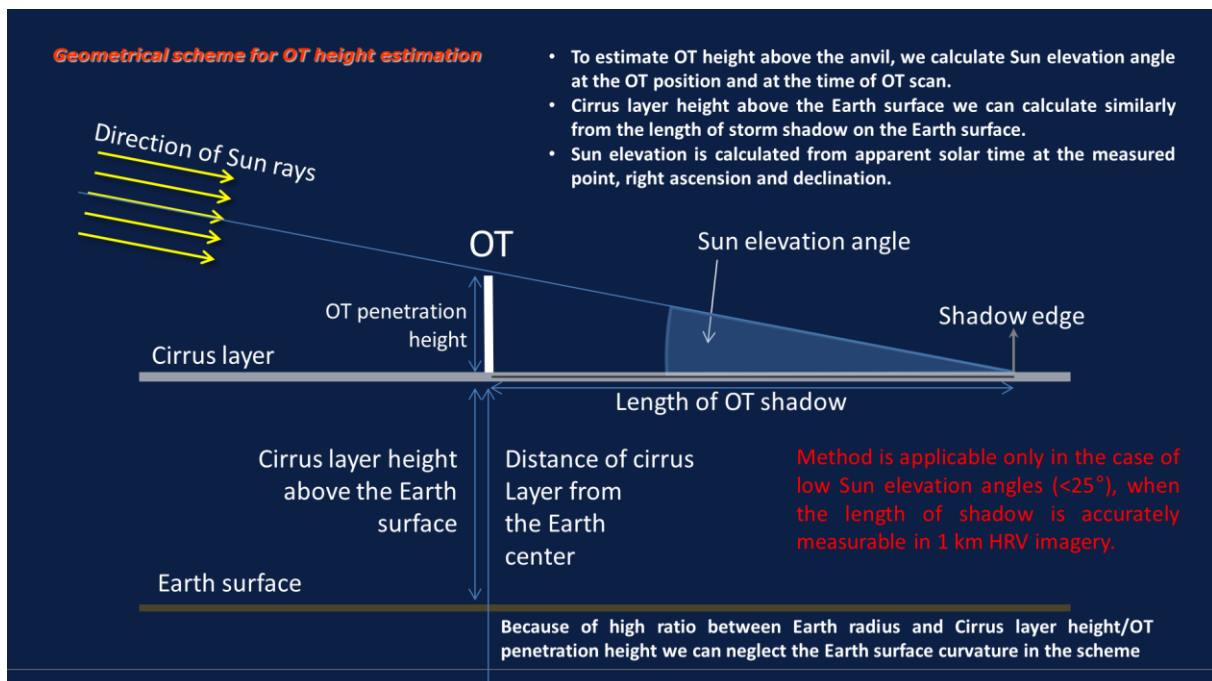


Figure 5.10. Geometrical scheme for OT height estimation. After visual detection of OT center position and its shadow edge all necessary calculations are done automatically by special visualisation tool.

This human-eye based method has various error sources:

#### a) Substantial errors

- Visual location of shadow base and shadow tail depends on the precision of OT center detection and in general on OT shape;
- Shadow of one OT can be broken by another OT shadow;
- Shadow tail casts out of anvil (out of projection area);
- Anvil cirrus cloud is too transparent or is not a plain;

- Observed cloud structures are not regular OTs and/or anvil cirrus clouds;
- Too long shadows when elevation is very low ( $<2^\circ$ ), shadow beyond terminator;
- Too short shadows when elevation is very high ( $>25^\circ$ );

b) Negligible errors

- Error resulting from parallax shift:
  - Manual correction is implemented in the tool; necessity of human adjustment.
  - In some cases it is hard to allocate proper cloud structure to the shadow.
- Error resulting from absolute anvil layer height above the Earth surface:
  - Error can be compensated manually.

Note: Above mentioned errors are relative to native MSG HRV image resolution and relate to subjective evaluation by observer.

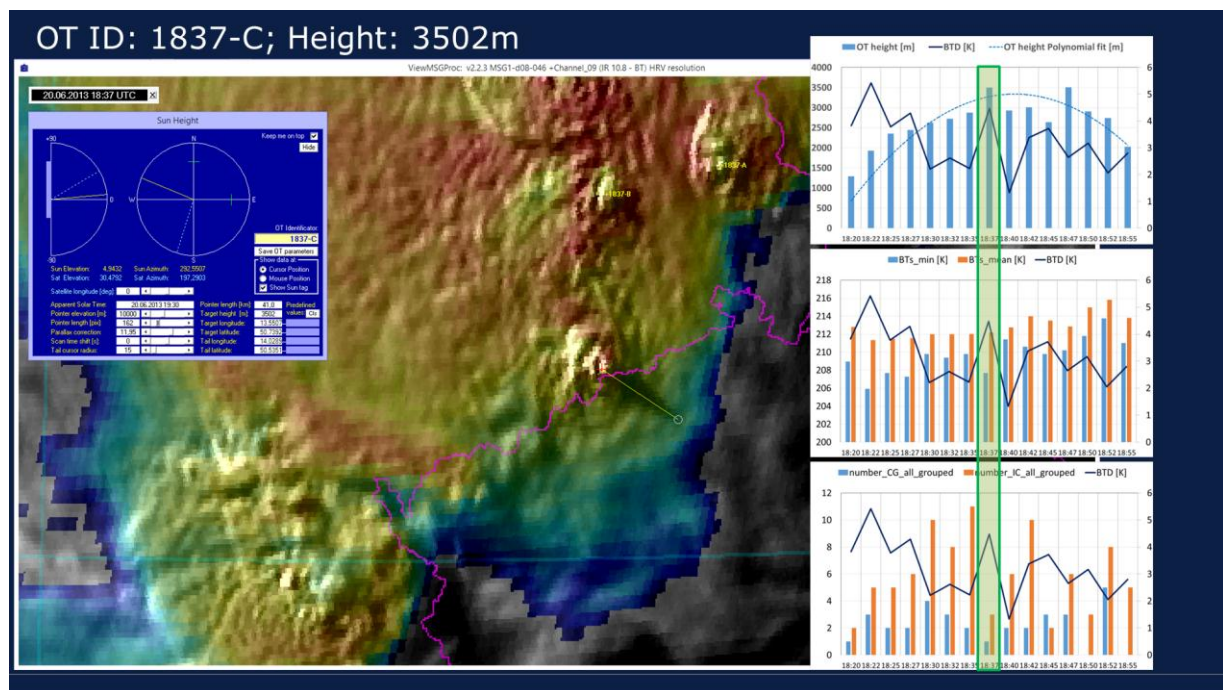


Figure 5.11. Example of OT height super rapid scan measurements by MSG-1 satellite from 20 June 2013. From complete database of OT created at ČHMÚ only OT with well pronounced shadows were selected for additional processing. On the right side panel time development of complete set of OT parameters is displayed: brightness temperature minimum, mean, difference against anvil, number of intra-cloud and cloud-to-ground lightning strokes.

In cooperation SHMÚ and ČHMÚ database of OT from super rapid scan measurements 2013 was created. Firstly “human eye based” approach (Setvák at al.) was applied to high resolution visible imagery, than automated OT detection using AdaBoost method (Radová at al.) on IR imagery was applied. Finally this

database was used at SHMÚ in visualisation tool for OT height measurement where all overshooting tops were inspected for shadows and for selected cases OT height was measured. Example of such measurement is shown on Figure 5.11.

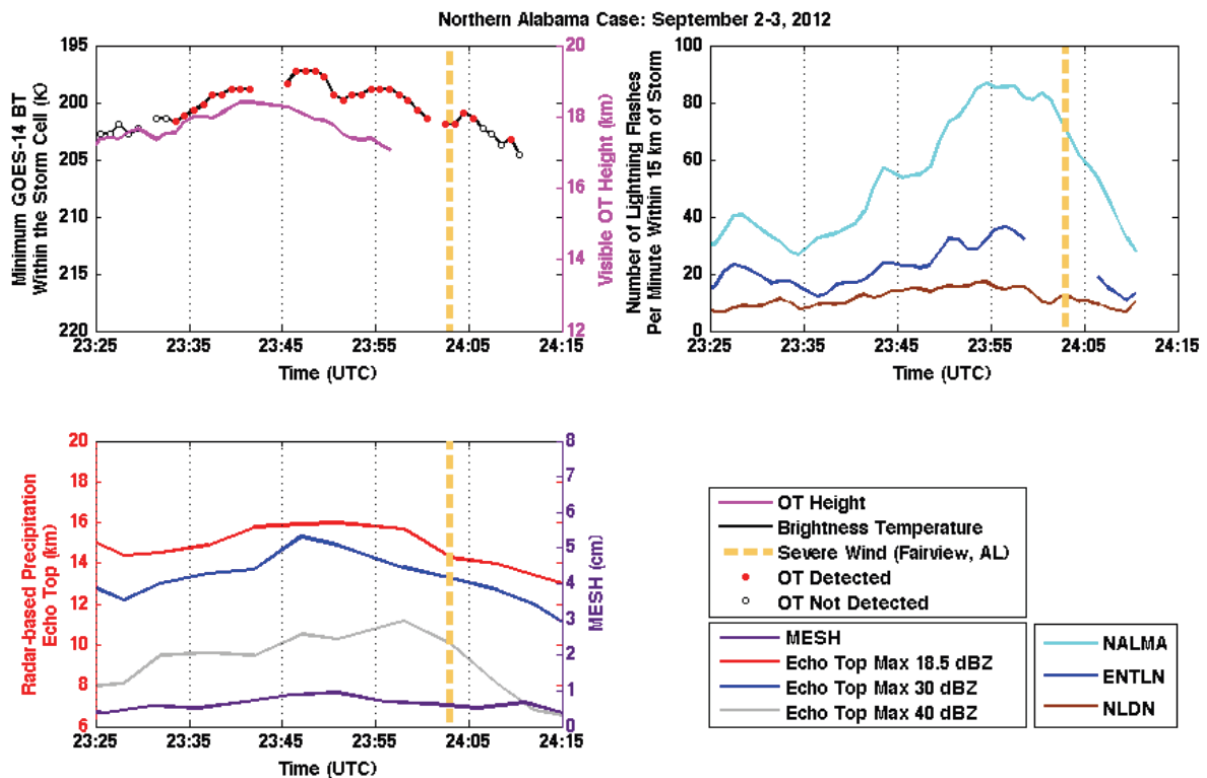
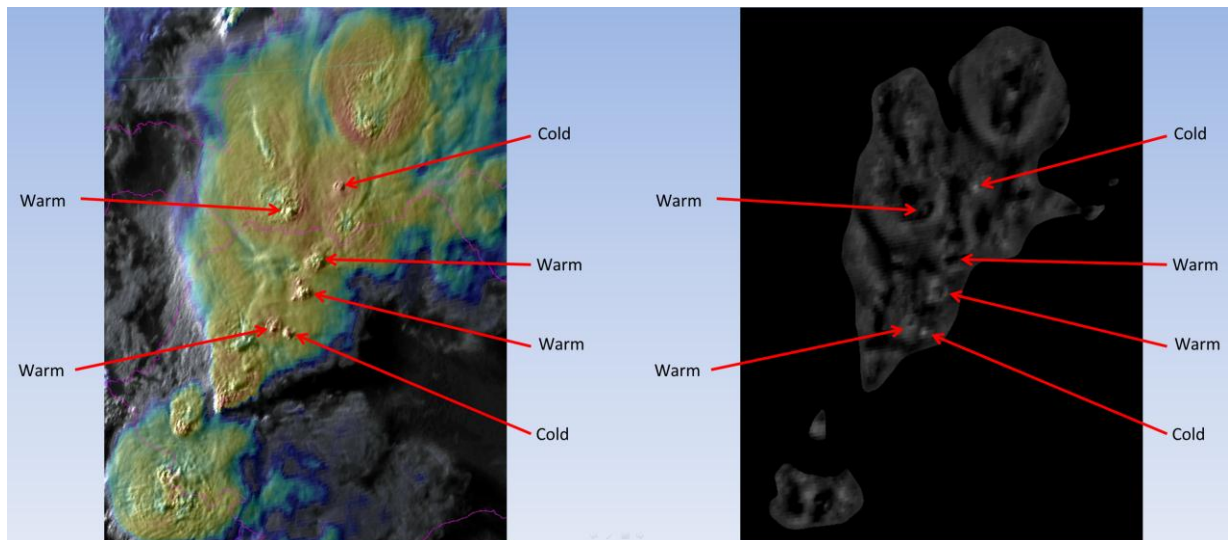


Figure 5.12. Upper-left: The GOES 14  $10.7\mu\text{m}$  BT minimum, objective OT detection time series and OT height estimations for storm on 2-3 September over Alabama, USA. Upper-right: The NALMA, ENTLN, and NLDN lightning networks flash detections. Lower-left: WSR-88D multi-reflectivity echo top time series from the Huntsville, Alabama radar and MESH time series. The time of a severe wind report is identified with a vertical yellow dashed line.

The aim of this experiment was to show that the severe wind and hail occurred near to or shortly after relatively rapid cloud top warming, indicating updraft decay that could have triggered a severe downdraft or allowed large hail to fall to the surface. It is evident from Figure 5.12 upper-left that overshooting top height well correlate with minimum infrared brightness temperatures detected by objective algorithm. Height measurement was limited to very low Sun elevations and was interrupted by Sun-set close to 23:57 UTC.

In cooperation with EUMETSAT Convection Working Group at SHMÚ we showed that overshooting tops of severe storms can be observed in various phases of life cycle from MSG satellites, especially using rapid scanning image updates. We performed convolution tests of IR imagery small structures, which showed strong differences in appearance of OT in VIS and IR spectral channels.

While on VIS imagery we observe lot of tower-like structures, on IR imagery some structures exhibit colder and another warmer spots or small areas in comparison to background cirrus clouds. Example is shown in Figure 5.13.



*Figure 5.13. Comparison of MSG HRV-IR composite image showing overshooting tops over severe storms (left) and IR image processed as convolution with narrow Gauss distribution (right).*

Numerical image post-processing – convolution of IR image with narrow Gauss function results into detection of local image extremes, both cold and warm spots. Comparing with high resolution visible image we are able to classify OT development phase. Mechanism of OT warming is not clear yet, hypothesis of warm air advection above collapsing OT – depression effect should be investigated in future.

But we are strongly limited by spatial resolution of current geostationary satellite generation. Next, third Meteosat generation will provide higher space, time and also spectral resolution, which promise better understanding of OT behavior in future.

## References Remote Sensing and Space Meteorology:

1. BEDKA, M. K. – WANG, C. – FELTZ, W. – ROGERS, R. – CAREY, D. L. – KAŇÁK, J. (2015). Examining Deep Convective Cloud Evolution Using Total Lightning, WSR-88D, and GOES-14 Super Rapid Scan Datasets. *AMS, WEATHER AND FORECASTING* 30:571-590 JUNE 2015; DOI: 10.1175/WAF-D-14-00062.1
2. BUCHA, T. et al. (2014). *Satelity v službách lesa*. SAP, Bratislava, 202 p. [in Slovak ]
3. FERANEC, J. – SOUKUP, T. – ČIŽMÁR, J. – ŠAFÁR, J. – KONTRA, P. (2015). CORINE land cover map of Europe. *Kartografické listy (Cartographic Letters)*, 23, 1, pp. 21-28.
4. KAŇÁK, J. (2015). Mature convection distribution over Europe based on 6-years Meteosat observations of anvils and overshooting tops. Conference poster P38: ECSS2015-120, European Conference on Severe Storms ECSS 2015, 14-18 September 2015, Wiener Neustadt, Austria.
5. KAŇÁK, J. – MÜLLER, M. (2014). Study on calibration stability and image sequence consistency in experimental 2.5-minute MSG rapid scan experiments. Proc. 2014 EUMETSAT Meteorological Satellite Conference, Geneva, Switzerland. EUMETSAT P.00516. <http://www.eumetsat.int/website/home/News/ConferencesandEvents/PreviousEvents/index.html>
6. KOPECKÁ, M. – ROSINA, K. – OŤAHEL', J. – FERANEC, J. – PAZÚR, R., – NOVÁČEK, J. (2015). Monitoring dynamiky zastavaných areálov (Monitoring the Dynamics of built-up areas). *Geographia Slovaca*, 30. Geografický ústav SAV, Bratislava, 98 p. [in Slovak ] Available at: [http://www.geography.sav.sk/journals/WEB\\_Geographia\\_Slovaca\\_30.pdf](http://www.geography.sav.sk/journals/WEB_Geographia_Slovaca_30.pdf)
7. KOPECKÁ, M. – VATSEVA, R. – FERANEC, J. – OŤAHEL', J. – ROSINA, K. (2014). Mapping and analyzing urban dynamics based on remote sensing for spatial planning and management. In 5th International Conference on Cartography and GIS. Bandrova, T., Konecny, M. (Eds.). Bulgarian Cartographic Association, Sofia, pp. 242-251.
8. PAZÚR, R. – KOPECKÁ, M. – FERANEC, J. (2015). Changes of artificial surfaces of Bratislava in 2006-2012 identified by the Urban Atlas data. In *Land Use/Cover Changes in Selected Regions in the World. Volume XI*. Asahikawa: International Geographical Union Commission on Land Use/Cover Change: Hokkaido University of Education, pp. 37-42.

9. PUCA, F. – PORCU, A. – RINOLLO, G. – VULPIANI, P. – BAGUIS, S. – BALABANOVA, E. – CAMPIONE, A. – ERTÜRK, S. – GABELLANI, R. – IWANSKI, M. – JURAŠEK, J. KAŇÁK, J. – KERÉNYI, G. – KOSHINCHANOV, G. – KOZINAROVA, P. – KRAHE, B. – LAPETA, E. – LÁBÓ, L. – MILANI, L'. – OKON, A. – ÖZTOPAL, P. – PAGLIARA, F. – PIGNONE, C. – RACHIMOW, N. – REBORA, E. – ROULIN, I. – SÖNMEZ, A. – TONIAZZO, D. – BIRON, D. – CASELLA, E. – CATTANI, S. – DIETRICH, F. – DI PAOLA, S. – LAVIOLA, V. – LEVIZZANI, D. – MELFI, A. – MUGNAI, G. – PANEGROSSI, M. – PETRACCA, P. – SANÒ, F. – ZAULI, P. – ROSCI, L. – DE LEONIBUS, E. A – GATTARI, F. (2014). The validation service of the hydrological SAF geostationary and polar satellite precipitation products. *Nat. Hazards Earth Syst. Sci.*, 14, 871-889.
10. SAČKOV, I. – BUCHA, T. – KIRÁLY, G. – BROLLY, G. – RAŠI, R. (2014). Individual tree and crown identification in the Danube floodplain forests based on airborne laser scanning data. In Zagajevski B., Kycko M., Reuter R. (Eds.). *Proceedings of the 34th EARSeL Symposium, 2nd Workshop of Special Interest Group on Forestry: Remote Sensing for forestry applications – New challenges, approaches and achievements.* Warsaw, Poland, June 17.-18.
11. SAČKOV, I. – SMREČEK, R. – TUČEK, J. (2014). Forest transportation survey based on airborne laser scanning data and GIS analyses. *GIScience & Remote Sensing*, 51(1), 83-98.
12. SETVÁK, M. – RADOVÁ, M. – KAŇÁK, J. – VALACHOVÁ, M. – BEDKA, K. – ŠŤÁSTKA, J. – NOVÁK, P. – KYZVAROVÁ, H. (2014). Comparison of the MSG 2.5-minute rapid scan data and products derived from these, with radar and lightning observations. *Proc. 2014 EUMETSAT Meteorological Satellite Conference, Geneva, Switzerland.* EUMETSAT P.63. WWW: <http://www.eumetsat.int/website/home/News/ConferencesandEvents/PreviousEvents/index.html>
13. SVIČEK, M. – KOVÁČIKOVÁ, I. et al. (2014). The 2014 campaign of remote-sensing control of area-based subsidies. Final report, NAFC-SSCRI Bratislava, 20 p.
14. SVIČEK, M. – KOVÁČIKOVÁ, I. et al. (2015). The 2015 campaign of remote-sensing control of area-based subsidies. Final report, NAFC-SSCRI Bratislava, 22 p.

## 6. INSTITUTIONS INVOLVED IN SPACE RESEARCH

Members of the National Committee of COSPAR with e-mail addresses.

The website of NC is <http://nccospar.saske.sk>.

Astronomical Institute (AI)  
Slovak Academy of Sciences (SAS)  
Stará Lesná  
059 60 Tatranská Lomnica  
J. Rybák ([choc@astro.ta3.sk](mailto:choc@astro.ta3.sk), NC member)

Faculty of Mathematics, Physics and Informatics (FMPI)  
Comenius University  
Mlynská dolina  
842 15 Bratislava  
J. Masarik ([Jozef.Masarik@fmph.uniba.sk](mailto:Jozef.Masarik@fmph.uniba.sk), NC member)

National Forest Centre  
T.G. Masaryka 22  
960 92 Zvolen  
contact: T. Bucha ([bucha@nlcsk.org](mailto:bucha@nlcsk.org))

Earth Science Institute (ESI)  
Slovak Academy of Sciences (SAS)  
Dubravska cesta 9  
840 05 Bratislava  
M. Revallo ([milos.revallo@savba.sk](mailto:milos.revallo@savba.sk), Secretary of NC)

Institute of Animal Biochemistry and Genetics  
Slovak Academy of Sciences (SAS)  
Moyzesova 61  
900 28 Ivanka pri Dunaji  
I. Hapala ([Ivan.Hapala@savba.sk](mailto:Ivan.Hapala@savba.sk), NC member)

Institute of Experimental Endocrinology (IEE BMC)  
Slovak Academy of Sciences (SAS)  
Dubravska cesta 9  
845 05 Bratislava  
R. Kvetňanský ([ueenkvet@savba.sk](mailto:ueenkvet@savba.sk), Vice- chair of NC)

Institute of Experimental Physics (IEP)  
Slovak Academy of Sciences (SAS)  
Watsonova 47  
040 01 Košice  
K. Kudela (kkudela@kosice.upjs.sk, Chair of NC, Representative  
of Slovak NC to COSPAR)

Institute of Geography (IGG)  
Slovak Academy of Sciences (SAS)  
Štefánikova 49  
814 73 Bratislava  
J. Feranec (feranec@savba.sk, NC member)

Institute of Materials and Machine Mechanics  
Slovak Academy of Sciences (SAS)  
Račianska 75  
831 02 Bratislava 3  
J. Lapin (ummslapi@savba.sk, lapin@up.upsav.sk, NC member)

Institute of Measurement Science (IMS)  
Slovak Academy of Sciences (SAS)  
Dúbravská 9  
842 19 Bratislava  
contact: I. Frollo ([frollo@savba.sk](mailto:frollo@savba.sk))

Institute of Normal and Pathological Physiology (INPP)  
Slovak Academy of Sciences (SAS)  
Sienkiewiczova 1  
813 71 Bratislava  
contact: F. Hlavačka ([Frantisek.Hlavacka@savba.sk](mailto:Frantisek.Hlavacka@savba.sk))

Slovak Central Observatory (SCO)  
Komárňanská 134  
947 01 Hurbanovo  
contact: Ivan Dorotovič ([ivan.dorotovic@suh.sk](mailto:ivan.dorotovic@suh.sk) )

Slovak Environmental Agency  
Remote Sensing Department  
Tajovského 28  
975 90 Banská Bystrica  
contact: J. Nováček ([jozef.novacek@sazp.sk](mailto:jozef.novacek@sazp.sk))

Slovak Hydrometeorological Institute  
Jeseniova 17  
833 15 Bratislava  
contact: J. Kaňák (jan.kanak@shmu.sk, NC member)

Slovak Organization for Space Activities  
Čukárska Paka 256  
93051 Veľká Paka (okr. Dunajská Streda)  
Contact: Michaela Musilova ([musilova@sosa.sk](mailto:musilova@sosa.sk))

Soil Science and Conservation Research Institute  
Gagarinova 10  
827 13 Bratislava  
contact: M. Sviček ([svicek@vupu.sk](mailto:svicek@vupu.sk))

Space Research in Slovakia 2014 – 2015  
National Committee of COSPAR in Slovak Republic  
Slovak Academy of Sciences  
Institute of Experimental Physics, SAS, Košice

Editors: Karel Kudela, Ján Feranec and Jana Štetiarová

Printed by CopyCenter Košice, April 2016  
ISBN 978-80-89656-09-7